Transmission Protocol Design for Covert Communications in UAV-Enabled Wireless Systems

by

Wenhao Zhang

A dissertation submitted in partial fulfillment
of the requirements for the degree of
Doctor of Philosophy
(The School of Systems Information Science)
in Future University Hakodate
September 2024

To my family

ACKNOWLEDGEMENTS

First and foremost, I am deeply grateful to Professor Xiaohong Jiang for his exceptional guidance and unwavering support throughout my Ph.D. journey at Future University Hakodate. His mentorship has not only shaped my research endeavors but also instilled in me invaluable life lessons. I extend my sincere appreciation to Professor Jiang's wife, Mrs. Li, for her kindness and support, which have made my time in Hakodate memorable. Their collective influence has enriched my academic pursuit and personal growth in ways I cannot fully express. I am profoundly grateful for their generosity and guidance, which have made this Ph.D. journey memorable and rewarding.

Besides my advisor, I would like to thank the rest of my thesis committee: Professor Hiroshi Inamura, Professor Masaaki Wada, Professor Ayahiko Nimi, and Professor Shigemi Ishida for their encouragement and insightful comments that not only help me to improve this thesis significantly but also inspire me to widen the area of my future research.

I would also like to express my sincere gratitude to Ji He of Xidian University, China, who helped me greatly improve the quality and clarity of my dissertation research and showed me the way to be an excellent researcher.

My sincere thanks also go to other members of our laboratory GuoZhu Zhao, Yan Liu, Xinzhe Pi, He Zhu, Jiaqing Bai, Zhen Jia, Zewei Guo, Meiyun Xie, Xin Guo, Yu Zhang and Jianing Wang, for their contributions in some way to this thesis.

Last but not the least, I would like to thank my family, especially my parents.

Words cannot express how grateful I am to them for all of the sacrifices they have made for me.

ABSTRACT

Transmission Protocol Design for Covert Communications in UAV-Enabled Wireless Systems

by

Wenhao Zhang

Unmanned aerial vehicle (UAV)- enabled wireless communication is emerging as a promising technology widely employed in modern wireless communication systems. However, the broadcast nature of wireless communications and the high-quality line-of-sight (LoS) air-to-ground links make UAV communications more vulnerable to security threats than traditional terrestrial wireless communications. Covert communication serves as a good solution to achieve secure communication in UAV-enabled wireless communication systems. This dissertation focuses on the protocol design and related performance analysis for covert communications in UAV-enabled wireless communication systems. We first focus on the single-receiver scenario, in which the transmitter UAV, ground receiver Bob and ground warden Willie are all equipped with antennas capable of operating in both omnidirectional microwave (OM) and directional mmWave (DM) transmission modes. We propose a covert transmission protocol based on hybrid OM/DM transmission mode selection, and develop related theoretical models to depict the system performance in terms of detection error probability (DEP), transmission outage probability (TOP), and effective covert rate. We

then consider a simple multi-receiver scenario, in which a UAV would like to disseminate common covert information (CI) to multiple ground users (GUs) within its coverage area while simultaneously evading the detection by a ground warden Willie outside the covered area. We design both one-hop and two-hop multicast transmission protocols for the concerned system, and develop related theoretical models to show the system performance in terms of detection error probability (DEP) and overall transmission time. We further consider a general multi-receiver scenario, in which a UAV would like to disseminate a common CI to multiple GUs diversely distributed within a circular area while simultaneously evading the detection by a ground warden Willie located in the center of the area. We propose two effective multicast group (MG) construction algorithms, develop a theoretical framework for the performance modeling of each MG, and explore the transmission time minimization in each MG. By integrating these components, we thus devise a complete and time-efficient covert multicast transmission protocol for the concerned system. Extensive numerical results are provided in this dissertation to illustrate the efficiency of the new transmission protocols for covert communications in UAV-enabled wireless communication systems. It is expected that the work in this dissertation can serve as a promising solution and also shed light on the protocol design for future UAV-enabled covert wireless communication systems.

TABLE OF CONTENTS

LIST OF FIGURES

Figure

LIST OF TABLES

Table

CHAPTER I

Introduction

In this chapter, we first introduce the background of UAV-enabled wireless communication systems and covert wireless communication. Then, we present the objective and main works of this dissertation. Finally, we give the outline and main notations of this dissertation.

1.1 UAV-Enabled Wireless Communication Systems

Unmanned Aerial Vehicles (UAVs), commonly known as drones, have significantly impacted various industries due to their high mobility, rapid deployment, and improved communication conditions. These features have led to the rapid growth and extensive use of UAVs in various applications, particularly in wireless communication. UAV-enabled wireless communication systems, which consist of one or more UAVs and ground terminals, can provide notable benefits over traditional terrestrial communication systems. As the demand for high-speed, interconnected communication services continues to increase, utilizing the advantages of UAVs to address communication challenges has become increasingly crucial [1].

UAV-enabled wireless communication systems are essential in both civilian and commercial domains. They play vital roles in weather monitoring, forest fire detection, and emergency search and rescue operations. Unlike traditional communica-

tion systems, which can be restricted by geographical and infrastructural limitations, UAVs can be quickly deployed to provide wireless connectivity in areas where ground-based infrastructure is either unavailable or damaged. This capability is particularly useful in urban areas with complex terrain or in regions where the existing communication infrastructure is compromised [2].

One of the primary advantages of UAV-enabled wireless communication systems is their cost-effectiveness. Traditional communication infrastructure, such as cell towers, requires substantial investment and time for installation. In contrast, UAVs can be deployed rapidly at a lower cost, making them an ideal choice for temporary or emergency communication needs. This economic efficiency, combined with their flexibility and mobility, makes UAVs a suitable option for both short-term and long-term communication solutions.

Another significant advantage of UAV-enabled wireless communication systems is their ability to establish line-of-sight (LoS) communication links. LoS links greatly enhance the capacity of communication systems, leading to improved data transmission rates and reliability. Furthermore, the dynamic deployment capabilities of UAVs allow them to adjust to different communication scenarios and physical environments in real-time. This adaptability enhances the system's resistance to interference and its overall performance in complex environments.

In conclusion, UAV-enabled wireless communication systems represent a substantial advancement in addressing the challenges of modern communication needs. Their high mobility, rapid deployment, cost-effectiveness, and improved communication conditions make them a compelling alternative to traditional terrestrial communication systems. As the demand for high-speed and reliable communication continues to grow, the role of UAVs in wireless communication is poised to expand, driving innovation and enhancing connectivity across various domains.

1.2 Security in UAV-Enabled Systems

1.2.1 Security Issues and Typical Approaches

UAVs play crucial roles in wireless communication systems. However, the broadcast nature of wireless transmissions and the lack of clear physical boundaries make wireless channels vulnerable to eavesdropping, leading to security vulnerabilities and potential attacks on UAVs. Particularly, compared to traditional terrestrial communication systems, LoS air-to-ground channels enhance signal strength for both legitimate users and eavesdroppers, making it easier for eavesdroppers to decode sensitive information [3]. This results in more significant security risks in UAV networks. Thus, ensuring the communication security of UAV-enabled wireless communication systems becomes an increasing concern.

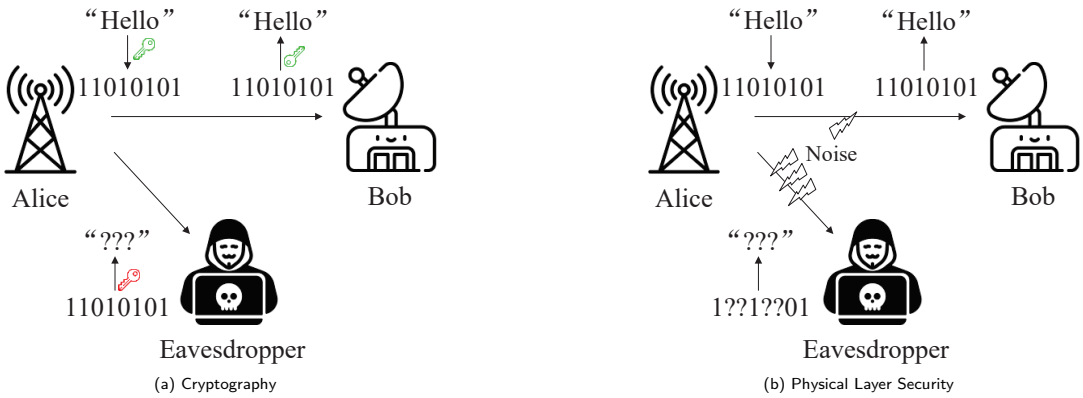

Figure 1.1: Illustration of the security approaches.

Cryptography is a well-known method for ensuring communication security. As illustrated in Fig. 1.1a, it employs key encryption and designs various encryption algorithms to safeguard private data transmission. However, encryption often requires a trusted key management center, which limits its applicability in complex networks. Additionally, it has been demonstrated that even the most robust cryptographic methods are at risk of being brutally cracked by quantum computing [4].

As an alternative approach, physical layer security can achieve information-theoretic

security by exploiting the inherent physical layer randomness of wireless channels [5]. As shown in Fig. 1.1b, the core idea of physical layer security technology lies in leveraging inherent transmission characteristics of wireless channels, such as differences between primary and eavesdropping channels, randomness, reciprocity, and secrecy. By intelligently constructing and designing transmit signals, it enhances the mutual information between the transmitter and intended user while minimizing information available to eavesdroppers. This approach effectively safeguards private information transmitted by preventing unauthorized interception, thereby enhancing communication privacy and security among legitimate users. Physical layer security offers significant advantages over traditional encryption methods by achieving security without relying on encryption and decryption processes. Furthermore, it leverages the timing and randomness of wireless channels to enhance security performance through signal processing techniques, such as power distribution strategies from the transmitter's perspective. However, it is important to note that while physical layer security aims to protect transmitted content from eavesdropping, extreme scenarios may still pose risks. Detection of illicit transmitter behavior by unauthorized parties could lead to potential tracking or exposure of transmitter's location information, posing security vulnerabilities in wireless communication networks.

1.2.2 Covert Communication

In recent years, covert communication has emerged as a novel approach to ensuring wireless security. The basic model for the covert communication problem is illustrated in Fig. 1.2. In this model, known as the "Prisoners' Problem" [6], Alice and Bob transmit covert messages to each other under the surveillance of the warden, Willie. If the warden detects their covert messages, he identifies the presence of their communication, suspects an escape plan, and punishes them to prevent further communication. If the warden fails to detect their communication, the prisoners have

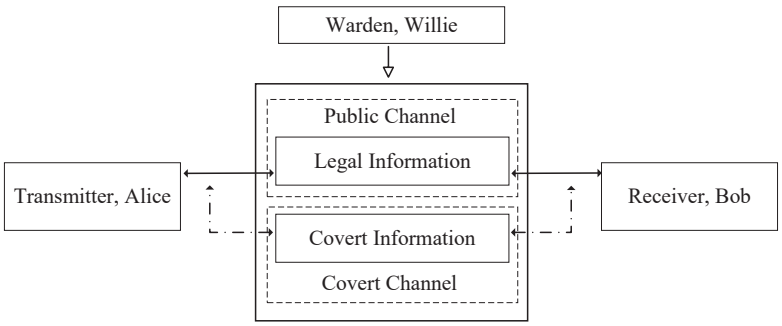

Figure 1.2: Illustration of the Prisoners' Problem.

successfully transmitted their messages without being detected. In covert communication, similar to the "Prisoners' Problem," Alice transmits secret information to Bob while a detector, Willie, attempts to detect the transmission process between Alice and Bob.

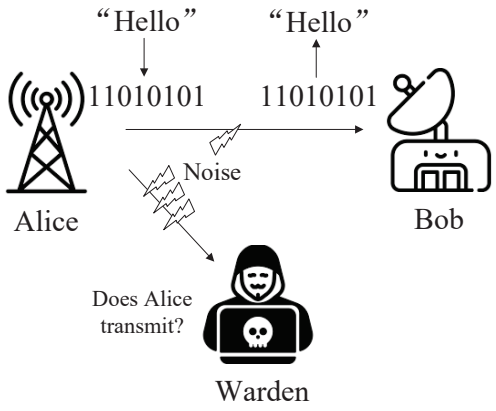

Figure 1.3: Illustration of the covert communication.

As shown in Fig. 1.3 that unlike the encryption and physical layer security techniques, covert communication focuses on minimizing the probability of detection by a warden, thereby hiding communication behaviors or processes. While encryption and physical layer security protect transmitted content, the revelation of communication behaviors can still lead to significant security issue. Covert communication offers new possibilities for addressing privacy protection challenges faced by UAV communication networks.

1.3 Why Covert Communication in UAV-Enabled Systems

As flying wireless networks, UAV networks are inherently vulnerable due to their openness, the broadcast nature of wireless media, and the long-distance LoS communication characteristics, which make them susceptible to attacks. Additionally, many applications not only require the safeguarding of data security but also need to ensure that the communication process remains undetected to prevent interference and eavesdropping by malicious users.

Covert communication in UAV-enabled systems is essential for secure and private data transmission. By hiding communication from unauthorized entities, it prevents eavesdropping and data breaches, which is crucial for governmental, commercial, and environmental operations.

In law enforcement and border control, covert communication allows UAVs to monitor suspects and secure borders without alerting those under surveillance. This enhances operational effectiveness and ensures the integrity of collected data. In commercial applications, private security companies use UAVs for discreet surveillance of property and assets, preventing potential intruders from detecting these efforts and thereby improving security. Covert communication also protects against corporate espionage by safeguarding sensitive communications during UAV-based inspections and operations.

In disaster response and management, UAVs equipped with covert communication can coordinate search and rescue operations without interference. This ensures that emergency response teams can communicate securely and efficiently, leading to more effective disaster management. Environmental monitoring benefits from covert communication by enabling discreet tracking of wildlife, preventing poaching and illegal activities. It also aids in monitoring illegal logging and fishing activities without alerting perpetrators, supporting conservation efforts.

Overall, covert communication enhances the security, efficiency, and effectiveness of UAV operations across various sectors, highlighting its importance as a critical area of research and development.

1.4 UAV Covert Communication Scenarios

1.4.1 Typical Scenarios

UAV covert communication encompasses various scenarios, including the UAV acting as a transmitter and the UAV acting as a relay. In the first scenario, the UAV directly sends information to one or more ground stations or receivers while avoiding detection by ground wardens. This scenario is crucial for targeted data delivery in applications such as surveillance and real-time monitoring in disaster-stricken areas. In the second scenario, ground stations transmit information through the UAV to ground users while ensuring the transmission process remains undetected by ground wardens. This scenario involves two-hop or multi-hop transmissions, extending communication range and network coverage in remote or obstructed areas. These capabilities enhance communication efficiency across various applications, including providing support in remote locations, establishing temporary networks during emergencies, and enabling coordinated communication in large-scale environments. Such examples highlight the versatility of UAVs in improving communication performance in challenging environments.

1.4.2 Considered Scenarios

This thesis explores covert protocol design for three typical scenarios of UAV systems where UAVs act as transmitters, i.e., the single-receiver, simple multi-receiver, and general multi-receiver scenarios. In the single-receiver scenario, the UAV communicates directly with a ground user. The simple multi-receiver scenario focuses

on GUs within the UAV's coverage area. The general multi-receiver scenario investigates covert performance in more complex network structures, where multiple GUs are diversely distributed within a circular area.

These scenarios utilize the broadcast wireless data transmission model, where signals are transmitted via radio waves and travel through the air without physical barriers, making them detectable by any device within the transmission range. The unicast protocol is employed for the single-receiver scenario, while the multicast protocol is adopted in simple and general multi-receiver scenarios to enhance transmission efficiency. Unicast is a one-to-one communication model where data is sent from a single transmitter to a specific receiver using a unique address, such as an IP address, ensuring targeted information delivery. In contrast, multicast enables a single transmitter to communicate simultaneously with multiple receivers identified by a multicast group address, optimizing bandwidth usage and reducing network congestion.

1.5 Objective and Main Works

This thesis focuses on the protocol design and related performance analysis for covert communications in UAV-enabled wireless communication systems. As shown in Fig. 1.4, our objective is to offer promising transmission protocols for covert communication in various UAV-enabled wireless systems. Towards this end, we first focus on the covert transmission protocol design of the single-receiver scenario and develop theoretical models to depict the system performance. We then consider a simple multi-receiver scenario, design both one-hop and two-hop multicast transmission protocols for the concerned system, and provide related theoretical models to show the system performance. We further consider a general multi-receiver scenario and devise a complete and time-efficient covert multicast transmission protocol for the concerned system.

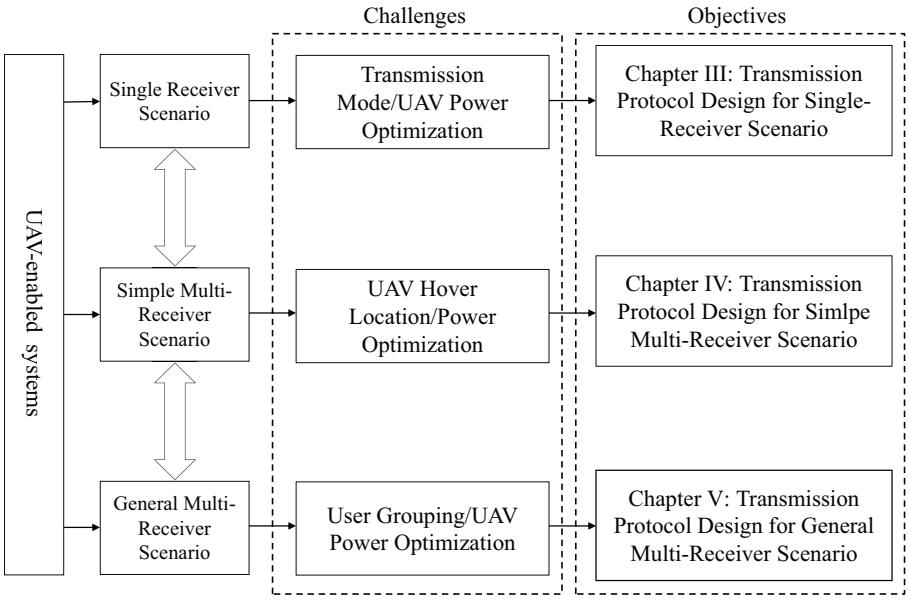

Figure 1.4: Objectives and main contributions of this thesis.

1.5.1 Transmission Protocol Design for Single-Receiver Scenario

This work focuses on the covert transmission protocol design for the single-receiver scenario of the UAV-enabled wireless systems. The existing works help us understand the covert communication with either microwave or mmWave technologies. Notice that these two technologies have their strength and weakness, so some recent work explored the dual-frequency antenna design to support both bands of communications [7–9] as well the related issue of network performance analysis [10, 11]. These works indicate that network performance can be significantly enhanced by supporting both microwave and mmWave in the communication system. Thus, a natural question that arises is *how to take the full advantages of microwave and mmWave to achieve a more efficient covert communication.* To this end, we explore covert communication in a UAV-enabled wireless system where UAV is equipped with a dual-band antenna and propose a covert transmission protocol based on the optimal selection between omnidirectional microwave and directional mmWave transmission mode to improve

the covert performance of the concerned system. The main contributions of this work are summarized as follows.

- We first develop theoretical frameworks for covert performance analysis of an A2G system under both the OM and DM transmission modes, in terms of the detection error probability (DEP), outage probability and effective covert rate (ECR). Specially, the uncertainty of LoS and non-line-of-sight (NLoS) of the A2G channel due to the movement of UAV is fully considered in the analysis. These frameworks reveal the inherent relationship between the key system parameters (i.e., UAV's location, transmission rate, transmit power) and the DEP, outage probability and ECR.

- We then explore the covert performance optimization of the concerned A2G wireless system under both the OM and DM transmission modes. Specifically, for a given position of UAV, we determine the optimal covert transmission power and transmission rate to achieve the maximal ECR while satisfying the DEP constraint.

- Based on the optimization results, we further propose a covert transmission protocol based on the OM/DM transmission mode selection, which allows the UAV to adaptively select between the OM and DM transmission modes at different locations to achieve the optimal covert transmission performance.

- Finally, extensive numerical results are provided to illustrate the effects of the key system parameters on the overall covert performance. The results indicate that the proposed covert transmission protocol based on the OM/DM transmission mode selection outperforms the pure OM or DM transmission mode in the considered single-receiver scenario of the UAV-enabled wireless system.

1.5.2 Transmission Protocol Design for Simple Multi-Receiver Scenario

This work explores the covert transmission protocol design for the simple multi-receiver scenario of UAV-enabled wireless systems. Notice that multicast communication, which effectively utilizes network radio resources to simultaneously transmit data to multiple users, serves as an important communication paradigm for enhancing transmission efficiency and overall network utility [12]. In particular, the multicast communication is promising to support the future explosively growing content-centric applications [13]. Thus, it is of great importance to investigate the covert multicast communication since it can greatly improve the efficiency of covert communication systems.

To the best of our knowledge, the existing works focus on unicast protocol design, overlooking the potential efficiency offered by multicast transmissions. Thus, the covert multicast in UAV-enabled wireless communication systems remains an unexplored issue. As the first attempt towards this direction, this work focuses on the scenario where the UAV acts as a flying base station to disseminate a common information to multiple GUs while avoiding detection by the ground warden, and proposes two covert multicast transmission protocols for the concerned system based on one-hop transmission and two-hop transmission, respectively. The main contributions of this work are summarized as follows.

- We first design two covert multicast transmission protocols. One is a One-Hop (OH) transmission protocol, where the UAV directly multicasts covert information to GUs. The other is a Two-Hop (TH) transmission protocol, in which the UAV transmits covert information to a relay, which then multicasts the received information to the remaining GUs.

- Next, we develop a theoretical framework to model the performance of both the detection error probability (DEP) at Willie and the overall transmission time

of the UAV under the OH transmission protocol. For a given hover location, we derive the mathematical expressions for the optimal transmit power and the corresponding minimum transmission time subject to covertness constraints. Additionally, we propose a particle swarm optimization (PSO)-based algorithm to jointly optimize the UAV's hover location and transmit power, achieving the overall minimum transmission time.

- We then develop the corresponding theoretical framework to model the performance of both the DEP at Willie and the overall transmission time of the UAV under the TH transmission protocol. For a selected relay, we derive the mathematical expressions for the optimal transmit power and the corresponding minimum transmission time, ensuring the covertness constraint is met. Additionally, we propose an exhaustive optimization algorithm to jointly optimize the relay selection and the UAV's transmit power for transmission time minimization.

- Finally, we present extensive numerical results for various GU distribution scenarios to compare the transmission time among the benchmark central-based hover location protocol, the One-Hop (OH) transmission protocol, and the Two-Hop (TH) covert transmission protocol. The numerical results demonstrate the efficiency of the proposed covert transmission protocols.

1.5.3 Transmission Protocol Design for General Multi-Receiver Scenario

This work further considers a general multi-receiver scenario, in which a UAV would like to disseminate a common CI to multiple GUs diversely distributed within a circular area while simultaneously evading the detection by a ground warden Willie located in the center of the area. The main contributions of this work are summarized as follows.

- We first develop two effective multicast group (MG) construction algorithms based on the K-means++ algorithm [14] and spiral mobile-based station placement algorithm [15] to group all GUs into multiple MGs.

- For each MG, we then establish a theoretical framework for its performance analysis in terms of DEP at warden and transmission time of UAV.

- Under the covertness constraint, we further formulate the optimal setting of transmission power at UAV for transmission time minimization as an optimization problem, and also derive the analytical results for the corresponding optimal transmission power and the minimum transmission time.

- By integrating the aforementioned procedures, we thus devise a complete multicast transmission protocol to achieve the minimum transmission time under the covertness constraint.

- Finally, we provide extensive numerical results under various system scenarios to illustrate the comparison between the simple point-to-point transmission and the proposed multicast transmission protocol, and thus to demonstrate the efficiency of the new multicast protocol.

1.6 Dissertation Outline

The remainder of this dissertation is organized as follows: Chapter II reviews the related works pertinent to this dissertation. Chapter III focuses on the design of the transmission protocol for covert communications in the single-receiver scenario. Chapter IV explores the design of transmission protocols for covert communications in the simple multi-receiver scenario, and Chapter V extends this exploration to the general multi-receiver scenario. Finally, we conclude the dissertation in Chapter VI.

1.7 Notations

The main notations of this dissertation are summarized in Table 1.1.

Table 1.1: Main Notations

Symbol	Definition
a	UAV (Alice)
b	Ground user (Bob)
w	Ground warden (Willie)
GUs	Ground users
P_a	Transmission power of Alice
l_{ij}	Horizontal distance between nodes i and j
d_{ij}	Distance between nodes i and j
h_i	Height of node i
$d_{aw}^{\min}$	Minimum distance between UAV and Willie
$d_{aw}^{\max}$	Maximum distance between UAV and Willie
$\mathbb{A} \in \{M, S\}$	Main lobe and side lobe, respectively
$\mathbb{B} \in \{L, N\}$	LoS channel and NLoS channel, respectively
$\mathbb{C} \in \{o, d\}$	OM transmission mode and DM transmission mode, respectively
G_{ij}	Total antenna gains of link $i \to j$
G_i^M	Main lobe gain of node i
G_i^S	Side lobe gain of node i
P_{ij}^L	Probability that the channel mode of link $i \to j$ is LoS link
P_{ij}^N	Probability that the channel mode of link $i \to j$ is NLoS link
$H_{ij}^{\mathbb{C},\mathbb{B}}$	Channel coefficient of link $i \to j$
$h_{ij}^{\mathbb{C},\mathbb{B}}$	Small scaling fading coefficient of link $i \to j$
$L_{ij}^{\mathbb{C},\mathbb{B}}$	Path loss of link $i \to j$

$\alpha_{\mathbb{B}}$	Path-loss exponent of $\mathbb{B}$
$\beta_{\mathbb{B}}$	Path-loss coefficient of $\mathbb{B}$
$S_{\mathbb{B}}$	Nakagami-m fading parameter of $\mathbb{B}$
$k_{\mathbb{B}}$	Rician factor of $\mathbb{B}$
θ_i	Elevation angle of UAV relative to node i
θ_i^h	Half-power beamwidth for the azimuth orientation in the horizontal direction of node i
$\theta_i^{e/d}$	Half-power beamwidth for the elevation/depression angles of node i
φ_i	Included angle of node i relative to UAV and node j
σ_b^2	Noise power at Bob
σ_w^2	Noise power at Willie
$\hat{\sigma}_n^2$	Nominal noise power
σ_g^2	Noise power at g-th GU
σ_r^2	Noise power at relay
ϵ	Covertness constraint
γ_{th}	Outage probability threshold
R_b	Target rate
π_0, π_1	Transmit probability and dose not transmit probability, respectively

CHAPTER II

Related Works

This chapter introduces the existing works related to our study in this thesis, including the works on achieving covert wireless communication and works on covert UAV-enabled wireless communication.

2.1 Covert Wireless Communication

Bash et al. first derive the information theory limitation called the square root law (SRL) for covert communication [16], pointing out that under the additive white Gaussian noise (AWGN) channel, Alice can only reliably and covertly send $\mathcal{O}(\sqrt{n})$ bits to Bob over n channel uses. Subsequently, the fundamental limit of covert communication is further studied under various wireless channels, including binary symmetric channels [17], discrete memory-less channels [18], and multiple input multiple output (MIMO) AWGN channels [19]. Following this line, extensive research works are dedicated to the study of covert communication in various network scenarios.

The authors in [20] first prove that a nonzero covert rate is possible over the AWGN channels and Rayleigh channels regardless of the finite or infinite channel use. Based on the results, the optimal power adaptation schemes are designed in [21]. Considering the channel uncertainty, the work [22] reveals the fundamental difference in the design of covert transmission schemes between the case of quasi-static fading

channel and the case of non-fading AWGN channel [23]. The jamming-assisted covert communication is also explored in different network scenarios, including those with full-duplex jamming receiver [24], those with Poisson point distributed jammer [25], those with randomly located warden [26], those with two-hop relaying [27], and those with intelligent reflecting surface (IRS) technology [28, 29]. Noticing that millimeter-wave (mmWave) technology can bring high bandwidth, covert communications with mmWave is examined in some recent works. The authors in [30] first consider a mmWave communication system with dual independent antenna arrays, and propose a covert transmission scheme where one antenna array is used to form a beam towards Bob for data transmission and the other is used for jamming. The covert rate maximization in mmWave systems is investigated in [31] through the joint optimization of beam training duration, training power, and transmission power. A multi-user beam training strategy is proposed in [32] to maximize the effective covert throughput. Besides, the authors in [33] consider a full-duplex covert mmWave communications scenario and explore the maximization of achievable covert rate by jointly optimizing the beamforming, transmit power, and jamming power.

2.2 Covert UAV-Enabled Wireless Communication

Currently, extensive contributions are devoted to the study of UAV-enabled covert wireless communication systems. For a UAV system where the UAV acts as the transmitter, the authors in [34] propose an iterative algorithm to efficiently optimize the UAV's trajectory and transmit power concurrently to achieve the maximal covert communication rate in the system. In [35], a geometric method algorithm is proposed to jointly determine the optimal UAV trajectory and transmit power for covert communication capacity maximization in a UAV system. The authors in [36] present an iterative algorithm to collectively optimize the time slot, transmit power, and trajectory of the UAV for covertness performance enhancement in a UAV system. The

works in [37] and [38] delve into the optimization of UAV transmit power and placement for covert rate maximization in two-dimensional and three-dimensional UAV systems. The work in [39] focuses on scenarios where the UAV acts as a relay, optimizing block length and transmit power at both the transmitter and UAV to enhance covert performance. Regarding the full-duplex UAV relay system, the authors in [40] formulate an optimization problem that jointly optimizes the transmit power of the transmitter and the jamming power of the UAV relay. They develop a penalty successive convex approximation scheme to tackle this optimization problem and achieve maximum covert throughput. Moreover, considering the delay-intolerant UAV relay system, the authors in [41] explore UAV location optimization to maximize effective throughput under the constraints of covertness and block length.

In light of the considerable advantage of IRS technology in reconfiguring the propagation environment, the authors in [42] propose a novel scheme for covert communication by integrating UAVs and IRS. In this scheme, the UAV carries an IRS to introduce additional randomness to channels, and the optimal transmit-to-jamming ratio is obtained to maximize the achievable covert transmission rate. The authors in [43] iteratively optimize the transmit power of the transmitter, the phase shift of the IRS, and the horizontal location of the UAV-IRS to maximize the covert transmission rate. The authors in [44] develop an iterative algorithm aiming to optimize the UAV 2D trajectory and IRS phase shift to maximize the average covert rate in a UAV-enabled wireless communication system. Furthermore, in [45], a deep reinforcement learning-based optimization algorithm is proposed for optimizing the UAV 3D trajectory and IRS phase shift to enhance covert communication performance.

Concerning multi-user systems, the authors in [46] devise an energy-efficient multi-UAV-mounted IRS covert communication scheme over the Terahertz band. They propose a block successive convex approximation approach to iteratively design the user scheduling, power allocation, maximum jamming power, IRS beamforming, and

UAVs' trajectory to improve covert throughput. Besides, the non-orthogonal multiple access (NOMA), which can facilitate multiple users to access services simultaneously over the same frequency, offers enhanced throughput to multi-user systems. Considering the UAV-assisted NOMA networks, the authors in [47] jointly optimize the hovering height and power to enhance covert performance. In addition, the authors in [48] propose an iterative block coordinate descent-based successive convex approximation method to maximize the average covert achievable rate for the considered UAV-assisted NOMA networks.

It is important to note that most existing research in the field primarily focuses on analyzing covert communication performance within a single frequency band. While this approach provides valuable insights, it inherently limits the scope of understanding and application, particularly in more complex and realistic scenarios. Additionally, multicast communication, which efficiently uses network radio resources to transmit data to multiple users simultaneously, plays a crucial role in enhancing both transmission efficiency and overall network utility. By enabling a single transmission to reach multiple receivers, multicast communication significantly reduces bandwidth consumption and increases the scalability of wireless networks.

Given the critical importance of these factors, it becomes imperative to extend the analysis of covert communication to dual frequency bands. Such an investigation would provide a more comprehensive understanding of how covert performance can be optimized by adapting the different frequencies, offering more flexible and resilient solutions for secure communication. Additionally, exploring covert multicast communication systems could reveal new strategies for balancing security and efficiency, enabling the development of more robust and versatile communication protocols.

CHAPTER III

Transmission Protocol Design for Single-Receiver Scenario

This chapter focuses on the single-receiver scenario, in which the transmitter UAV, ground receiver Bob and ground warden Willie are all equipped with antennas capable of operating in both omnidirectional microwave (OM) and directional mmWave (DM) transmission modes. We propose a covert transmission protocol based on a hybrid OM/DM transmission mode selection scheme, where the UAV can dynamically select between the OM and DM transmission modes according to the link conditions of the two transmission modes, leading to an enhanced covert communication performance. Related theoretical models are also developed to depict the system performance in terms of detection error probability (DEP), transmission outage probability (TOP), and effective covert rate. Finally, extensive numerical results are provided to illustrate the efficiency of the new transmission protocol under the single-receiver scenario.

3.1 System Model and Preliminaries

3.1.1 System Model

We investigate a UAV-enabled covert communication system as depicted in Fig. 3.1, wherein a UAV (Alice, a) undertakes surveillance tasks (e.g., imaging) over a specific

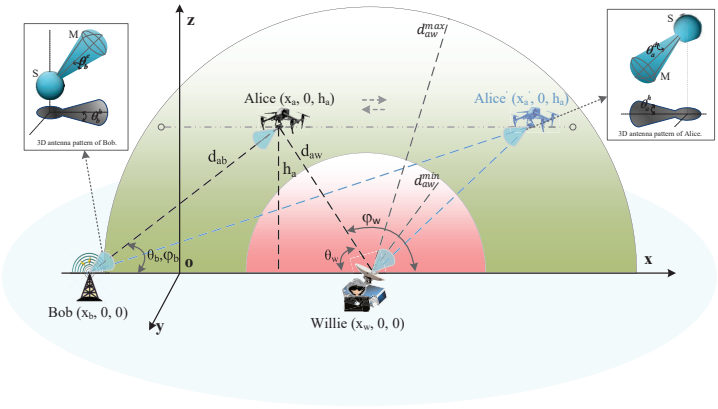

Figure 3.1: Illustration of the concerned UAV-enabled communication system model.

geographical area and requires the urgent transmission of critical information to an intended user (Bob, b), all the while avoiding detection by a warden (Willie, w). Alice, Bob, and Willie are all equipped with antennas capable of operating in both OM and DM transmission modes [7–9]. It is assumed that Alice uses a consistent transmission power P_a, limited by a maximum power constraint P_{max}, and patrols the surveillance area at a uniform height h_a. The distance between Alice and Willie is denoted as d_{aw}. A minimum distance constraint $d_{aw}^{\min}$ is in place to shield the UAV from detection by visual or radar mechanisms. Additionally, given the finite resolution of the UAV's imaging equipment, a maximum distance constraint, $d_{aw}^{\max}$, is essential.

3.1.2 Antenna Model

Due to UAV moves in 3D space, we adopt the 3D sectorized antenna pattern like [49, 50], which is essential to model the links from air to ground. As shown in Fig. 3.1, θ_i^h ($i \in \{a, b, w\}$) is the half-power beamwidth for the azimuth orientation in the horizontal direction, θ_i^e (resp. θ_i^d) is the half-power beamwidth for the elevation (resp. depression) angles in the ground or air node i. Considering the antenna gain G_i^M within the half-power beamwidth (i.e., main lobe) and gain G_i^S outside the half-power beamwidth (i.e., side lobe). Let $G_i^{\mathbb{A}}$ denote the antenna gain of node i, here

$\mathbb{A} \in \{M, S\}$, the total directivity gain of DM for link $i \to j$ thus determined as $G_{ij} = G_i^{\mathbb{A}} G_j^{\mathbb{A}}$, where $j \in \{b, w\}$ with $i \neq j$. To improve the signal quality at Bob, Alice dynamically adjusts the steering orientation of the antenna array toward Bob, such that she can maximize antenna array gain G_a^M. Thus, the directional antenna gain of Alice→ Bob link is determined as $G_{ab} = G_a^M G_b^{\mathbb{A}}$. Note that in the process of Alice's movement, Willie may be located in the half-power beamwidth direction of the antenna array of Alice→ Bob link, and the antenna array gain of Alice for Willie is the main lobe gain G_a^M, otherwise, the side lobe gain G_a^S. Thus, the antenna gain of Alice→ Willie link is determined as

$$G_{aw} = G_w^{\mathbb{A}} \times \begin{cases} G_a^M, & \varphi_w - \varphi_b \leq \theta_a^d, \\ G_a^S, & otherwise, \end{cases} \tag{3.1}$$

where φ_w (resp. φ_b) is the included angle of Willie (resp. Bob) relative to UAV and Bob (resp. Willie). Considering an actual situation, a uniform planar square array (UPA) is adopted to model the sectorized pattern at node i. As per [50], the directional antenna gain and the associated probability can be approximated as

$$G_i^{\mathbb{A}} = \begin{cases} G_i^M = \mathcal{N}_i, & P_i^M = \frac{\theta_i^h}{2\pi} \times \frac{\theta_i^e}{\pi}, \\ G_i^S = \frac{\sqrt{\mathcal{N}_i} - \frac{\sqrt{3}}{2\pi} \mathcal{N}_i \sin\left(\frac{3\pi}{2\sqrt{\mathcal{N}_i}}\right)}{\sqrt{\mathcal{N}_i} - \frac{\sqrt{3}}{2\pi} \sin\left(\frac{3\pi}{2\sqrt{\mathcal{N}_i}}\right)}, & P_i^S = 1 - \frac{\theta_i^h}{2\pi} \times \frac{\theta_i^e}{\pi}, \end{cases} \tag{3.2}$$

where $\mathcal{N}_i$ denotes the number of antenna elements at the node i, P_i^M and P_i^S denote the associated probability of antenna gain G_i^M and G_i^S, respectively.

3.1.3 Propagation Model

To characterize the A2G wireless channel feature, the channel from UAV to Bob/Willie is modeled as the combination of NLoS and LoS channels. Specifically,

we denote $P_{aj}^{\mathbb{B}}$ ($\mathbb{B} \in \{L, N\}$) as the probability of the channel from the UAV to node j is either LoS or NLoS channel. Following the model presented in [37], we have $P_{ij}^{L} = (1 + \sigma \exp(-f[\theta_j - \sigma]))^{-1}$ and $P_{ij}^{N} \triangleq 1 - P_{ij}^{L}$, where $\theta_j = \frac{180}{\pi} \arcsin(\frac{h_a}{d_{ij}})$ is the degree of the elevation angle for node j relative to UAV, $d_{ij} = \sqrt{(x_i - x_j)^2 + h_a^2}$ is the distance between UAV and node j, σ and f represent the S-curve parameters, dependent on the specific communication environment.

In this work, we account for both large scale fading and small scale fading. Consequently, the channel coefficient of link $i \to j$ is denoted as $H_{ij}^{\mathbb{C},\mathbb{B}} = h_{ij}^{\mathbb{C},\mathbb{B}} \sqrt{L_{ij}^{\mathbb{C},\mathbb{B}}}$, where $h_{ij}^{\mathbb{C},\mathbb{B}}$ and $L_{ij}^{\mathbb{C},\mathbb{B}}$ respectively denote the channel fading coefficient and the path loss coefficient. Here, $\mathbb{C} \in \{o, d\}$ designates the transmission mode of node i, where o denotes the OM transmission mode, while d stands for the MD transmission mode. $L_{ij}^{\mathbb{C},\mathbb{B}}$ is calculated using $L_{ij}^{\mathbb{C},\mathbb{B}} = \beta_{\mathbb{B}}^{\mathbb{C}} d_{ij}^{-\alpha_{\mathbb{B}}^{\mathbb{C}}}$, where $\beta_{\mathbb{B}}^{\mathbb{C}}$ and $\alpha_{\mathbb{B}}^{\mathbb{C}}$ are the constant coefficient and path-loss exponent, respectively. In the following, we introduce $h_{ij}^{\mathbb{C},\mathbb{B}}$ in both the transmission modes.

3.1.3.1 Small scale fading of microwave channel

Considering of the combination of LoS and multipath scatterers of NLoS, the microwave channels are modeled as Rician fading to characterize the propagation effect as [51]. Thus, the fading coefficient $h_{ij}^{o,\mathbb{B}}$ is given by

$$h_{ij}^{o,\mathbb{B}} = \sqrt{\frac{k_{\mathbb{B}}}{k_{\mathbb{B}} + 1}} \hat{h}_{ij} + \sqrt{\frac{1}{k_{\mathbb{B}} + 1}} \tilde{h}_{ij}, \tag{3.3}$$

where $|\hat{h}_{ij}| = 1$ and $\tilde{h}_{ij} \sim \mathcal{CN}(0, 1)$ denote the components of LoS channel and NLoS Rayleigh fading, respectively. $k_{\mathbb{B}}$ denotes the Rician factor which is determined as [51, 52]

$$k_{\mathbb{B}}(\theta_j) = \begin{cases} k_0 \exp\left(\frac{2}{\pi}(\ln k_{\frac{\pi}{2}} - \ln k_0)\theta_j\right), & LoS, \\ 0, & NLoS, \end{cases} \tag{3.4}$$

k_0 and $k_{\frac{\pi}{2}}$ are constant coefficients determined by the specific environment. Thus, the fading coefficient $|h_{ij}^{o,\mathbb{B}}|^2$ follows a non-central chi-squared distribution with two degrees of freedom, and its corresponding CDF is given by as [51, 53]

$$F_{|h_{ij}^{o,\mathbb{B}}|^2}(x) = 1 - Q_1\left(\sqrt{2k_{\mathbb{B}}}, \sqrt{2(k_{\mathbb{B}}+1)x}\right), \tag{3.5}$$

where $Q_1(\cdot,\cdot)$ is the standard Marcum-Q function.

3.1.3.2 Small scale fading of mmWave channel

The mmWave channel is usually characterized by the Nakagami-m fading with shape parameter $S_{\mathbb{B}} \geq 1/2$ as in [50, 54]. Thus, the fading coefficient $|h_{ij}^{d,\mathbb{B}}|^2$ follows a normalized gamma distribution with shape parameter of $S_{\mathbb{B}}$. Suppose $S_{\mathbb{B}}$ is an integer, the CDF of $|h_{ij}^{d,\mathbb{B}}|^2$ is closely approximated as [55, 56]

$$F_{|h_{ij}^{d,\mathbb{B}}|^2}(x) = \sum_{r=0}^{S_{\mathbb{B}}} \binom{S_{\mathbb{B}}}{r} (-1)^r e^{-r\xi_{\mathbb{B}}x}. \tag{3.6}$$

where $\xi_{\mathbb{B}} = S_{\mathbb{B}}(S_{\mathbb{B}}!)^{-1/S_{\mathbb{B}}}$.

3.1.4 Noise Uncertainty Model

In practice, the background noise is uncertain due to its complex composition (including thermal noise, quantization noise, imperfect filters, ambient wireless signals, etc.), dynamic environment, and calibration error. Therefore, it is practical to use noise uncertainty to realize covert communication in mobile communication scenarios. Thus, we adopt a typical bounded noise uncertainty model, where the noise power σ_i^2 of node i lies in a finite range around the nominal noise power $\hat{\sigma}_n^2$. As per [57], the noise power σ_i^2 is modeled by a logarithmic uniform distribution, and its probability

density function (PDF) can be characterized as

$$f_{\sigma_i^2}(x) = \begin{cases} \frac{1}{2\ln(\rho)x}, & \frac{1}{\rho}\hat{\sigma}_n^2 \leq \sigma_i^2 \leq \rho\hat{\sigma}_n^2, \\ 0, & otherwise, \end{cases} \tag{3.7}$$

where ρ ($\rho > 1$) is the parameter that quantifies the level of the uncertainty of the noise.

3.1.5 Metric Definitions

Some basic definitions involved in this work are as follows.

Detection Error Probability (DEP) P_{ew}: Let H_0 (the null hypothesis) and H_1 (the alternative hypothesis) denote that Alice does not transmit and transmits covert information, respectively. Let D_0 and D_1 indicate Willie make a decision to accept H_0 and H_1, respectively. The DEP P_{ew} is defined as the probability that Willie makes a wrong decision on whether or not UAV is transmitting covert messages, which is

$$P_{ew} = P_{FA} + P_{MD}, \tag{3.8}$$

where $P_{FA} = \mathbb{P}(D_1|H_0)$ is the false alarm probability that Willie is in favor of H_1 while H_0 is true, $P_{MD} = \mathbb{P}(D_0|H_1)$ is the missed detection probability that Willie is in favor of H_0 while H_1 is true.

Detection Probability (DP) P_w: The detection probability P_w is defined as the probability that Willie makes the correct decision. This implies that the decision D_0 is made when H_0 occurs and the decision D_1 is made when H_1 occurs, so P_w can be determined as $P_w = \mathbb{P}(D_0|H_0) + \mathbb{P}(D_1|H_1)$.

Outage Probability P_{out}: The outage probability P_{out} is defined as the probability that the channel capacity $C_{ab} = W\log_2(1+\gamma_{ab})$ cannot support a given target rate R_b (i.e., $P_{out} = \mathbb{P}(C_{ab} < R_b) = \mathbb{P}(\gamma_{ab} < \gamma_{th})$), where W is the bandwidth of link

$a \to b$, γ_{ab} is the signal-noise-ratio (SNR), and γ_{th} is the threshold of SNR which can be calculated as $\gamma_{th} = 2^{\frac{R_b}{W}} - 1$.

Effective Covert Rate (ECR) R_{ab}: The effective covert rate R_{ab} is defined as the average *successfully* transmitted amount of information, which can be denoted as $R_{ab} = R_b \times (1 - P_{out})$, where R_b is the target rate and P_{out} is the outage probability.

3.2 Transmission Mode and Detection Strategy

In this section, we first respectively introduce the OM transmission mode and the DM transmission mode, and then present the detection strategy at Willie.

3.2.1 Preliminaries

The results in [58, 59] indicate that a secret key is needed between legitimate terminals to ensure the reliability and covert performance for covert communications. Same as [58], in this work we assume that Alice and Bob share a secret key of sufficient length which is secret from Willie.

3.2.2 OM Transmission Mode

When UAV adopts the OM transmission mode, the signal $y_b(i)$ $(i = 1, 2, \cdots, n)$ received by Bob at i-th channel use is given by

$$y_b^o(i) = \sqrt{P_a} H_{ab}^{o,\mathbb{B}} x_a(i) + n_b(i), \tag{3.9}$$

and the signal $y_w^o(i)$ for i-th channel use at Willie is determined as

$$y_w^o(i) = \sqrt{P_a} H_{aw}^{o,\mathbb{B}} x_a(i) + n_w(i), \tag{3.10}$$

where $x_a(i)$ is the i-th symbol transmitted from Alice, which follows a zero-mean Gaussian distribution, i.e., $\mathbb{E}[|x_a(i)|^2] = 1$. Besides, $n_b(i)$ and $n_w(i)$ are the received noise at Bob and Willie, respectively, and the PDF is given by (3.7).

3.2.3 DM Transmission Mode

When UAV adopts the DM transmission mode, the signal $y_b^d(i)$ received by Bob at the i-th channel use is given by

$$y_b^d(i) = \sqrt{P_a G_{ab}} H_{ab}^{d,\mathbb{B}} x_a(i) + n_b(i), \tag{3.11}$$

and the signal $y_w^d(i)$ received by Willie at i-th channel use is given by

$$y_w^d(i) = \sqrt{P_a G_{aw}} H_{aw}^{d,\mathbb{B}} x_a(i) + n_w(i). \tag{3.12}$$

The transmitted symbol $x_a(i)$ and noise obey the same distribution as the OM transmission mode.

3.2.4 Detection Strategy at Willie

Based on the observations over all time slots, Willie attempts to determine whether Alice conducts transmission or not. According to [23], the optimal decision rule at Willie to minimize the detection error probability is determined as

$$T_w = \frac{1}{n} \sum_{i=1}^{n} |y_w(i)|^2 \underset{D_0}{\overset{D_1}{\gtrless}} \tau, \tag{3.13}$$

where $\sum_{i=1}^{n} |y_w(i)|^2$ is the total power received by Willie in a given block, τ is the decision threshold, and n is the total number of channel uses in a block. According to (3.10), when Alice adopts the OM transmission mode, the received signal $y_w^o(i)$ at

Willie is given by

$$T_w^o = \begin{cases} \sigma_w^2, & H_0, \\ P_a L_{aw}^{o,\mathbb{B}} |h_{aw}^{o,\mathbb{B}}|^2 + \sigma_w^2, & H_1. \end{cases} \tag{3.14}$$

Similarly, according to (3.12), when Alice adopts the DM transmission mode, the received signal $y_w^d(i)$ received at Willie can be expressed as

$$T_w^d = \begin{cases} \sigma_w^2, & H_0, \\ P_a G_{aw} L_{aw}^{d,\mathbb{B}} |h_{aw}^{d,\mathbb{B}}|^2 + \sigma_w^2, & H_1. \end{cases} \tag{3.15}$$

3.3 Covert Performance Analysis under the OM Transmission Mode

In this section, we derive the optimal detection threshold and the corresponding minimum DEP/optimal DP at Willie, as well as the expected minimum DEP from Alice's perspective. Lastly, the ECR under OM transmission mode is investigated.

3.3.1 Detection Performance

To determine the DEP at Willie, we first analyze the false alarm probability and the missed detection probability. Based on (3.13) and (3.14), the false alarm probability P_{FA}^o is given by

$$P_{FA}^o = \mathbb{P}(T_w^o > \tau | H_0) = \mathbb{P}\left(\sigma_w^2 \frac{\chi_{2n}^2}{n} > \tau\right), \tag{3.16}$$

where χ_{2n}^2 denotes a random value that follows chi-squared distribution with $2n$ degrees of freedom. From the strong law of large numbers, we know that $\frac{\chi_{2n}^2}{n}$ converges to 1. Based on Lebesgue's Dominated Convergence Theorem [60], the false alarm

probability P_{FA}^{o} can be derived as

$$P_{FA}^{o}=\mathbb{P}(\sigma_{w}^{2}>\tau)=\begin{cases}1, & \tau<\frac{\hat{\sigma}_{n}^{2}}{\rho},\\ 1-\frac{\ln(\rho\tau)-\ln\hat{\sigma}_{n}^{2}}{2\ln\rho}, & \frac{\hat{\sigma}_{n}^{2}}{\rho}\leq\tau\leq\rho\hat{\sigma}_{n}^{2},\\ 0, & \tau>\rho\hat{\sigma}_{n}^{2}.\end{cases}\tag{3.17}$$

Similarly, the missed detection probability can be derived as

$$\begin{aligned}P_{MD}^{o}&=\mathbb{P}(T_{w}^{o}<\tau|H_{1})=\mathbb{P}(k_{a}^{o}+\sigma_{w}^{2}<\tau)\\&=\begin{cases}1, & \tau>k_{a}^{o}+\rho\hat{\sigma}_{n}^{2},\\ \frac{\ln(\rho(\tau-k_{a}^{o}))-\ln\hat{\sigma}_{n}^{2}}{2\ln\rho}, & k_{a}^{o}+\frac{\hat{\sigma}_{n}^{2}}{\rho}\leq\tau\leq k_{a}^{o}+\rho\hat{\sigma}_{n}^{2},\\ 0, & \tau<k_{a}^{o}+\frac{\hat{\sigma}_{n}^{2}}{\rho},\end{cases}\end{aligned}\tag{3.18}$$

where $k_{a}^{o}=P_{a}L_{aw}^{o,\mathbb{B}}|h_{aw}^{o,\mathbb{B}}|^{2}$. According to (3.17) and (3.18), we can analyze the optimal detection threshold and the minimization DEP for Willie under OM transmission mode as follows.

Lemma 1. *When Alice adopts the OM transmission mode, the optimal threshold τ^{*} for Willie's detector is in the interval*

$$\tau^{*}\in\begin{cases}[\rho\hat{\sigma}_{n}^{2},k_{a}^{o}+\frac{\hat{\sigma}_{n}^{2}}{\rho}], & \rho\hat{\sigma}_{n}^{2}<k_{a}^{o}+\frac{\hat{\sigma}_{n}^{2}}{\rho},\\ k_{a}^{o}+\frac{\hat{\sigma}_{n}^{2}}{\rho}, & \rho\hat{\sigma}_{n}^{2}\geq k_{a}^{o}+\frac{\hat{\sigma}_{n}^{2}}{\rho},\end{cases}\tag{3.19}$$

and the corresponding minimum DEP $P_{ew}^{*,o}$ is given by

$$P_{ew}^{*,o}=\begin{cases}0, & \rho\hat{\sigma}_{n}^{2}<k_{a}^{o}+\frac{\hat{\sigma}_{n}^{2}}{\rho},\\ 1-\frac{\ln(\rho k_{a}^{o}+\hat{\sigma}_{n}^{2})-\ln\hat{\sigma}_{n}^{2}}{2\ln\rho}, & \rho\hat{\sigma}_{n}^{2}\geq k_{a}^{o}+\frac{\hat{\sigma}_{n}^{2}}{\rho},\end{cases}\tag{3.20}$$

where $k_{a}^{o}=P_{a}L_{aw}^{o,\mathbb{B}}|h_{aw}^{o,\mathbb{B}}|^{2}$, ρ and $\hat{\sigma}_{n}^{2}$ are the parameters that quantify the size of the

uncertainty and nominal noise power, respectively, as defined in 3.1.4.

Proof. To find the optimal threshold, we consider the optimization problem $\min_\tau P_{ew}^o = P_{FA}^o + P_{MD}^o$. According to (3.17) and (3.18), the following two cases are considered.

Case I: When $\rho\hat{\sigma}_n^2 < k_a^o + \frac{\hat{\sigma}_n^2}{\rho}$, for any $\tau \in [\rho\hat{\sigma}_n^2, k_a^o + \frac{\hat{\sigma}_n^2}{\rho}]$, we have $P_{ew}^o = P_{FA}^o + P_{MD}^o = 0$.

Case II: When $\rho\hat{\sigma}_n^2 \geq k_a^o + \frac{\hat{\sigma}_n^2}{\rho}$, the DEP $P_{ew}^o = P_{FA}^o + P_{MD}^o$ can be written as

$$P_{ew}^o = \begin{cases} 1, & \tau < \frac{\hat{\sigma}_n^2}{\rho}, & \text{(3.21a)} \\ 1 - \dfrac{\ln(\rho\tau) - \ln\hat{\sigma}_n^2}{2\ln\rho}, & \frac{\sigma_n^2}{\rho} \leq \tau < k_a^o + \frac{\hat{\sigma}_n^2}{\rho}, & \text{(3.21b)} \\ 1 - \dfrac{\ln\tau - \ln(\tau - k_a^o)}{2\ln\rho}, & k_a^o + \frac{\hat{\sigma}_n^2}{\rho} \leq \tau \leq \rho\hat{\sigma}_n^2, & \text{(3.21c)} \\ \dfrac{\ln(\rho(\tau - k_a^o)) - \ln\hat{\sigma}_n^2}{2\ln\rho}, & \rho\hat{\sigma}_n^2 < \tau \leq k_a^o + \rho\hat{\sigma}_n^2, & \text{(3.21d)} \\ 1, & \tau > k_a^o + \rho\hat{\sigma}_n^2\ . & \text{(3.21e)} \end{cases}$$

We can see from (3.21b), when $\frac{\sigma_n^2}{\rho} \leq \tau < k_a^o + \frac{\hat{\sigma}_n^2}{\rho}$, P_{ew}^o is a decreasing function of τ. Thus, when $\tau = k_a^o + \frac{\hat{\sigma}_n^2}{\rho}$, P_{ew}^o gets the minimum value which equals to (3.21c). From (3.21d), when $\rho\hat{\sigma}_n^2 < \tau \leq k_a^o + \rho\hat{\sigma}_n^2$, P_{ew}^o is a increasing function of τ. Thus, when $\tau = \rho\hat{\sigma}_n^2$, P_{ew}^o gets the minimum value which equals to (3.21c). Overall, the DEP gets the minimum value $P_{ew}^{*,o}$ for Willie if and only if $\tau \in [k_a^o + \frac{\hat{\sigma}_n^2}{\rho}, \rho\hat{\sigma}_n^2]$. After deriving the first-order derivative of P_{ew}^o with respect to τ, we have

$$\frac{\partial P_{ew}^o}{\partial \tau} = \frac{k_a^o}{2\tau(\tau - k_a^o)\ln\rho} > 0. \tag{3.22}$$

Obviously, P_{ew}^o is monotonically increasing in the interval. Thus, the optimal decision threshold τ^* for Willie is $\tau^* = k_a^o + \frac{\hat{\sigma}_n^2}{\rho}$ and the corresponding minimum DEP $P_{ew}^{*,o}$ is

$$P_{ew}^{*,o} = 1 - \frac{\ln(\rho k_a^o + \hat{\sigma}_n^2) - \ln\hat{\sigma}_n^2}{2\ln\rho}. \tag{3.23}$$

Based on Case I and Case II, we have (3.19) and (3.20). □

Corollary 1. *When Alice adopts the OM transmission mode, the optimal detection probability $P_w^{*,o}$ at Willie can be given as*

$$P_w^{*,o} = \begin{cases} 1, & \rho\hat{\sigma}_n^2 < k_a^o + \frac{\hat{\sigma}_n^2}{\rho}, \\ \frac{\ln(\rho k_a^o + \hat{\sigma}_n^2) - \ln\hat{\sigma}_n^2}{2\ln\rho}, & \rho\hat{\sigma}_n^2 \geq k_a^o + \frac{\hat{\sigma}_n^2}{\rho}, \end{cases} \tag{3.24}$$

where $k_a^o = P_a L_{aw}^{o,\mathbb{B}} |h_{aw}^{o,\mathbb{B}}|^2$, ρ and $\hat{\sigma}_n^2$ are the parameters that quantify the size of the uncertainty and nominal noise power, respectively, as defined in 3.1.4.

Proof. According to the definitions of DEP and DP, we have

$$\begin{aligned} P_w^o &= \mathbb{P}(D_0|H_0) + \mathbb{P}(D_1|H_1) \\ &= \mathbb{P}(H_0) - \mathbb{P}(D_1|H_0) + \mathbb{P}(H_1) - \mathbb{P}(D_0|H_1) \\ &= 1 - (P_{FA} + P_{MD}). \end{aligned} \tag{3.25}$$

Then, by substituting the minimum detection error probability of (3.20) into (3.25), we can get the optimal detection probability as (3.24). □

Since only the statistical information of channel Alice → Willie is available, we use the expected measure of $P_{ew}^{*,o}$ to evaluate the covertness. From (3.20), we note that $\mathbb{E}[P_{ew}^{*,o}]$ is related to the numerical integration of $|h_{aw}^{o,\mathbb{B}}|^2$. To this end, we first present the following lemma.

Lemma 2. *If $h_{aw}^{o,\mathbb{B}}$ ($\mathbb{B} \in \{L, N\}$) is the channel fading coefficient of the microwave channel, we have*

$$\begin{aligned} \int_0^a x f_{|h_{aw}^{o,\mathbb{B}}|^2}(x)dx = &\frac{\gamma\left(\frac{2}{\nu(\sqrt{2k_{\mathbb{B}}})}, [2a(k_{\mathbb{B}}+1)]^{\frac{\nu(\sqrt{2k_{\mathbb{B}}})}{2}} e^{\mu(\sqrt{2k_{\mathbb{B}}})}\right)}{(k_{\mathbb{B}}+1)\nu(\sqrt{2k_{\mathbb{B}}}) e^{\frac{2\mu(\sqrt{2k_{\mathbb{B}}})}{\nu(\sqrt{2k_{\mathbb{B}}})}}} \\ &- a\exp\left(-[2a(k_{\mathbb{B}}+1)]^{\frac{\nu(\sqrt{2k_{\mathbb{B}}})}{2}} e^{\mu(\sqrt{2k_{\mathbb{B}}})}\right), \end{aligned} \tag{3.26}$$

where $a \geq 0$, $f_{|h_{aw}^{o,\mathbb{B}}|^2}$ *is the PDF of* $|h_{aw}^{o,\mathbb{B}}|^2$, $\gamma(\cdot,\cdot)$ *is the lower incomplete gamma function.* $\mu(x)$ *and* $\nu(x)$ *are the polynomial expressions of* x *as in [61, 62], which are respectively given by*

$$\mu(x) \triangleq \begin{cases} -\ln 2, & x = 0, \\ -3.0888 \times 10^{-10} x^6 + 1.8362 \times 10^{-7} x^5 & \\ -3.7185 \times 10^{-5} x^4 + 3.4103 \times 10^{-3} x^3 & \\ -0.1624 \times x^2 - 1.4318 x + 0.7409, & 10 \leq x \leq 8000, \end{cases} \tag{3.27}$$

and

$$\nu(x) \triangleq \begin{cases} 2, & x = 0, \\ 5.1546 \times 10^{-11} x^6 - 3.1961 \times 10^{-8} x^5 & \\ +6.3859 \times 10^{-6} x^4 - 5.4159 \times 10^{-4} x^3 & \\ +1.9833 \times 10^{-2} x^2 + 0.9044 x + 0.9439, & 10 \leq x \leq 8000. \end{cases} \tag{3.28}$$

Proof. The detailed proof is presented in Appendix A.1. □

Considering the uncertainty of the LoS/NLoS channels, the probability $P_{aw}^{\mathbb{B}}$ should be considered in the calculation of $\mathbb{E}[P_{ew}^{*,o}]$. According to Lemma 2, we can derive $\mathbb{E}[P_{ew}^{*,o}]$ as the following theorem.

Theorem 3.1. *When Alice adopts the OM transmission mode, the expected value* $\mathbb{E}[P_{ew}^{*,o}]$ *from Alice's perspective is given as (3.29)*

$$\mathbb{E}[P_{ew}^{*,o}] = \sum_{\mathbb{B}\in\{L,N\}} P_{aw}^{\mathbb{B}} \left[1-\exp(\Theta_{\mathbb{B}}^{o})\right] \left\{ 1 - \frac{1}{2\ln\rho} \left\{ \ln\left[\rho P_a L_{aw}^{o,\mathbb{B}} \right.\right.\right. \\ \left.\left.\left. \times \left(\frac{\gamma\left(\frac{2}{\nu(\sqrt{2k_{\mathbb{B}}})}, -\Theta_{\mathbb{B}}^{o}\right)}{(k_{\mathbb{B}}+1)\nu(\sqrt{2k_{\mathbb{B}}}) e^{\frac{2\mu(\sqrt{2k_{\mathbb{B}}})}{\nu(\sqrt{2k_{\mathbb{B}}})}}} - \varrho^{o}\exp(\Theta_{\mathbb{B}}^{o}) \right) + \hat{\sigma}_n^2 \right] - \ln\hat{\sigma}_n^2 \right\} \right\}, \tag{3.29}$$

where $\varrho^{o} = \frac{(\rho^2-1)\hat{\sigma}_n^2}{\rho P_a L_{aw}^{o,\mathbb{B}}}$*, and* $\Theta_{\mathbb{B}}^{o}$ *is defined as*

$$\Theta_{\mathbb{B}}^{o} = -e^{\mu(\sqrt{2k_{\mathbb{B}}})} \left(2(k_{\mathbb{B}}+1)\varrho^{o}\right)^{\frac{\nu(\sqrt{2k_{\mathbb{B}}})}{2}}. \tag{3.30}$$

Proof. For convenience, let's write $k_1^{o} = \rho\hat{\sigma}_n^2$ and $k_2^{o} = k_a^{o} + \frac{\hat{\sigma}_n^2}{\rho}$. According to (3.20) in Lemma 1, we have

$$\begin{aligned} \mathbb{E}[P_{ew}^{*,o}] &= \mathbb{E}_{k_1^{o}<k_2^{o}}[P_{ew}^{*,o}]\mathbb{P}(k_1^{o}<k_2^{o}) + \mathbb{E}_{k_1^{o}\geq k_2^{o}}[P_{ew}^{*,o}]\mathbb{P}(k_1^{o}\geq k_2^{o}) \\ &= \mathbb{P}(k_1^{o}\geq k_2^{o}) \left(1 - \frac{\ln(\rho P_a L_{aw}^{o,\mathbb{B}}\mathbb{E}_{k_1^{o}\geq k_2^{o}}\left[|h_{aw}^{o,\mathbb{B}}|^2\right] + \hat{\sigma}_n^2) - \ln\hat{\sigma}_n^2}{2\ln\rho}\right), \end{aligned} \tag{3.31}$$

where $\mathbb{P}(k_1^{o}\geq k_2^{o})$ can be derived as

$$\begin{aligned} \mathbb{P}(k_1^{o}\geq k_2^{o}) &= \mathbb{P}\left(\rho\hat{\sigma}_n^2 \geq P_a L_{aw}^{o,\mathbb{B}}|h_{aw}^{o,\mathbb{B}}|^2 + \frac{\hat{\sigma}_n^2}{\rho}\right) \\ &= 1 - Q_1\left(\sqrt{2k_{\mathbb{B}}}, \sqrt{2(k_{\mathbb{B}}+1)\varrho^{o}}\right). \end{aligned} \tag{3.32}$$

To provide some deep analytical insights on the average value of $P_{ew}^{*,o}$, we adopt a tight exponential-type approximation for the standard Marcum-Q function $Q_1(\cdot,\cdot)$, which is $Q_1(x,y) \approx \exp\left(-e^{\mu(x)}y^{\nu(x)}\right)$ where $\mu(x)$ and $\nu(x)$ are given by (3.27) and (3.28), respectively. The root means square error (RMSE) of approximation is less

than 0.005 (refer to [62] for details). Thus, Eq. (3.32) can be rewritten as

$$\mathbb{P}(k_1^o \geq k_2^o) = 1 - \exp(\Theta_{\mathbb{B}}^o). \tag{3.33}$$

For the expectation term in (3.31), we have

$$\begin{aligned}\mathbb{E}_{k_1^o \geq k_2^o}\left[|h_{aw}^{o,\mathbb{B}}|^2\right] &= \mathbb{E}\left[|h_{aw}^{o,\mathbb{B}}|^2 \middle| |h_{aw}^{o,\mathbb{B}}|^2 \leq \varrho^o\right] \\ &\overset{(a)}{=} \frac{\gamma\left(\frac{2}{\nu(\sqrt{2k_{\mathbb{B}}})}, \Theta_{\mathbb{B}}^o\right)}{(k_{\mathbb{B}}+1)\nu(\sqrt{2k_{\mathbb{B}}})e^{\frac{2\mu(\sqrt{2k_{\mathbb{B}}})}{\nu(\sqrt{2k_{\mathbb{B}}})}}} - \varrho^o \exp(\Theta_{\mathbb{B}}^o),\end{aligned} \tag{3.34}$$

where step (a) is due to Lemma 2. Finally, substituting (3.33) and (3.34) into (3.31), $\mathbb{E}[P_{ew}^{*,o}]$ can be given by (3.29). □

3.3.2 Effective Covert Rate

According to the definition mentioned in Section 3.1.5, the ECR R_{ab}^o can be given as the following theorem.

Theorem 3.2. *When UAV adopts the OM transmission mode in the concerned UAV-enabled communication system, the ECR R_{ab}^o of the system is determined as*

$$R_{ab}^o = \frac{R_b}{\ln \rho}\left[\mathcal{F}_{Ei}^o(\rho) - \mathcal{F}_{Ei}^o\left(\frac{1}{\rho}\right)\right], \tag{3.35}$$

where R_b is the target rate, and function $\mathcal{F}^o(x)$ is defined as

$$\mathcal{F}_{Ei}^o(x) = \sum_{\mathbb{B}\in\{L,N\}} \frac{P_{ab}^{\mathbb{B}}}{\nu(\sqrt{2k_{\mathbb{B}}})} \mathrm{Ei}\left(-e^{\mu(\sqrt{2k_{\mathbb{B}}})}\left(\frac{2(k_{\mathbb{B}}+1)\gamma_{th}\hat{\sigma}_n^2 x}{P_a L_{ab}^{o,\mathbb{B}}}\right)^{\frac{\nu(\sqrt{2k_{\mathbb{B}}})}{2}}\right), \tag{3.36}$$

where $\nu(x)$ is given in (3.28), $\mathrm{Ei}(x)$ *is the exponential integral defined as $\int_{-\infty}^{x} \frac{e^t}{t} dt$,*

$P_{ab}^{\mathbb{B}}$ and γ_{th} are respectively declared in Section 3.1.3 and 3.1.5.

Proof. To derive the ECR, we first need to determine the outage probability P_{out}^{o} at Bob. Considering the uncertainty of the LoS/NLoS channel, the outage probability P_{out}^{o} under the OM transmission mode can be determined by

$$P_{out}^{o} = \sum_{\mathbb{B}\in\{L,N\}} P_{ab}^{\mathbb{B}} \times \mathbb{P}\left(\gamma_{ab}^{o} < \gamma_{th}\right). \tag{3.37}$$

According to (3.9), the SNR at Bob is determined by $\gamma_{ab}^{o} = P_a L_{ab}^{o,\mathbb{B}} |h_{ab}^{o,\mathbb{B}}|^2/\sigma_b^2$. Thus, the outage probability at Bob P_{out}^{o} is given by

$$\begin{aligned}
\mathbb{P}\left(\gamma_{ab}^{o} < \gamma_{th}\right) &= \mathbb{P}\left(|h_{ab}^{o,\mathbb{B}}|^2 < \frac{\sigma_b^2\gamma_{th}}{P_a L_{ab}^{o,\mathbb{B}}}\right) \\
&\overset{(a)}{=} 1 - \int_{\frac{\hat{\sigma}_n^2}{\rho}}^{\rho\hat{\sigma}_n^2} \exp\left(-e^{\mu(\sqrt{2k_{\mathbb{B}}})}\left(\frac{2(k_{\mathbb{B}}+1)\gamma_{th}x}{P_a L_{ab}^{o,\mathbb{B}}}\right)^{\frac{\nu(\sqrt{2k_{\mathbb{B}}})}{2}}\right)\frac{1}{2x\ln\rho}dx \\
&\overset{(b)}{=} 1 - \frac{1}{\nu(\sqrt{2k_{\mathbb{B}}})\ln\rho}\mathrm{Ei}\left(-e^{\mu(\sqrt{2k_{\mathbb{B}}})}\left(\frac{2(k_{\mathbb{B}}+1)\gamma_{th}\rho\hat{\sigma}_n^2}{P_a L_{ab}^{o,\mathbb{B}}}\right)^{\frac{\nu(\sqrt{2k_{\mathbb{B}}})}{2}}\right) \\
&\quad + \frac{1}{\nu(\sqrt{2k_{\mathbb{B}}})\ln\rho}\mathrm{Ei}\left(-e^{\mu(\sqrt{2k_{\mathbb{B}}})}\left(\frac{2(k_{\mathbb{B}}+1)\gamma_{th}\hat{\sigma}_n^2}{P_a L_{ab}^{o,\mathbb{B}}\rho}\right)^{\frac{\nu(\sqrt{2k_{\mathbb{B}}})}{2}}\right)
\end{aligned} \tag{3.38}$$

where step (a) is calculated based on the CDF of $|h_{ab}^{o,\mathbb{B}}|^2$ and the approximation of the standard Marcum-Q function, and step (b) is due to $\int e^{ax^n}x^{-1}dy = \mathrm{Ei}(ax^n)/n$ [63, Eq. (2.325.7)]. Then, substituting (3.38) into (3.37), we can obtain (3.35). □

3.4 Covert Performance Analysis under the DM Transmission Mode

This section explores the minimal DEP/optimal DP under the optimal detection threshold at Willie. Moreover, it examines the anticipated minimal DEP from Alice's viewpoint and subsequently deduces the ECR within the DM transmission mode.

3.4.1 Detection Performance

In instances where Alice refrains from transmitting information, Willie only receives background noise. Consequently, under the DM transmission mode, the false alarm probability P_{FA}^{d} aligns with equation (3.17). When Alice initiates information transmission, an examination of the derivation presented in (3.18) enables us to compute the missed detection probability P_{MD}^{d}, by substituting the parameter k_a^o in (3.18) with $k_a^d = P_a G_{aw} L_{aw}^{d,\mathbb{B}} |h_{aw}^{d,\mathbb{B}}|^2$. Utilizing both P_{FA}^{d} and P_{MD}^{d}, we can further infer the optimal detection threshold and the minimum detection error probability at Willie, as articulated in the subsequent lemma.

Lemma 3. *When Alice adopts the DM transmission mode, the optimal detection threshold τ^* for Willie's detector lies within the interval*

$$\tau^* \in \begin{cases} [\rho\hat{\sigma}_n^2, k_a^d + \frac{\hat{\sigma}_n^2}{\rho}], & \rho\hat{\sigma}_n^2 < k_a^d + \frac{\hat{\sigma}_n^2}{\rho}, \\ k_a^d + \frac{\hat{\sigma}_n^2}{\rho}, & \rho\hat{\sigma}_n^2 \geq k_a^d + \frac{\hat{\sigma}_n^2}{\rho}, \end{cases} \tag{3.39}$$

and the corresponding minimum DEP $P_{ew}^{*,d}$ is given as

$$P_{ew}^{*,d} = \begin{cases} 0, & \rho\hat{\sigma}_n^2 < k_a^d + \frac{\hat{\sigma}_n^2}{\rho}, \\ 1 - \frac{\ln(\rho k_a^d + \hat{\sigma}_n^2) - \ln\hat{\sigma}_n^2}{2\ln\rho}, & \rho\hat{\sigma}_n^2 \geq k_a^d + \frac{\hat{\sigma}_n^2}{\rho}, \end{cases} \tag{3.40}$$

where $k_a^d = P_a G_{aw} L_{aw}^{d,\mathbb{B}} |h_{aw}^{d,\mathbb{B}}|^2$, ρ and $\hat{\sigma}_n^2$ are the parameters that quantify the size of the uncertainty and nominal noise power, respectively, which are defined in Section 3.1.4.

Proof. The proof is similar to Lemma 1, we omit it here. □

Corollary 2. *When Alice adopts the DM transmission mode, the optimal detection*

probability $P_w^{*,d}$ at Willie can be given as

$$P_w^{*,d} = \begin{cases} 1, & \rho\hat{\sigma}_n^2 < k_a^d + \frac{\hat{\sigma}_n^2}{\rho}, \\ \frac{\ln(\rho k_a^d + \hat{\sigma}_n^2) - \ln\hat{\sigma}_n^2}{2\ln\rho}, & \rho\hat{\sigma}_n^2 \geq k_a^d + \frac{\hat{\sigma}_n^2}{\rho}, \end{cases} \tag{3.41}$$

where $k_a^d = P_a G_{aw} L_{aw}^{d,\mathbb{B}} |h_{aw}^{d,\mathbb{B}}|^2$, ρ and $\hat{\sigma}_n^2$ are the parameters that quantify the size of the uncertainty and nominal noise power, respectively, as defined in Section 3.1.4.

Proof. The proof is similar to Corollary 1, we omit it here. □

Similar to Theorem 3.1, Alice and Bob primarily depend on the anticipated measure of $P_{ew}^{;d}$ to assess covert operation within the DM transmission scheme. It should be noted that $\mathbb{E}[P_{ew}^{;d}]$ exhibits a relationship with the numerical integration of $|h_{aw}^{d,\mathbb{B}}|^2$. Therefore, prior to deriving $\mathbb{E}[P_{ew}^{*,d}]$, we initially introduce the following lemma.

Lemma 4. *let $h_{aw}^{d,\mathbb{B}}$ ($\mathbb{B} \in \{L, N\}$) as the channel fading coefficient of the mmWave channel, and $f_{|h_{aw}^{d,\mathbb{B}}|^2}$ as the PDF of $|h_{aw}^{d,\mathbb{B}}|^2$, we have*

$$\int_0^a x f_{|h_{aw}^{d,\mathbb{B}}|^2}(x)dx = \sum_{r=1}^{S_{\mathbb{B}}} \binom{S_{\mathbb{B}}}{r} (-1)^r \left[a e^{-r\xi_{\mathbb{B}} a} - \frac{1 - e^{-r\xi_{\mathbb{B}} a}}{r\xi_{\mathbb{B}}} \right]. \tag{3.42}$$

Proof. The detailed proof is presented in Appendix A.2. □

It is imperative to acknowledge that the uncertainties of both the channel model and the antenna gain should be concurrently contemplated. Consequently, when UAV engages the DM transmission scheme, the expected value of $P_{ew}^{*,d}$ can be expressed as follows.

Theorem 3.3. *When Alice adopts the DM transmission mode, the expected value*

$\mathbb{E}[P_{ew}^{*,d}]$ *from Alice's perspective is given as (3.43)*

$$\begin{aligned}\mathbb{E}[P_{ew}^{*,d}] = &\sum_{\mathbb{A}\in\{M,S\}} P_w^{\mathbb{A}} \sum_{\mathbb{B}\in\{L,N\}} P_{aw}^{\mathbb{B}} \,(1+\Theta_{\mathbb{B}}^d)\Bigg\{1-\frac{1}{2\ln\rho}\Bigg\{\ln\Bigg[\rho P_a G_a^{\mathbb{A}} G_w^{\mathbb{A}} L_{aw}^{d,\mathbb{B}} \\ &\times\left(\varrho^d\Theta_{\mathbb{B}}^d - \sum_{r=1}^{S_{\mathbb{B}}}\binom{S_{\mathbb{B}}}{r}(-1)^r\frac{1-e^{-r\xi_{\mathbb{B}}\varrho^d}}{r\xi_{\mathbb{B}}}\right)+\hat{\sigma}_n^2\Bigg]-\ln\hat{\sigma}_n^2\Bigg\}\Bigg\},\end{aligned} \tag{3.43}$$

where $\varrho^d = \frac{(\rho^2-1)\hat{\sigma}_n^2}{\rho P_a G_a^{\mathbb{A}} G_w^{\mathbb{A}} L_{aw}^{d,\mathbb{B}}}$*, and* $\Theta_{\mathbb{B}}^d$ *is defined as*

$$\Theta_{\mathbb{B}}^d = \sum_{r=1}^{S_{\mathbb{B}}}\binom{S_{\mathbb{B}}}{r}(-1)^r e^{-r\xi_{\mathbb{B}}\varrho^d}. \tag{3.44}$$

Proof. For the sake of clarity, let $k_1^d = \rho\hat{\sigma}_n^2$ and $k_2^d = k_a^d + \frac{\hat{\sigma}_n^2}{\rho}$. According to (3.40) in Lemma 3, we have

$$\begin{aligned}\mathbb{E}[P_{ew}^{*,d}] &= \mathbb{E}_{k_1^d<k_2^d}[P_{ew}^{*,d}]\mathbb{P}(k_1^d<k_2^d) + \mathbb{E}_{k_1^d\geq k_2^d}[P_{ew}^{*,d}]\mathbb{P}(k_1^d\geq k_2^d) \\ &= \mathbb{P}(k_1^d\geq k_2^d)\times\Bigg\{1-\frac{1}{2\ln\rho}\Bigg[-\ln\hat{\sigma}_n^2 \\ &+\ln\left(\rho P_a G_a^{\mathbb{A}} G_w^{\mathbb{A}} L_{aw}^{d,\mathbb{B}}\mathbb{E}_{k_1^d\geq k_2^d}\left[|h_{aw}^{d,\mathbb{B}}|^2\right]+\hat{\sigma}_n^2\right)\Bigg]\Bigg\}.\end{aligned} \tag{3.45}$$

First, we derive the first term on the right-hand side as follows

$$\begin{aligned}\mathbb{P}(k_1^d\geq k_2^d) &= \mathbb{P}\left(\rho\hat{\sigma}_n^2 \geq P_a G_a^{\mathbb{A}} G_w^{\mathbb{A}} L_{aw}^{d,\mathbb{B}}|h_{aw}^{d,\mathbb{B}}|^2+\frac{\hat{\sigma}_n^2}{\rho}\right) \\ &= \mathbb{P}\left(|h_{aw}^{d,\mathbb{B}}|^2\leq\varrho^d\right) = \sum_{r=0}^{S_{\mathbb{B}}}\binom{S_{\mathbb{B}}}{r}(-1)^r e^{-r\xi_{\mathbb{B}}\varrho^d}.\end{aligned} \tag{3.46}$$

For the second term on the right-hand side, we have

$$\begin{aligned}\mathbb{E}_{k_1^d\geq k_2^d}\left[|h_{aw}^{d,\mathbb{B}}|^2\right] &= \mathbb{E}\left[|h_{aw}^{d,\mathbb{B}}|^2\middle||h_{aw}^{d,\mathbb{B}}|^2\leq\varrho^d\right]\ {}^{(a)} \\ &= \sum_{r=1}^{S_{\mathbb{B}}}\binom{S_{\mathbb{B}}}{r}(-1)^r\left[\varrho^d e^{-r\xi_{\mathbb{B}}\varrho^d}-\frac{1-e^{-r\xi_{\mathbb{B}}\varrho^d}}{r\xi_{\mathbb{B}}}\right],\end{aligned} \tag{3.47}$$

where step (a) is due to Lemma 4. Finally, substituting (3.46) and (3.47) into (3.45), we can obtain (3.43) after simplification. □

3.4.2 Effective Covert Rate

Now, we explore another performance metric of the system under the DM transmission mode, i.e., the ECR R_{ab}^{d}, which can be included as the following theorem.

Theorem 3.4. *When UAV adopts the DM transmission mode, the ECR R_{ab}^{d} of the concerned UAV-enabled communication system is given by*

$$R_{ab}^{d} = \frac{R_b}{2\ln\rho} \times \left[\mathcal{F}_{Ei}^{d}\left(\frac{1}{\rho}\right) - \mathcal{F}_{Ei}^{d}(\rho)\right], \tag{3.48}$$

where function $\mathcal{F}^{d}(x)$ is defined as

$$\mathcal{F}_{Ei}^{d}(x) = \sum_{\mathbb{A}\in\{M,S\}} P_b^{\mathbb{A}} \sum_{\mathbb{B}\in\{L,N\}} P_{ab}^{\mathbb{B}} \sum_{r=1}^{S_{\mathbb{B}}} \binom{S_{\mathbb{B}}}{r} (-1)^r \mathrm{Ei}\left(\frac{-r\xi_{\mathbb{B}}\gamma_{th}\hat{\sigma}_n^2 x}{P_a G_a^M G_b^{\mathbb{A}} L_{ab}^{d,\mathbb{B}}}\right). \tag{3.49}$$

where $P_b^{\mathbb{A}}$ and $P_{ab}^{\mathbb{B}}$ are given in Section 3.1.2 Section 3.1.3, respectively.

Proof. To conduct an analysis of the ECR, it is essential to ascertain the outage probability P_{out}^{d} at Bob. Owing to the uncertainties associated with both the LoS/NLoS channel and the antenna gains, P_{out}^{d} under the DM transmission mode can be calculated as

$$P_{out}^{d} = \sum_{\mathbb{A}\in\{M,S\}} P_b^{\mathbb{A}} \times \sum_{\mathbb{B}\in\{L,N\}} P_{ab}^{\mathbb{B}} \times P_{out}^{d}. \tag{3.50}$$

According to (3.11), the SNR at Bob is given as $\gamma_{ab}^{d} = P_a G_{ab} L_{ab}^{d,\mathbb{B}} |h_{ab}^{d,\mathbb{B}}|^2/\sigma_b^2$. Thus, the

outage probability at Bob $P_{out}^{d} = \mathbb{P}\left(\gamma_{ab}^{d} < \gamma_{th}\right)$ can be calculated as

$$\begin{aligned} P_{out}^{d} &= \mathbb{P}\left(P_a G_a^M G_b^{\mathbb{A}} L_{ab}^{d,\mathbb{B}} |h_{ab}^{d,\mathbb{B}}|^2/\sigma_b^2 < \gamma_{th}\right) \\ &= 1 + \sum_{r=1}^{S_{\mathbb{B}}} \binom{S_{\mathbb{B}}}{r} (-1)^r \int_{\frac{\hat{\sigma}_n^2}{\rho}}^{\rho\hat{\sigma}_n^2} \exp\left(\frac{-r\xi_{\mathbb{B}}\gamma_{th}x}{P_a G_a^M G_b^{\mathbb{A}} L_{ab}^{d,\mathbb{B}}}\right) \frac{1}{2x\ln\rho} dx \\ &= 1 + \sum\nolimits_{r=1}^{S_{\mathbb{B}}} \binom{S_{\mathbb{B}}}{r} (-1)^r \frac{1}{2\ln\rho} \mathrm{Ei}\left(\frac{-r\xi_{\mathbb{B}}\gamma_{th}\rho\hat{\sigma}_n^2}{P_a G_a^M G_b^{\mathbb{A}} L_{ab}^{d,\mathbb{B}}}\right) \\ &\quad - \sum\nolimits_{r=1}^{S_{\mathbb{B}}} \binom{S_{\mathbb{B}}}{r} (-1)^r \frac{1}{2\ln\rho} \mathrm{Ei}\left(\frac{-r\xi_{\mathbb{B}}\gamma_{th}\hat{\sigma}_n^2}{P_a G_a^M G_b^{\mathbb{A}} L_{ab}^{d,\mathbb{B}}\rho}\right), \end{aligned} \tag{3.51}$$

Then, substituting (3.51) into (3.50), we can obtain (3.48). □

3.5 Performance Optimization

In this section, we study the ECR maximization under the DEP constraints for both the OM and DM transmission modes.

3.5.1 Maximum ECR Under OM Transmission Mode

From Theorem 3.2, we note that the ECR R_{ab} is related to the transmission power P_a and target rate R_b. A large P_a and R_b result in a small $\mathbb{E}[P_{ew}^{*,\mathbb{C}}]$ and a large P_{out}, respectively. Thus, for a certain position $U(x, y, z)$ during the movement, the UAV intends to find its optimal transmission power P_a and optimal target rate R_b to maximize $R_{ab,U}$ with the covertness constraint. The corresponding optimal problem

under the OM transmission mode can be formulated as the follows

$$\bar{R}_{ab,U}^{*,o} = \max_{P_a, R_b} R_{ab,U}^{o}, \tag{3.52a}$$

$$s.t.\ \mathbb{E}[P_{ew}^{*,o}] \geq 1 - \epsilon, \tag{3.52b}$$

$$0 \leq P_a \leq P_{max}, \tag{3.52c}$$

$$R_b > 0. \tag{3.52d}$$

where $\bar{R}_{ab,U}^{*,o}$ denotes the maximum of $R_{ab,U}^{o}$, ϵ is the covertness constraint. Due to transcendental functions, we hardly cannot obtain the closed-form solutions for the jointly optimal transmission power and target rate. However, we can leverage the power of Lagrange Multipliers to find a numerical solution. By applying the Karush-Kuhn-Tucker (KKT) conditions, the solution for the optimization problem (3.52) can be given as the following theorem.

Theorem 3.5. *For the UAV-enabled communication system, when UAV adopts the OM transmission mode at location U, the maximum effective covert rate can be determined as*

$$\bar{R}_{ab,U}^{*,o} = \frac{R_b^{*,o}}{\ln \rho} \left(\mathcal{F}_{Ei}^{*,o}(\rho) - \mathcal{F}_{Ei}^{*,o}(\frac{1}{\rho}) \right), \tag{3.53}$$

where $\mathcal{F}_{Ei}^{*,o}(x)$ is obtained by substituting $P_a^{*,o}$ and $R_b^{*,o}$ into (3.36), $P_a^{*,o} = min\{P_{max}, \tilde{P}_a^o\}$ denotes the optimal transmission power, $\tilde{P}_a^o$ is the solution of $1 - \epsilon - \mathbb{E}[P_{ew}^{*,o}] = 0$, and $R_b^{*,o}$ indicates the optimal target rate, which is the solution of $\mathcal{F}_{Ei}^{o}(\frac{1}{\rho}) - \mathcal{F}_{Ei}^{o}(\rho) - \mathcal{F}_{e}^{o}(\rho) + \mathcal{F}_{e}^{o}(\frac{1}{\rho}) = 0$ with substituting $P_a^{*,o}$ for P_a, where $\mathcal{F}_{Ei}^{o}(x)$ is given in (3.36), and

$$\mathcal{F}_{e}^{o}(x) = \sum_{\mathbb{B} \in \{L,N\}} P_{ab}^{\mathbb{B}} \frac{2^{R_b - 1} R_b \ln 2}{\gamma_{th}} \exp\left(-e^{\mu(\sqrt{2k_{\mathbb{B}}})} \left(\frac{2(k_{\mathbb{B}} + 1)\gamma_{th}\hat{\sigma}_n^2 x}{P_a L_{ab}^{o,\mathbb{B}}} \right)^{\frac{\nu(\sqrt{2k_{\mathbb{B}}})}{2}} \right). \tag{3.54}$$

Proof. It is observed that due to the highly non-linear terms present in (3.52), obtaining an explicit analytic solution for P_a and R_b is not feasible. In this situation, the KKT conditions are the suitable approach to solve this non-linear optimization problem. The associated Lagrange function corresponding to the constrained optimization problem can be given as

$$\mathcal{L} = -R^o_{ab,U} + \lambda(1 - \epsilon - \mathbb{E}[P^{*,o}_{ew}]) + \mu(-P_a) + \omega(P_a - P_{max}) + \vartheta(-R_b), \tag{3.55}$$

where λ, μ and ω are the Lagrange multipliers. The KKT conditions are determined as

$$\frac{\partial \mathcal{L}}{\partial P_a} = 0, \tag{3.56a}$$
$$\frac{\partial \mathcal{L}}{\partial R_b} = 0, \tag{3.56b}$$
$$g1 = 1 - \epsilon - \mathbb{E}[P^{*,o}_{ew}] \leq 0, \tag{3.56c}$$
$$g2 = P_a - P_{max} \leq 0, \tag{3.56d}$$
$$-P_a \leq 0, \tag{3.56e}$$
$$\lambda(1 - \epsilon - \mathbb{E}[P^{*,o}_{ew}]) = 0, \tag{3.56f}$$
$$\mu(-P_a) = 0, \tag{3.56g}$$
$$\omega(P_a - P_{max}) = 0, \tag{3.56h}$$
$$\vartheta(-R_b) = 0, \tag{3.56i}$$
$$\{\lambda, \mu, \omega, \vartheta\} \geq 0, R_b > 0. \tag{3.56j}$$

To find all the stationary points of P_a that satisfy the conditions, we first calculate the derivative of (3.56a)

$$\frac{\partial \mathcal{L}}{\partial P_a} = \frac{1}{4P_a \ln \rho}\left(2A^o_1 - \lambda\left(\frac{A^o_2 + A^o_3}{A^o_4} + A^o_5\right)\right) - \mu + \omega = 0. \tag{3.57}$$

where

$$A_1^o = \sum_{\mathbb{B}\in\{L,N\}} P_{ab}^{\mathbb{B}} R_b \left(\exp\left(-e^{\mu(\sqrt{2k_{\mathbb{B}}})} \left(\frac{2(k_{\mathbb{B}}+1)\gamma_{th}\hat{\sigma}_n^2\rho}{P_a L_{ab}^{o,\mathbb{B}}} \right)^{\frac{\nu(\sqrt{2k_{\mathbb{B}}})}{2}} \right) - \exp\left(-e^{\mu(\sqrt{2k_{\mathbb{B}}})} \left(\frac{2(k_{\mathbb{B}}+1)\gamma_{th}\hat{\sigma}_n^2}{\rho P_a L_{ab}^{o,\mathbb{B}}} \right)^{\frac{\nu(\sqrt{2k_{\mathbb{B}}})}{2}} \right) \right), \tag{3.58}$$

$$A_2^o = \sum_{\mathbb{B}\in\{L,N\}} P_{aw}^{\mathbb{B}} \left(1 - e^{\Theta_{\mathbb{B}}^o}\right) 2\rho P_a L_{aw}^{o,\mathbb{B}} \left(\nu(\sqrt{2k_{\mathbb{B}}}) \times (-\Theta_{\mathbb{B}}^o)^{\frac{2}{\nu(\sqrt{2k_{\mathbb{B}}})}} - 2e^{-\Theta_{\mathbb{B}}^o} \gamma\left(\frac{2}{\nu(\sqrt{2k_{\mathbb{B}}})}, -\Theta_{\mathbb{B}}^o \right) \right), \tag{3.59}$$

$$A_3^o = \sum_{\mathbb{B}\in\{L,N\}} P_{aw}^{\mathbb{B}} \left(e^{-\Theta_{\mathbb{B}}^o} - 1\right) 2^{\frac{\nu(\sqrt{2k_{\mathbb{B}}})}{2}} \rho P_a L_{aw}^{o,\mathbb{B}} \nu(\sqrt{2k_{\mathbb{B}}})^2 \times e^{\frac{4\mu(\sqrt{2k_{\mathbb{B}}})}{\nu(\sqrt{2k_{\mathbb{B}}})} + \mu(\sqrt{2k_{\mathbb{B}}})} \left(\frac{(k_{\mathbb{B}}+1)(\rho^2-1)\hat{\sigma}_n^2}{\rho P_a L_{aw}^{o,\mathbb{B}}} \right)^{\frac{\nu(\sqrt{2k_{\mathbb{B}}})+2}{2}}, \tag{3.60}$$

$$A_4^o = \sum_{\mathbb{B}\in\{L,N\}} P_{aw}^{\mathbb{B}} \left((k_{\mathbb{B}}+1)\hat{\sigma}_n^2 \nu(\sqrt{2k_{\mathbb{B}}}) e^{\frac{4\mu(\sqrt{2k_{\mathbb{B}}})}{\nu(\sqrt{2k_{\mathbb{B}}})}} \left(e^{-\Theta_{\mathbb{B}}^o} - \rho^2 + 1\right) + 2\rho P_a L_{aw}^{o,\mathbb{B}} e^{-\Theta_{\mathbb{B}}^o} \gamma\left(\frac{2}{\nu(\sqrt{2k_{\mathbb{B}}})}, -\Theta_{\mathbb{B}}^o \right) \right), \tag{3.61}$$

$$A_5^o = \sum_{\mathbb{B}\in\{L,N\}} P_{aw}^{\mathbb{B}} \Theta_{\mathbb{B}}^o \nu(\sqrt{2k_{\mathbb{B}}}) \left(2\ln\rho + \ln\hat{\sigma}_n^2 - \ln\left((1-\rho^2)\hat{\sigma}_n^2 e^{\Theta_{\mathbb{B}}^o} + \frac{2\rho P_a L_{aw}^{o,\mathbb{B}} e^{-\frac{4\mu(\sqrt{2k_{\mathbb{B}}})}{\nu(\sqrt{2k_{\mathbb{B}}})}} \gamma\left(\frac{2}{\nu(\sqrt{2k_{\mathbb{B}}})}, -\Theta_{\mathbb{B}}^o \right)}{(k_{\mathbb{B}}+1)\nu(\sqrt{2k_{\mathbb{B}}})} + \hat{\sigma}_n^2 \right) \right). \tag{3.62}$$

From (3.57), we can see it involves three Lagrange multipliers λ, μ, ω. First of all, $P_a > 0$ is essential to ensure successful transmission between Alice and Bob, which satisfies (3.56e). Then, based on (3.56g), we can conclude that $\mu = 0$. Next, according to (3.56f), (3.56h) and (3.56j), the following four cases are considered respect to λ and ω.

Case I ($\lambda = 0$ and $\omega = 0$): we observe that (3.52) turns into an unconstrained problem, rendering both (3.52b) and (3.52c) ineffective. Consequently, this case im-

plies that $g1 < 0$ and $g2 < 0$. It means the covert constraint ϵ is large enough, even if the transmission power P_{max} were sufficiently large, it could still achieve the covert communication. Using $\tilde{P}_a^o$ denotes the transmission power satisfying $g1 = 0$, thus the optimal transmission power $P_a^{*,o} = min\{P_{max}, \tilde{P}_a^o\}$.

Case II ($\lambda = 0$ and $\omega > 0$): we have $g1 < 0$ and $g2 = 0$. According to (3.56d), we find that $P_a^{*,o} = P_{max}$. Substituting $P_a^{*,o}$ and $\lambda = 0$ into (3.57), and $P_a^{*,o}$ into $g1$, we can obtain $\omega = -\frac{A_1^{*,o}}{2P_a \ln \rho} > 0$, and the relationship of covertness constraint ϵ with respect to $P_a^{*,o}$, which are the applicable ranges of this optimal solution.

Case III ($\lambda > 0$ and $\omega = 0$): we have $g1 = 0$ and $g2 < 0$. According to (3.56c), we can determine the optimal transmission power $P_a^{*,o} = \tilde{P}_a^o$. Similarly, we substitute $P_a^{*,o}$ and $\omega = 0$ into (3.57), and $P_a^{*,o}$ into $g2$, we can obtain the applicable ranges of this case, which are $\lambda = \frac{2A_1^{*,o}A_4^{*,o}}{A_2^{*,o}+A_3^{*,o}+A_4^{*,o}A_5^{*,o}} > 0$, and $P_a^{*,o} < P_{max}$.

Case IV ($\lambda > 0$ and $\omega > 0$): we have $g1 = 0$ and $g2 = 0$. According to (3.56c) and (3.56d), we find that $P_a^{*,o} = \tilde{P}_a^o$ and $P_a^{*,o} = P_{max}$, respectively. Since both equations are the function of $P_a^{*,o}$, leading to a contradictory conclusion, thus ignoring this case.

Overall, by considering these four cases, we can conclude that the optimal transmission power $P_a^{*,o} = min\{P_{max}, \tilde{P}_a^o\}$.

Finally, we calculate the derivative of (3.56b) which respect to R_b, it can be given by

$$\frac{\partial \mathcal{L}}{\partial R_b} = \frac{1}{\ln \rho}\left(\mathcal{F}^o(\frac{1}{\rho}) - \mathcal{F}^o(\rho) - \mathcal{F}_e^o(\rho) + \mathcal{F}_e^o(\frac{1}{\rho})\right) - \vartheta = 0, \tag{3.63}$$

where $\mathcal{F}^o(x)$ is given in (3.36). To ensure a positive rate, it is essential that $R_b > 0$, which implies $\vartheta = 0$. The optimal value of $R_b^{*,o}$ can be obtained by solving (3.63) with $\vartheta = 0$ and $P_a^{*,o}$. □

3.5.2 Maximum ECR Under DM Transmission Mode

Same as Section 3.5.1, we first establish the optimal problem as follow

$$\bar{R}_{ab,U}^{*,d} = \max_{P_a, R_b} R_{ab,U}^{d}, \tag{3.64a}$$

$$s.t.\ \mathbb{E}[P_{ew}^{*,d}] \geq 1 - \epsilon, \tag{3.64b}$$

$$0 \leq P_a \leq P_{max}, \tag{3.64c}$$

$$R_b > 0. \tag{3.64d}$$

Theorem 3.6. *For the considered UAV-enabled communication system, when UAV adopts the DM transmission mode at location U, the maximum effective covert rate can be determined as*

$$\bar{R}_{ab,U}^{*,d} = \frac{R_b^{*,d}}{2\ln\rho} \times \left(\mathcal{F}_{Ei}^{*,d}(\frac{1}{\rho}) - \mathcal{F}_{Ei}^{*,d}(\rho) \right), \tag{3.65}$$

where $\mathcal{F}_{Ei}^{*,d}(x)$ is obtained by substituting $P_a^{*,d}$ and $R_b^{*,d}$ into (3.49), $P_a^{*,d} = min\{P_{max}, \tilde{P}_a^d\}$ denotes the optimal transmission power, $\tilde{P}_a^d$ is the solution of $1 - \epsilon - \mathbb{E}[P_{ew}^{*,d}] = 0$, and $R_b^{*,d}$ indicates the optimal target rate, which is the solution of $\mathcal{F}_{Ei}^{d}(\rho) - \mathcal{F}_{Ei}^{d}(\frac{1}{\rho}) + \mathcal{F}_{e}^{d}(\rho) - \mathcal{F}_{e}^{d}(\frac{1}{\rho}) = 0$ with substituting $P_a^{*,d}$ for P_a, where $\mathcal{F}_{Ei}^{d}(x)$ is given in (3.49), and

$$\mathcal{F}_{e}^{d}(x) = \sum_{\mathbb{A}\in\{M,S\}} P_b^{\mathbb{A}} \sum_{\mathbb{B}\in\{L,N\}} P_{ab}^{\mathbb{B}} \frac{2^{R_b} R_b \ln 2}{\gamma_{th}} \sum_{r=1}^{S_{\mathbb{B}}} \binom{S_{\mathbb{B}}}{r} (-1)^r e^{-\frac{r\gamma_{th}\hat{\sigma}_n^2 \xi_{\mathbb{B}} x}{P_a G_a^M G_b^{\mathbb{A}} L_{ab}^{d,\mathbb{B}}}}. \tag{3.66}$$

Proof. The derivation process follows a similar approach to Theorem 3.5. Therefore, we omit it here. □

3.6 Covert Transmission Protocol

Although mmWave has a larger bandwidth than low-frequency microwave, it also has the disadvantage of faster attenuation. Thus, with the dynamic change of the distance from UAV to Bob and Willie, respectively, the hybrid OM/DM transmission mode of the UAV would be superior to the pure OM or DM transmission mode in terms of covert performance. To confirm our idea, we propose a covert transmission protocol based on hybrid OM/DM transmission mode selection which allows UAV to adaptively switch between the OM and DM transmission modes based on (3.53) and (3.65). Specifically, for a given position U=(x_a, y_a, h_a) of UAV, we first calculate d_{ab} and d_{aw}. Then, we substitute them into (3.53) and (3.65) to obtain the maximum ECR. We select the optimal transmission mode I_{ECR} by comparing $\bar{R}^{*,o}_{ab,U}$ and $\bar{R}^{*,d}_{ab,U}$, where I_{ECR} is the indicator of the optimal selection mode for maximizing the ECR, which are respectively denoted as

$$I_{ECR} = \begin{cases} \text{OM mode}, & \bar{R}^{*,o}_{ab,U} \geq \bar{R}^{*,d}_{ab,U}, \\ \text{DM mode}, & otherwise. \end{cases} \tag{3.67}$$

Overall, the proposed covert transmission protocol based on the OM/DM transmission mode selection can be summarized in Protocol 1.

3.7 Numerical Results

In this section, we provide a wealth of numerical results to compare the performance of OM and DM transmission modes from various perspectives, revealing the respective advantages of these two modes and demonstrating that the hybrid OM/DM transmission mode is superior to the pure OM or DM mode.

To analyze the covert performance, we assume that the UAV possesses location

Protocol 1: Covert Transmission Protocol based on the OM/DM Transmission Mode Selection

Input: UAV's location $U(x_a, y_a, h_a)$, Bob's location $U(x_b, y_b, h_b)$, Willie's location $U(x_w, y_w, h_w)$.

Step 1: Calculate the distances d_{ab} and d_{aw}, respectively;

Step 2: Substitute d_{ab} and d_{aw} into (3.53) to get the theoretical optimal $\bar{R}_{ab}^{*,o}$ under the OM mode;

Step 3: Substitute d_{ab} and d_{aw} into (3.65) to get the theoretical optimal $\bar{R}_{ab}^{*,d}$ under the DM mode;

Step 4: Obtain I_{ECR} by comparing $\bar{R}_{ab}^{*,o}(x_a, y_a, h_a)$ with $\bar{R}_{ab}^{*,d}(x_a, y_a, h_a)$ according to (3.67);

Step 5: The UAV transmit information according to I_{ECR} with the optimal transmit power.

knowledge of not only Bob but also Willie. This assumption is justified by the UAV's ability to employ cameras or radar systems to detect suspicious areas where Willie may be present, as elucidated in [64]. We thus consider Bob is located at $(-500, 0, 0)$, Willie is located at $(1000, 0, 0)$, UAV flies at a fixed altitude of $h_a = 500m$, the minimum and maximum safe distance limit for UAV flight are $d_{aw}^{min} = 300m$ and $d_{aw}^{max} = 1500m$, respectively. The OM transmission mode of Alice transmits at a typical frequency 2.5GHZ with 40MHz bandwidth as [65], and the DM transmission mode transmits at a typical mmWave frequency 73GHz and with 100MHz bandwidth as [66, 67]. We summarize the considered parameters in Table 3.1, unless explicitly mentioned.

3.7.1 Analysis of Expected Minimum DEP

We first explore the impact of parameter ρ which is used to quantify the level of the noise uncertainty on the expected minimum DEP $\mathbb{E}[P_{ew}^*]$ at Willie. As depicted in Fig. 3.2, $\mathbb{E}[P_{ew}^*]$ keeps increasing as ρ increases. This is because the greater level of noise uncertainty, the more conducive to hiding the message transmission of Alice. We also can observe that, for a given position of Alice, i.e., $x_a = 1000m$ and $x_a = 1360m$, the DM transmission mode is superior to the OM transmission mode in terms of

Table 3.1: Network Parameter Settings

Network Parameters	**Values**
UPA antenna elements ($\mathcal{N}_a$, $\mathcal{N}_b$, $\mathcal{N}_w$)	6, 18, 18
S-curve parameters (σ, f) as [37]	4.88, 0.429
OM channel coefficients (α_L^o, α_N^o, β_L^o, β_N^o) as [68, 69]	$1.64, 2.71, 10^{-6}, 10^{-7}$
DM channel coefficients (α_L^d, α_N^d, β_L^d, β_N^d) as [68, 69]	$2, 3, 10^{-6.11}, 10^{-7.18}$
Rician factor (k_0, $k_{\pi/2}$) as [51, 52]	5 dBm, 15 dBm
Nakagami-m fading parameters (S_L, S_N) as [30]	3, 2
Nominal noise power $\hat{\sigma}_n^2$	-80 dBm
Noise uncertainty level ρ	2 dB
Target rate R_b	1 Mbits/s/Hz
Covertness constraint ϵ	0.2

covert performance. Due to the fast fading characteristic of mmWave, the probability of misjudgment under the DM mode is higher than that in the OM mode. From Fig. 3.2, we can further observe that, for the DM transmission mode, $\mathbb{E}[P_{ew}^*]$ of Willie is higher when $x_a = 1000m$ than that one when $x_a = 1360m$, which is opposite of the OM transmission mode. The reason behind the phenomena can be explained that, Alice always steers her main lobe of the antennas to Bob. When $x_a = 1360m$, Willie is also located in the boresight direction of the main lobe, such that he can obtain more power from Alice, thereby reducing $\mathbb{E}[P_{ew}^*]$.

We then investigate the impact of the transmission power of Alice P_a on the expected minimum DEP $\mathbb{E}[P_{ew}^*]$ with $\rho = 2$dB and $x_a = \{1000m, 1360m\}$. As shown in Fig. 3.3, it can be observed that $\mathbb{E}[P_{ew}^*]$ is monotonically decreasing with respect to P_a. That is because as the transmission power increases, it is not conducive to hiding the information in the background noise. Also, as P_a increases, the expected minimum DEP performance in OM transmission mode degrades faster than in DM transmission mode. Because the mmWave attenuates faster than the microwave, and

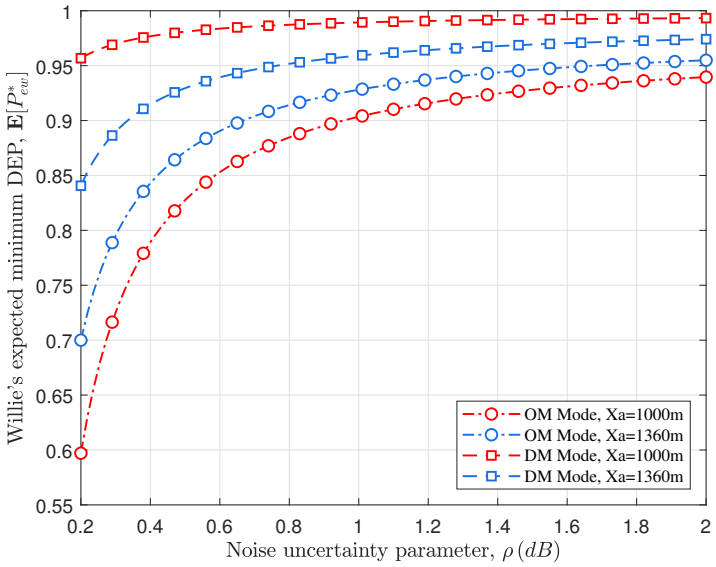

Figure 3.2: The expected minimum DEP $\mathbb{E}[P^*_{ew}]$ vs. noise uncertainty ρ.

the received power at Willie remains lower under the same transmission power.

To explore the impact of the position of Alice x_a on the expected minimum DEP $\mathbb{E}[P^*_{ew}]$, we summarize in Fig. 3.4 to show how $\mathbb{E}[P^*_{ew}]$ varies with x_a for the setting of $P_a = \{15\text{dBm}, 20\text{dBm}\}$. From Fig. 3.4, we can see that $\mathbb{E}[P^*_{ew}]$ first decreases as x_a increases from $-200m$ to $1000m$, and then increases after $1000m$ under the OM transmission mode. It is due to the fact that Alice just moves right above Willie, the distance between them is the closest, and Willie can detect the transmission behavior of Alice more accurately. For the DM transmission mode, we can see that when $x_a = 1360m$, $\mathbb{E}[P^*_{ew}]$ decreases sharply to the minimal value and then gradually increases as x_a increases. This interesting phenomenon can be explained as when $x_a = 1360m$, Willie is just in the half-power beam width direction of the antenna array of link Alice $\rightarrow$ Bob and he can obtain more power benefiting from the main lobe antenna gain of Alice. But as x_a increases, the distance between Willie and Alice will increase and the received power at Willie will decrease causing an increasing $\mathbb{E}[P^*_{ew}]$.

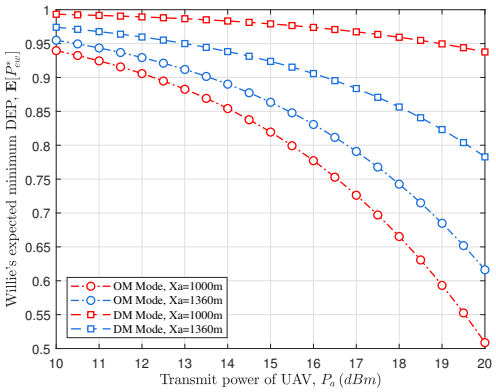

Figure 3.3: The expected minimum DEP $\mathbb{E}[P^*_{ew}]$ vs. transmission power P_a.

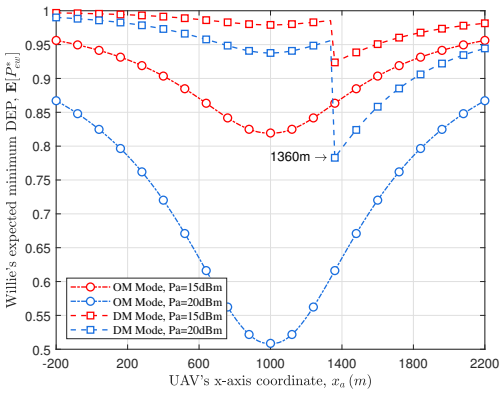

Figure 3.4: The expected minimum DEP $\mathbb{E}[P^*_{ew}]$ vs. horizontal position x_a.

3.7.2 Analysis of Outage Probability

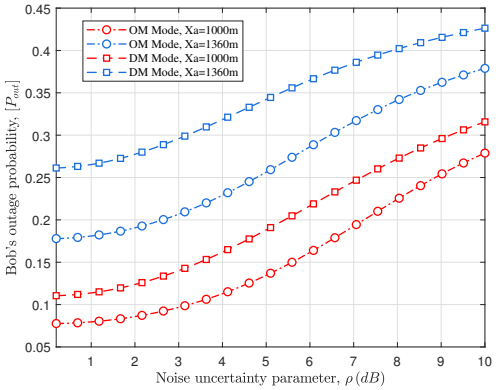

Figure 3.5: Outage probability P_{out} vs. noise uncertainty parameter ρ.

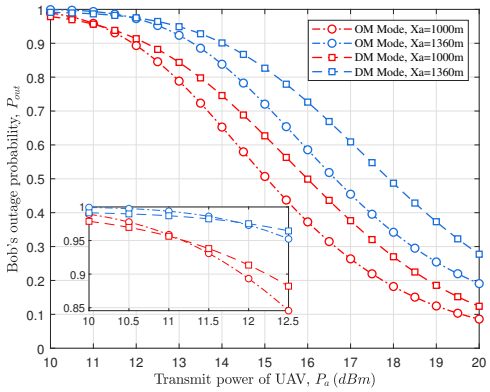

Figure 3.6: Outage probability P_{out} vs. transmission power P_a.

We plot Fig. 3.5 to explore the impact of noise uncertainty parameter ρ on the outage probability P_{out} under both OM and DM transmission modes. From Fig. 3.5, we can see that as ρ increases, P_{out} gradually increases. A larger ρ leads to a lower SNR at Bob such that the outage probability is higher. Note that we also can find that under a given x_a and ρ, the OM transmission mode outperforms the DM transmission

mode in terms of the outage probability performance. This phenomenon can be attributed to the fast fading of mmWave resulting in a small SNR at Bob.

Fig. 3.6 is used to study the impact of transmission power P_a on the outage probability P_{out}. We can see from Fig. 3.6 that the outage probability P_{out} monotonically decreases with respect to P_a. Obviously, a larger P_a will lead to a higher SNR resulting in a lower outage probability. A further careful observation of Fig. 3.6 indicates that when Alice transmits with a small P_a, P_{out} under the OM transmission mode is higher than the one under the DM transmission mode, but once P_a exceeds a certain value, P_{out} under the OM transmission mode is lower than the one under the DM transmission mode. Note that when Alice transmits with a lower power, mmWave directional antenna can offset a tiny part of channel fading. Thus, the outage probability under the DM transmission mode is lower than that one under the OM transmission mode. But, the channel fading of mmWave is much faster than the microwave, such that when Alice transmits with a big power, the received power of Bob under the DM transmission mode is less than the one under the OM transmission mode, resulting in a higher outage probability.

To further study the changing trend of the outage probability P_{out} varying with the target rate R_b under both transmission modes, we draw Fig. 3.7. We can observe that as the target rate R_b increases, the outage probability P_{out} also increases. It can be easily explained based on the definition of the outage probability. Besides, it also implies that there is a trade-off relationship between P_{out} and R_b which validates the rationality of optimizing R_b in this work.

3.7.3 Analysis of Maximum ECR

To explore the impact of the maximum power constraint P_{max} on the maximum ECR $\bar{R}_{ab}^{*}$ under both two modes, we summarize in Fig. 3.8 how it varies with P_{max} for the setting of $x_a \in \{1000m, 1360m\}$. From Fig. 3.8, we can see that as P_{max} increases,

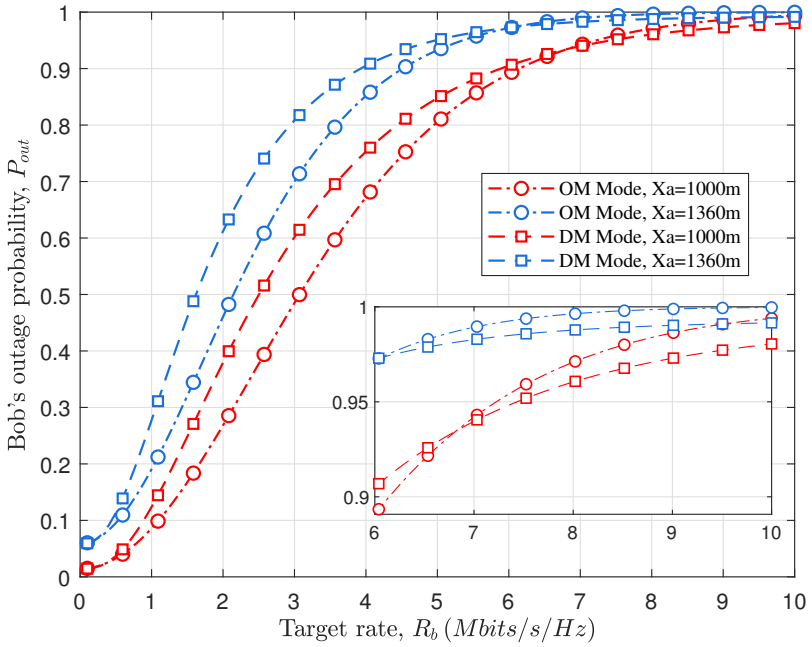

Figure 3.7: Outage probability P_{out} vs. target rate R_b with $P_a = 20$dBm.

$\bar{R}^*_{ab}$ gradually increases and then tends to a constant under the OM transmission mode. It can be explained as that a larger P_{max} can allow Alice uses more power to transmit information resulting in a smaller P_{out}. But the covert performance constraint limits that P_a cannot increase all the time. Thus, when P_{max} is enough large, $\bar{R}^*_{ab}$ reaches its maximum value and keeps constant. For the DM transmission mode, due to the fast fading of mmWave, even given a large P_{max}, the received power at Willie is still tiny, causing a high DEP. Thus, Alice can improve the ECR by increasing P_a.

We then investigate the impact of the covertness constraint ϵ on the maximum ECR $\bar{R}^*_{ab}$. The results are summarized in Fig. 3.9. We can observe from Fig. 3.9 that as ϵ increases, $\bar{R}^*_{ab}$ first increases and then tends to remain unchanged. This can be explained as follows. As the covertness constraint is gradually relaxed, Alice can adopt a large P_a to transmit the covert information and thus $\bar{R}^*_{ab}$ increases. But when P_a is large enough, the transmission power remains unchanged due to the maximum

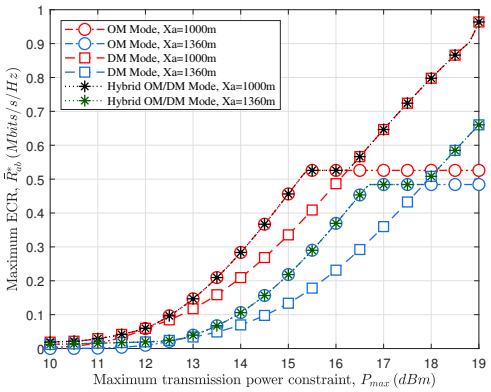

Figure 3.8: Maximum ECR $\bar{R}^*_{ab}$ vs. P_{max} with $x_a \in \{1000m, 1360m\}$.

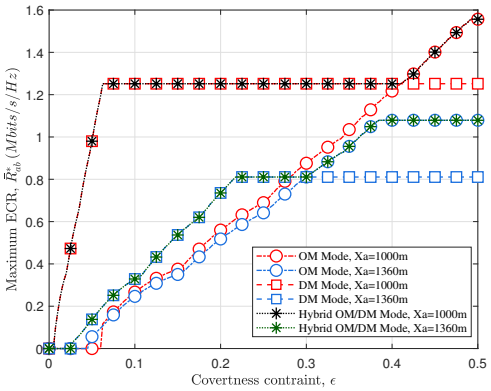

Figure 3.9: Maximum ECR $\bar{R}^*_{ab}$ vs. ϵ with $x_a \in \{1000m, 1360m\}$.

power constraint P_{max}. We further observe from Fig. 3.9 that under the hybrid mode, adopting the OM transmission mode can achieve better performance when the covertness constraint is relaxed enough. While adopting the DM transmission mode is better when the covertness constraint is strict.

Finally, we investigate the performance of different x_a during the movement of Alice. We summarize in Fig. 3.10 how the covert performance varies with x_a for a setting of $\rho = 2$dB and $P_{max} = 20$dBm. We can see from Fig. 3.10 that during Alice's movement from $(-200, 0, 500)$ to $(2200, 0, 500)$, the covert performance first decreases and then increases and finally decreases under both transmission modes. The interesting behavior can be explained as follows. When Alice moves away from Bob and closes to Willie, due to the negative effects brought by the path attenuation and covertness constraint, R^*_{ab} will decrease quickly. When Alice moves away from Willie, the power received by Willie decreases, and it can increase P_a appropriately to improve the transmission efficiency. When Alice moves far away from Willie and Bob enough, Alice can adopt a larger transmission power satisfying the covertness constraint, however, it cannot offset the negative impact of large-scale attenuation on transmission performance. Thus, $\bar{R}^*_{ab}$ will decrease. Moreover, from Fig 3.10, we can

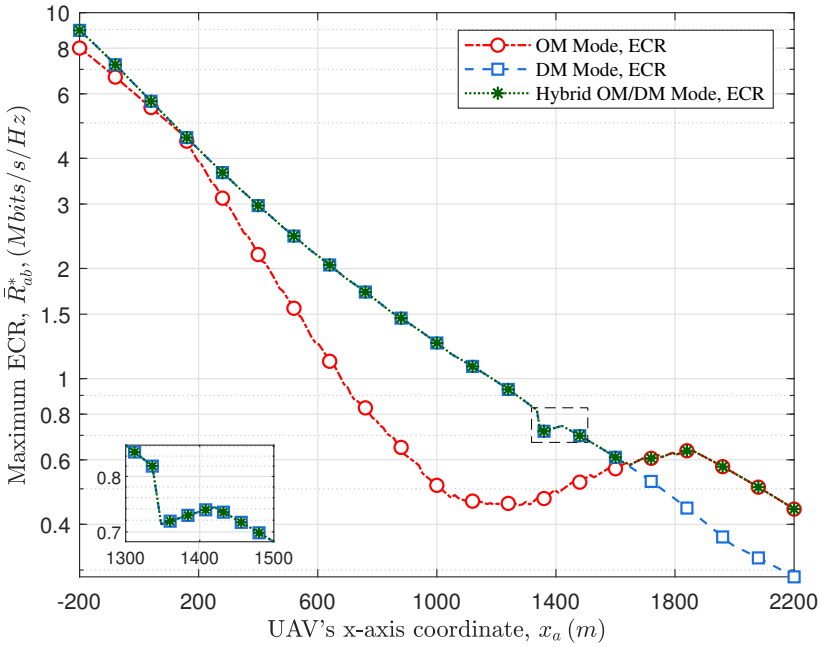

Figure 3.10: Covert performance $\bar{R}^*_{ab}$ vs. horizontal position of UAV x_a.

see that when Alice is far away from Willie, the DM transmission mode outperforms the OM transmission mode in terms of $\bar{R}^*_{ab}$, but when Alice moves a certain distance away from Willie, the OM transmission mode is better. On the one hand, the power received by Bob is smaller due to the rapid attenuation of mmWave; on the other hand, Willie is in the main lobe radiation range such that Willie has good detection performance. By comparing the two modes, we can derive the optimal transmission mode as Fig. 3.10 in the hybrid microwave/mmWave UAV-enabled communication system.

3.8 Summary

This chapter investigated covert communication in a hybrid microwave or mmWave UAV-enabled wireless communication system. Based on our theoretical performance analysis and covert performance optimization under both OM and DM transmission modes, we proposed a new covert transmission protocol based on the OM/DM

transmission mode selection for covert performance enhancement. The results in this chapter revealed that the hybrid transmission mode could lead to a significant improvement in covert performance compared to the pure OM or DM mode in the concerned UAV-enabled communication system. It is expected that this work can provide meaningful insights into the covert transmission protocol design in more general and more complicated UAV networks, e.g., UAVs with multiple band antennas, UAV swarms, etc.

CHAPTER IV

Transmission Protocol Design for Simple Multi-Receiver Scenario

This chapter considers a simple multi-receiver scenario, in which a UAV would like to disseminate common covert information (CI) to multiple ground users (GUs) within its coverage area while simultaneously evading the detection by a ground warden Willie outside the covered area. We design two covert multicast transmission protocols for the concerned system based on one-hop transmission and two-hop transmission. In the one-hop multicast protocol, according to link conditions from the UAV to all GUs, the UAV determines an optimal transmit power and optimal hover location to directly multicast the CI to all GUs with the minimum transmission time. In the two-hop multicast protocol, the UAV first selects an optimal transmit power and an optimal relay from GUs according to the link conditions among GUs, UAV and Willie, and then the UAV unicasts the CI to the relay, which further multicasts the CI to all other GUs. Related theoretical models are also developed to depict the system performance in terms of detection error probability (DEP) and overall transmission time. Finally, extensive numerical results are provided to illustrate the efficiency of the new transmission protocol under the simple multi-receiver scenario.

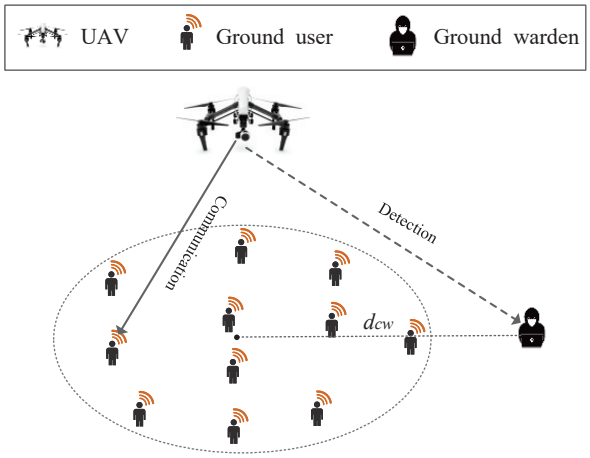

Figure 4.1: Illustration of the system model.

4.1 Preliminaries

4.1.1 System Model

As shown in Fig. 5.1, the UAV (Alice, a) acts as a flying base station in a three-dimensional area with the altitude h. It disseminates a common CI of M bits to G GUs, denoted by the set $\mathbb{G} = \{1, 2, \cdots, G\}$. Meanwhile, a ground warden (Willie, w) wants to detect the transmission. In this system, GUs are randomly distributed following the Poisson point process with a density of λ within a circular area of radius r covered by the UAV. At the same time, Willie is situated outside of this circular area, at a distance of d_{cw} from the center of this circular area. Let $\mathbf{q}_a = [x_a, y_a]$ denotes the horizontal coordinate of the UAV, and the horizontal coordinates of the g-th GU and Willie are denoted as $\mathbf{q}_g = [x_g, y_g]$ and $\mathbf{q}_w = [x_w, y_w]$, respectively. Thus, the horizontal distance from the UAV to the g-th GU and the distance from the UAV to Willie are given by $l_{ag} = \|\mathbf{q}_a - \mathbf{q}_g\|$ and $l_{aw} = \|\mathbf{q}_a - \mathbf{q}_w\|$, respectively. The distance from the UAV to the g-th GU and the distance from the UAV to Willie are given by $d_{ag} = \sqrt{l_{ag}^2 + h^2}$ and $d_{aw} = \sqrt{l_{aw}^2 + h^2}$, respectively.

4.1.2 Channel Model

4.1.2.1 Air to Ground Channel Model

The air-to-ground (A2G) channels from the UAV to ground nodes (i.e., GUs and Willie) are modeled as a combination of non-line-of-sight (NLoS) and probabilistic line-of-sight (LoS) channels. Following the model presented in [37], the probability of the LoS channel from the UAV to the g-th GU and Willie can be respectively given by

$$P_{LoS}(\theta_g) = \frac{1}{1 + \sigma \exp\left(-f[\theta_g - \sigma]\right)}, \tag{4.1}$$

and

$$P_{LoS}(\theta_w) = \frac{1}{1 + \sigma \exp\left(-f[\theta_w - \sigma]\right)}, \tag{4.2}$$

where σ and f represent the S-curve parameters related the specific communication environment; $\theta_g = \frac{180^\circ}{\pi} \arctan(\frac{h}{l_{ag}})$ and $\theta_w = \frac{180^\circ}{\pi} \arctan(\frac{h}{l_{aw}})$ are the degree of the elevation angles for the g-th GU relative to the UAV and Willie relative to the UAV, respectively.

In most UAV application scenarios, the LoS component dominates the NLoS component. Similar to [37, 47, 70], we consider the NLoS component to be negligible. Under this assumption, the channel gain H_{ag} from the UAV to the g-th GU can be given by

$$H_{ag} = P_{LoS}(\theta_g) d_{ag}^{\alpha_L}, \tag{4.3}$$

where $\alpha_L < 0$ is the A2G LoS channel fading loss exponent. The channel gain H_{aw} from the UAV to Willie can be given by

$$H_{aw} = P_{LoS}(\theta_w) d_{aw}^{\alpha_L}. \tag{4.4}$$

4.1.2.2 Ground to Ground Channel Model

The ground-to-ground (G2G) channels among GUs and Willie are assumed to follow the quasi-static Rayleigh fading channel model, where each channel remains constant in one slot while changing independently and randomly from one slot to another. Suppose that a GU is acting as a relay (r), the channel from the relay to the g-th GU is denoted by h_{rg} ($r, g \in \mathbb{G}, r \neq g$), the associated channel gain H_{rg} can be given by

$$H_{rg} = |h_{rg}|^2 l_{rg}^{\alpha_N}, \tag{4.5}$$

where l_{rg} is the distance from the relay to the g-th GU and $\alpha_N < 0$ is the G2G channel fading loss exponent. The channel from the relay to Willie is denoted by h_{rw}, the associated channel gain H_{rw} can be given by

$$H_{rw} = |h_{rw}|^2 l_{rw}^{\alpha_N}, \tag{4.6}$$

where l_{rw} is the distance from the relay to Willie.

Besides, we assume the UAV, GUs and Willie only have the knowledge of the statistical characterizations of the channel state information.

4.2 Transmission Protocols

In this work, we design two covert multicast transmission protocols for the concerned system, which are based on one-hop (OH) transmission and two-hop (TH) transmission, respectively.

4.2.1 OH Transmission Protocol

Under the OH transmission protocol, given the hover location of the UAV, the UAV directly multicasts CI to the GUs. Specifically, the UAV first flies to the target

optimal hover location and divides the CI into m blocks. To confuse Willie, the UAV selects each time slot with probability π_1 (i.e., does not select this time slot with probability $\pi_0 = 1 - \pi_1$) to transmit a block. If the UAV decides to transmit one block in a time slot, it encodes this block with a secret Gaussian codebook pre-shared among the UAV and GUs to ensure reliable transmission. This block is thus encoded into n real value symbols $\mathbf{x} = (\mathbf{x}[1], \cdots, \mathbf{x}[i])$, where each symbol satisfies $\mathbf{x}[i] \sim \mathcal{N}(0, 1)$ and $i = 1, 2, \cdots, n$. Finally, she multicasts each symbol $\mathbf{x}[i]$ to the GUs with the optimal transmit power. The overall OH transmission protocol can be summarized as Protocol 2.

Protocol 2: OH Transmission Protocol

Input: UAV's location $U(x_a, y_a, h_a)$, Bob's location $U(x_b, y_b, h_b)$, Willie's location $U(x_w, y_w, h_w)$.
Step 1: Calculate optimal transmit power with a given hover location;
Step 2: Search the joint solution of the optimal transmit power and hover location;
Step 3: Calculate the target blocks size m;
Step 4: Fly to the target optimal hover location;
Step 5: Divide information into m blocks;
Step 6: Encode one block into target n symbols;
Step 7: Select each time slot to transmit one block with a probability of π_1;
Step 8: Multicast these n symbols of one block to the GUs within one time slot;
Step 9: Repeat Step 6-8 until all blocks are multicast to the GUs.

4.2.2 TH Transmission Protocol

Under the TH transmission protocol, we first select a GU to act as the relay (r), then the UAV transmits CI to this relay, and finally the relay multicasts CI to the remaining GUs. Particularly, the UAV flies to the location just above the relay, then similar to OH transmission protocol, she divides the CI into blocks, selects a time slot with probability π_1, and encodes each block into n real value symbols. Instead of multicasting CI to the GUs of the OH transmission scheme, the UAV transmits

symbols of each block to the relay in a selected time slot. The relay is assumed to equipped with two independent antennas for reception and transmission, enabling it to operate in half-duplex (HD) transmission mode. Additionally, the relay is assumed to adopt the decode-and-forward (DF) mode with no processing delay [71]. Therefore the relay then decodes the signals and re-encodes them into symbols using the same codebook and approach as the UAV. After that, the relay forwards these symbols of one block to the remaining GUs in a multicast manner during the following time slot when the UAV does not transmit information. The overall OH transmission protocol can be summarized as Protocol 3.

Protocol 3: TH Transmission Protocol

Input: UAV's location $U(x_a, y_a, h_a)$, Bob's location $U(x_b, y_b, h_b)$, Willie's location $U(x_w, y_w, h_w)$.
Step 1: Calculate optimal transmit power for the UAV with a selected relay;
Step 2: Search the joint solution of the optimal transmit power and relay;
Step 3: Calculate the target blocks size m;
Step 4: Fly to the location above the relay;
Step 5: Divide information into m blocks;
Step 6: Encode one block into target n symbols;
Step 7: Select each time slot to transmit one block with a probability of π_1;
Step 8: Transmit these n symbols of one block to the relay within one time slot;
Step 9: The relay decodes the received signals into blocks;
Step 10: The relay re-encodes the blocks into n symbols;
Step 11: The relay transmit one block when the UAV does not transmit information (i.e., with a probability of $\pi_0 = 1 - \pi_1$);
Step 12: The UAV repeat Step 6-8 until all blocks are transmit to the relay;
Step 13: The relay repeat Step 9-11 until all blocks are multicast to the remaining GUs.

4.3 Covert Transmission Time Minimization Under the OH Transmission Protocol

As the UAV adopts the OH transmission protocol, the performance of covert multicast transmission depends on the GU with the worst channel condition and the

detection performance of Willie, which are both highly influenced by the hovering location $\mathbf{U}(\mathbf{q}_a, h)$ (i.e., horizontal location $\mathbf{q}_a$ and altitude h) and the transmit power of the UAV. According to Protocol 2, in this section, given the altitude h of the UAV, we jointly design the UAV's horizontal location $\mathbf{q}_a$ and the transmit power P_a to minimize the completion transmission time subject to the covertness constraint. Specifically, we first present the optimal DEP at Willie. Based on the optimal DEP, we formulate the minimal covert transmission time as an optimization problem and give the mathematical results. The optimization location is non-convex and challenging to solve directly. We thus propose a PSO-based optimization algorithm to solve it.

4.3.1 Detection Error Probability at Willie

Based on the observations over all time slots, Willie attempts to determine whether the transmission happened or not among the UAV and GUs. To achieve this, Willie adopts the hypothesis test to distinguish between the null hypothesis $\mathcal{H}_0$, which infers that the UAV or the relay did not conduct transmission, and the alternative hypothesis $\mathcal{H}_1$, which suggests that either the UAV or the relay did transmit. The received two types of signals can be given by

$$\begin{cases} H_0: & \mathbf{y}_w[i] = \mathbf{n}_w[i], \\ H_1: & \mathbf{y}_w[i] = \sqrt{P_a H_{aw}}\mathbf{x}[i] + \mathbf{n}_w[i], \end{cases} \tag{4.7}$$

where $\mathbf{n}_w[i]$ is the AWGN with mean zero and variance σ_w^2 at Willie. Assume that Willie adopts the optimal statistical hypothesis test that minimizes ξ, with the UAV transmission probability of π_1, as per [16], the optimal DEP ξ^* at Willie can be determined as

$$\xi^* \geq \min(\pi_0, \pi_1) - \max(\pi_0, \pi_1)\mathcal{V}_T(\mathbb{P}_1^n, \mathbb{P}_0^n), \tag{4.8}$$

where $\mathcal{V}_T(\mathbb{P}_1^n, \mathbb{P}_0^n)$ is the total variation between $\mathbb{P}_1^n$ and $\mathbb{P}_0^n$. $\mathbb{P}_0^n$ (resp. $\mathbb{P}_1^n$) is the distribution of the sequence $\mathbf{y}_w = \{\mathbf{y}_w[i]\}_{i=1}^n$ received in n channel use when $\mathcal{H}_0$ (resp. $\mathcal{H}_1$) is true.

Due to the intractability of the expression $\mathcal{V}_T(\mathbb{P}_1^n, \mathbb{P}_0^n)$, similar to [16], we can obtain an upper bound of it according to Pinsker's inequality, which is determined as

$$\mathcal{V}_T(\mathbb{P}_1^n, \mathbb{P}_0^n) \leq \sqrt{\frac{1}{2}\mathcal{D}(\mathbb{P}_1^n, \mathbb{P}_0^n)}, \tag{4.9}$$

where $\mathcal{D}(\mathbb{P}_1^n, \mathbb{P}_0^n)$ denotes the relative entropy (also known as Kullback-Leibler (KL) divergence) between $\mathbb{P}_1^n$ and $\mathbb{P}_0^n$. From the chain rule for relative entropy, we have

$$\mathcal{D}(\mathbb{P}_1^n, \mathbb{P}_0^n) = n\mathcal{D}(\mathbb{P}_1,\mathbb{P}_0). \tag{4.10}$$

According to (4.7), and based on the derivations in Appendix. B.1, the KL divergence $\mathcal{D}(\mathbb{P}_1, \mathbb{P}_0)$ from $\mathbb{P}_1$ to $\mathbb{P}_0$ can be calculated as

$$\mathcal{D}(\mathbb{P}_1, \mathbb{P}_0) = \frac{1}{2}\left[\gamma_{aw} - \ln\left(1 + \gamma_{aw}\right)\right], \tag{4.11}$$

where $\gamma_{aw} = \frac{P_a H_{aw}}{\sigma_w^2}$ denotes the received signal-noise ratio (SNR), P_a is the transmit power of UAV.

Overall, the lower bound of the optimal DEP ξ^* at Willie can be expressed as

$$\xi^* \geq \min(\pi_0, \pi_1) - \max(\pi_0, \pi_1)\sqrt{\frac{n}{4}\left(\gamma_{aw} - \ln\left(1 + \gamma_{aw}\right)\right)}. \tag{4.12}$$

4.3.2 Transmission Time Formulation

For the g-th GU, let T_g denote the transmission time for the UAV to disseminate CI to this GUs and let X_g represent the corresponding total time slots required to

complete the CI dissemination. Then we have

$$T_g = X_g \Delta t. \tag{4.13}$$

Since UAV selects each time slot with probability π_1 to transmit a block, X_g can be formulated as the negative binomial distribution [72]. Thus, the expected value $\mathbb{E}[X_g]$ of X_g can be given as $\mathbb{E}[X_g] = \frac{m_g}{\pi_1}$, here m_g is the number of blocks. Therefore, (4.13) can be rewritten as

$$T_g = \frac{m_g \Delta t}{\pi_1}. \tag{4.14}$$

The number of blocks m_g that the UAV needs to transmit CI to the g-th GU can be determined as

$$m_g = \frac{M}{C_g \Delta t}. \tag{4.15}$$

By substituting (4.15) into (4.14), T_g can be further given by

$$T_g = \frac{M}{\pi_1 C_g}. \tag{4.16}$$

To achieve the minimum covert transmission time, we need calculate the effective multicast throughput C_g of the UAV to the g-th GU. According to Protocol 2, the received signal at the g-th GU for the i-th symbol under the OH transmission scheme can be given by

$$\mathbf{y}_g[i] = \sqrt{P_a H_{ag}}\mathbf{x}[i] + \mathbf{n}_g[i], \tag{4.17}$$

where P_a is the transmit power of the UAV; $\mathbf{n}_g[i] \sim \mathcal{N}(0, \sigma_g^2)$ is the AWGN with mean zero and variance σ_g^2 at the g-th GU.

Based on the received signals, according to [73], the effective throughput C_g can be given as

$$C_g = \pi_1 n R(1 - \eta_g), \tag{4.18}$$

where R is the target rate and η_g is decoding error probability at g-th GU. As per [73], η_g can be determined as

$$\eta_g = Q\left(\frac{\sqrt{n}(1+\gamma_{ag})(\ln(1+\gamma_{ag}) + \frac{1}{2}\ln n - R\ln 2)}{\sqrt{\gamma_{ag}(\gamma_{ag}+2)}}\right), \tag{4.19}$$

where $Q(\cdot)$ is the Q-function; $\gamma_{ag} = \frac{P_a H_{ag}}{\sigma_g^2}$ denotes the received SNR and σ_g^2 is the power of AWGN at g-th GU, respectively. To make (4.19) mathematically tractable for the minimization of transmission time, we employ a linear approximation function for the Q-function as detailed in [74]. Thus, the decoding error η_g can be rewrite as

$$\eta_g \approx \begin{cases} 1, & \gamma_{ag} < \vartheta - \frac{1}{2\varsigma}, \\ -\varsigma(\gamma_{ag} - \vartheta) + \frac{1}{2}, & \vartheta - \frac{1}{2\varsigma} \leq \gamma_{ag} \leq \vartheta + \frac{1}{2\varsigma}, \\ 0, & \gamma_{ag} > \vartheta + \frac{1}{2\varsigma}. \end{cases} \tag{4.20}$$

where $\varsigma = \sqrt{\frac{n}{2\pi(\exp(2R)-1)}}$ and $\vartheta = \exp(R) - 1$.

We focus on the case where $0 < \eta < 1$. By substituting this specific case of (4.20) into (4.18), we can consequently determine the transmission time from UAV to g-th GU as follows

$$T_g = \frac{2M}{\pi_1 n R\,(1 + 2\varsigma(\gamma_{ag} - \vartheta))}. \tag{4.21}$$

Notice that the overall transmission time is fundamentally limited by the bottleneck link. Based on (4.21), the problem of minimizing the overall transmission time while ensuring the covertness can be formulated as

$$\min_{P_a, \mathbf{q}_a} \max_{g \in \mathbb{G}} \quad T_g, \tag{4.22a}$$

$$s.t. \quad \xi^* \geq \min(\pi_0, \pi_1) - 2\min(\pi_0, \pi_1)\epsilon \tag{4.22b}$$

where P_a denotes the transmit power of the UAV with the OH transmission protocol,

$\mathbf{q}_a$ is the hover location of the UAV, $\mathbb{G}$ is the set of GUs, $\epsilon > 0$ is the covertness constraint, (4.22b) represents the covertness requirement.

4.3.3 Transmit Power Optimization with the Given Hovering Location

The optimization problem presented in (4.22) involves multiple variables, constituting a challenging joint optimization problem. To simplify the resolution of this complex problem, we decompose it into sub-problems and solve them separately. First, given the horizontal location $\mathbf{q}_a$ of the UAV, the optimal transmit power and the corresponding minimum transmission time can be summarized in the following theorem.

Theorem 4.1. *For the considered UAV multicast system, when the UAV transmits M bits CI to the GUs positioned at the horizontal coordinate $\mathbf{q}_a$ and altitude h over n channel use in each time slot, along with the target rate R, prior transmission probability π_1 and the covertness constraint ϵ. The optimal transmit power P_a^* and the associated minimum transmission time T^* for the optimization problem (4.22) are determined as*

$$P_a^* = \frac{4\epsilon\sigma_w^2}{H_{aw}}\sqrt{\frac{2}{n}}\frac{\min(\pi_0,\pi_1)}{\max(\pi_0,\pi_1)}, \tag{4.23}$$

and

$$T^* = \frac{2M}{\pi_1 nR\left(1+2\varsigma(\gamma_{a\hat{g}}^* - \vartheta)\right)}, \tag{4.24}$$

where $\gamma_{a\hat{g}}^* = \frac{P_a^* H_{a\hat{g}}}{\sigma_{\hat{g}}^2}$; $\hat{g}$ represents the farthest GU from the UAV; ς and ϑ are given in (4.20); H_{aw} and $H_{a\hat{g}}$ can be obtained by substituting $\mathbf{q}_a$ and h into (4.3) and (4.4), respectively.

Proof. According to (4.3), given the hover location $\mathbf{U}(\mathbf{q}_a, h)$ of the UAV, we can conclude that the worst communication link from the UAV to GUs is the one farthest from the UAV to GU, using $\hat{g}$ denotes the GU farthest from the UAV. Then, based on this worst communication link, we explore the optimal transmit power of the UAV to

minimize the transmission time. It is easy to find that T is a decreasing function of P_a. To achieve the minimum transmission time, we need first to calculate the optimal transmit power while satisfying the covertness constraint. According to (4.12) and (4.22b), we know that the covertness requirement can be rewritten as

$$\frac{P_a H_{aw}}{\sigma_w^2} - \ln\left(1 + \frac{P_a H_{aw}}{\sigma_w^2}\right) \leq \frac{16\epsilon^2}{n}\left(\frac{\min(\pi_0, \pi_1)}{\max(\pi_0, \pi_1)}\right)^2. \tag{4.25}$$

Given the typically low transmit power in covert communications and thus a low SNR, we can leverage the Taylor series expansion and the inequality $\ln(1+x) \geq x - \frac{x^2}{2}$. Consequently, (4.25) can be further approximated as

$$\frac{P_a H_{aw}}{\sigma_w^2} \leq 4\epsilon\sqrt{\frac{2}{n}}\frac{\min(\pi_0, \pi_1)}{\max(\pi_0, \pi_1)}. \tag{4.26}$$

The optimal transmit power P_a^* is attained by setting the inequality in (4.26) as equality. Therefore, P_a^* is determined as (4.23), and the corresponding minimum transmission time T^* is determined as (4.24). □

4.3.4 Joint Optimization of the Transmit Power and Horizontal Location

In this subsection, we intend to jointly explore the optimal transmit power and horizontal location of the UAV to achieve the overall minimum transmission time. The optimal problem is challenging to solve mathematically since the variability in the worst communication links is associated with different horizontal locations. We thus adopt the PSO algorithm [75] to find the optimal horizontal location of the UAV. In the PSO algorithm, a swarm of particles moves in a D-dimensional search space to optimize the fitness function. During the searching process, each particle assesses its fitness for every iteration and adjusts its position based on its historical and global

best positions. The m-th particle's position is determined as

$$\mathbf{o}_m(k+1) = \mathbf{o}_m(k) + \mathbf{v}_m(k+1), \tag{4.27}$$

where k is the iteration index; $\mathbf{o}_m(k)$ is current position and $\mathbf{v}_m(k+1)$ is the velocity of the m-th particle, which is given by

$$\begin{aligned} \mathbf{v}_m(k+1) =& w\mathbf{v}_m(k) + c_1\psi_1(\mathbf{P}_m - \mathbf{o}_m(k)) \\ &+ c_2\psi_2(\mathbf{P}_g - \mathbf{o}_m(k)), \end{aligned} \tag{4.28}$$

where w is the inertial weight coefficient of each particle; c_1 and c_2 are acceleration constants; ψ_1 and ψ_2 are the local and global learning coefficients; $\mathbf{P}_m$ and $\mathbf{P}_g$ represent the local best and global best particle's positions.

In this work, the fitness function refers to the minimum transmission time, each particle's position is bounded by the concerned area, we need to check if the new position satisfies this constraint. Algorithm 1 illustrates the details of the PSO-based optimization algorithm that jointly solves the transmit power and hovering location of UAV.

4.4 Covert Transmission Time Minimization Under the TH Transmission Protocol

In this section, the UAV adopts the TH transmission protocol to minimize the completion transmission time. According to Protocol 2, we need select the optimal GU from GUs to serve as the relay, and determine the optimal transmit power P_a of the UAV subject to the covertness constraint. Concretely, we first present the optimal DEP at Willie, leveraging this optimal DEP, we then formulate the minimization of covert transmission time as an optimization problem. The optimization problem

Algorithm 1: PSO-based location optimization algorithm

Data: Location of GUs and Willie; Target rate R; Number of channel use n; Noise variance of GUs and Willie σ_g and σ_w; Altitude of the UAV h; CI size M; Channel fading loss exponent α; Covertness constraint ϵ; Number of particles m_{max}; Max value of iterations k_{max};

Result: Optimal transmit power P_a^*, Horizontal location $\mathbf{q}_a^*$; Minimum transmission time T^*;

Initialize random positions and velocities for m_{max} particles;
for $k = 1; k < k_{max}; k++$ **do**
  for $m = 1; m < m_{max}; m++$ **do**
    Update m-th particle's position by (4.27);
    Check and correct the particle's position in the concerned area;
    Calculate the optimal transmit power P_a and minimum transmission time $T_m(k)$ according to Theorem 4.1 with the current particle's position $\mathbf{o}_m(k)$;
    if $T_m(k)$ *is less than personal minimum transmission time* T_m^* **then**
      $T_m^* = T_m(k)$;
      $\mathbf{P}_m = \mathbf{o}_m(k)$;
    end
    if $T_m(k)$ *is less than global minimum transmission time* T_g^* **then**
      $P_a^* = P_a$;
      $T_g^* = T_m(k)$;
      $\mathbf{P}_g = \mathbf{o}_m(k)$;
    end
  end
end
$\mathbf{q}_a = \mathbf{P}_g$; $T^* = T_g^*$;

is non-convex and challenging to solve directly, we thus propose an exhaustive optimization algorithm to solve the joint problem.

4.4.1 Detection Error Probability at Willie

Similar to Section 4.3.1, to detect the transmission of the UAV to the relay with the TH transmission protocol, Willie should distinguishes the following two received signals.

$$\begin{cases} H_0: & \mathbf{y}_w[i] = \sqrt{P_r H_{rw}}\mathbf{t}[i] + \mathbf{n}_w[i], \\ H_1: & \mathbf{y}_w[i] = \sqrt{P_a H_{aw}}\mathbf{x}[i] + \mathbf{n}_w[i], \end{cases} \tag{4.29}$$

where P_r is the predetermined transmit power at the relay; $\mathbf{t}[i] = \mathbf{x}[i]$ is the transmit symbol from the relay. We suppose that Willie adopts the optimal statistical hypothesis test to minimize the optimal DEP ξ^*. The lower bound of the optimal ξ^* can be determined as

$$\xi^* \geq \min(\pi_0, \pi_1) - \max(\pi_0, \pi_1)\sqrt{\frac{n\mathcal{D}(\mathbb{P}_1, \mathbb{P}_0)}{2}}. \tag{4.30}$$

The KL divergence $\mathcal{D}(\mathbb{P}_1, \mathbb{P}_0)$ from $\mathbb{P}_1$ to $\mathbb{P}_0$ can be calculated as

$$\mathcal{D}(\mathbb{P}_1, \mathbb{P}_0) = \frac{1}{2}\left[\gamma_{aw} - \ln\left(1 + \gamma_{aw}\right)\right], \tag{4.31}$$

where $\gamma_{aw} = \frac{P_a H_{aw}}{P_r H_{rw} + \sigma_{\hat{w}}^2}$, P_a and P_r are the transmit power of the UAV and the relay, respectively.

Thus, the lower bound of the optimal DEP ξ^* at Willie can be expressed as

$$\xi^* \geq \min(\pi_0, \pi_1) - \max(\pi_0, \pi_1)\sqrt{\frac{n}{4}\left(\gamma_{aw} - \ln\left(1 + \gamma_{aw}\right)\right)}. \tag{4.32}$$

4.4.2 Transmission Time Formulation

Similar to Section 4.3.2, with the selected relay, to achieve the minimum covert transmission time, we need to calculate the effective throughput C_g of the concerned system. According to Protocol 3, under the TH transmission scheme, for the i-th symbol, the received signal at the relay $\mathbf{y}_r[i]$, the received signal at the g-th remaining GU when the UAV transmits CI $\mathbf{y}_g^u[i]$, and the received signal at the g-th remaining GU when the relay transmits CI $\mathbf{y}_g^r[i]$ are respectively given by

$$\mathbf{y}_r[i] = \sqrt{P_a H_{ar}}\mathbf{x}[i] + \mathbf{n}_r[i], \tag{4.33}$$

$$\mathbf{y}_g^u[i] = \sqrt{P_a H_{ag}}\mathbf{x}[i] + \mathbf{n}_g[i], \tag{4.34}$$

$$\mathbf{y}_g^r[i] = \sqrt{P_r H_{rg}}\mathbf{t}[i] + \mathbf{n}_g[i], \tag{4.35}$$

where H_{ar} is similar to the notion in (4.3), denotes the channel gain from the UAV to the relay; $\mathbf{n}_r[i] \sim \mathcal{N}(0, \sigma_r^2)$ is the AWGN at the relay. Additionally, following the approach in [76, 77], the GU g is assumed to use maximum ratio combining (MRC) to take advantage of receiving two independent copies of each symbol. Consequently, the SNR at GU g with MRC is determined as $\gamma_{arg} = \frac{P_a H_{ag} + P_r H_{rg}}{\sigma_g^2}$.

Based on the signals received at the GUs, the decoding error probability of the block at the GUs is higher when relying solely on direct links from the UAV compared to using MRC-based relay links. Thus, our focus is the MRC-based relay links. According to [77], the overall decoding correct probability is the intersection of the decoding correct probability at the relay and the decoding correct probability at the g-th GU with MRC. Therefore, the overall decoding error probability, which represents the likelihood of at least one decoding error occurring in the system, can be given by

$$\eta_{ag} = 1 - (1 - \eta_{ar})(1 - \eta_{arg}), \tag{4.36}$$

where η_{ar} and η_{arg} are the decoding error probabilities at the selected relay and g-th GU with MRC, respectively. Additionally, since the UAV transmits a block with probability π_1, the relay transmits a block with probability π_0, the overall probability of transmitting a block is $\min(\pi_0, \pi_1)$. Therefore, the effective throughput C_g can be expressed as

$$C_g = \min(\pi_0, \pi_1) nR(1 - \eta_{ar})(1 - \eta_{arg}). \tag{4.37}$$

Similar to (4.20), we employ a linear approximation function for the decoding error probability. Thus, the decoding error probability η_{ar} at the selected relay can be determined as

$$\eta_{ar} \approx \begin{cases} 1, & \gamma_{ar} < \vartheta - \frac{1}{2\varsigma}, \\ -\varsigma(\gamma_{ar} - \vartheta) + \frac{1}{2}, & \vartheta - \frac{1}{2\varsigma} \leq \gamma_{ar} \leq \vartheta + \frac{1}{2\varsigma}, \\ 0, & \gamma_{ar} > \vartheta + \frac{1}{2\varsigma}, \end{cases} \tag{4.38}$$

and the decoding error probability η_{arg} at g-th GU can be given by

$$\eta_{arg} \approx \begin{cases} 1, & \gamma_{arg} < \vartheta - \frac{1}{2\varsigma}, \\ -\varsigma(\gamma_{arg} - \vartheta) + \frac{1}{2}, & \vartheta - \frac{1}{2\varsigma} \leq \gamma_{arg} \leq \vartheta + \frac{1}{2\varsigma}, \\ 0, & \gamma_{arg} > \vartheta + \frac{1}{2\varsigma}. \end{cases} \tag{4.39}$$

We focus on the case where $0 < \eta_{ar} < 1$ and $0 < \eta_{arg} < 1$. By substituting these specific cases of (4.38) and (4.39) into (4.36), we can consequently determine the transmission time from UAV to g-th GU as follows

$$T_g = \frac{4M}{\min(\pi_0, \pi_1) nR(1 + 2\varsigma(\gamma_{ar} - \vartheta))(1 + 2\varsigma(\gamma_{arg} - \vartheta))}. \tag{4.40}$$

Notice that the overall transmission time is fundamentally limited by the bottle-

neck link. Based on (4.40), the problem of minimizing the overall transmission time while ensuring the covertness can be formulated as

$$\min_{P_a, r\in\mathbb{G}} \max_{g\in\mathbb{G}} \quad T_g, \tag{4.41a}$$

$$s.t. \quad \xi^* \geq \min(\pi_0, \pi_1) - 2\min(\pi_0, \pi_1)\epsilon, \tag{4.41b}$$

where P_a denotes the transmit power of the UAV with the TH transmission protocol, r is the selected GU acting as the relay, $\mathbb{G}$ is the set of GUs, $\epsilon > 0$ is the covertness constraint, (4.41b) represents the covertness requirement.

4.4.3 Transmit Power Optimization with the Selected Relay

The optimization problem presented in (4.41) involves multiple variables, constituting a challenging joint optimization problem. To simplify the solution of this complex problem, we decompose it into sub-problems and solve them separately. First, given the selected relay, the optimal transmit power and the corresponding minimum transmission time can be summarized in the following theorem.

Theorem 4.2. *For the considered UAV multicast system, when the UAV transmits M bits CI to the GUs positioned above of the selected relay r and altitude h over n channel use in each time slot, along with the target rate R, the fixed transmit power P_r at the relay and the covertness constraint ϵ. The optimal transmit power P_a^* for the optimization problem (4.41) is determined as*

$$P_a^* = \frac{4\epsilon\sigma_w^2}{H_{aw}e^{\kappa_{rw}}\kappa_{rw}E_1(\kappa_{rw})}\sqrt{\frac{2}{n}}\frac{\min(\pi_0, \pi_1)}{\max(\pi_0, \pi_1)}, \tag{4.42}$$

where $E_1(\cdot)$ is the exponential integral, defined as $E_1(z) = \int_z^\infty e^{-t}t^{-1}dt$ [63], and $\kappa_{rw} = \frac{\sigma_w^2}{P_r l_{rw}^{\alpha_N}}$. The corresponding expected minimum transmission time T^* is thus

determined as

$$T^* = \frac{4M}{\min(\pi_0, \pi_1) nR(1 + 2\varsigma(\gamma_{ar}^* - \vartheta))(1 + 2\varsigma(\bar{\gamma}_{ar\hat{g}}^* - \vartheta))}, \tag{4.43}$$

where $\gamma_{ar}^* = \frac{P_a^* H_{ar}}{\sigma_r^2}$ *and* $\bar{\gamma}_{ar\hat{g}}^* = \frac{P_a^* H_{a\hat{g}} + P_r l_{r\hat{g}}^{\alpha} N}{\sigma_{\hat{g}}^2}$*;* $\hat{g}$ *represents the farthest GU from the relay;* ς *and* ϑ *are given in (4.20).*

Proof. According to (4.5), given the selected relay, we can conclude that the worst communication link from the relay to GUs is the one farthest from the relay to GU, using $\hat{g}$ denotes the GU farthest from the selected relay. Then, based on this worst communication link, we explore the optimal transmit power of the UAV to minimize the transmission time. It is easy to find that T is a decreasing function of P_a. To achieve the minimum transmission time, we need first to calculate the optimal transmit power while satisfying the covertness constraint. Notice that both the UAV and relay only know the channel state information from Willie, we need to calculate the average KL divergence. According to (4.32) and (4.41b), we know that the covertness requirement can be rewritten as

$$\mathbb{E}\left[\frac{P_a H_{aw}}{P_r H_{rw} + \sigma_w^2} - \ln\left(1 + \frac{P_a H_{aw}}{P_r H_{rw} + \sigma_w^2}\right)\right] \leq \frac{16\epsilon^2}{n}\left(\frac{\min(\pi_0, \pi_1)}{\max(\pi_0, \pi_1)}\right)^2. \tag{4.44}$$

Given the typically low transmit power in covert communications and thus a low SNR, we can leverage the Taylor series expansion and the inequality $\ln(1+x) \geq x - \frac{x^2}{2}$. Consequently, (4.44) can be further approximated as

$$\mathbb{E}\left[\frac{P_a H_{aw}}{P_r H_{rw} + \sigma_w^2}\right] \leq 4\epsilon\sqrt{\frac{2}{n}}. \tag{4.45}$$

The expected value of KL divergence can be given by

$$\begin{aligned}\mathbb{E}\left[\frac{P_a H_{aw}}{P_r H_{rw}+\sigma_w^2}\right] &= \int_0^{\infty} \frac{P_a H_{aw}}{P_r l_{rw}^{\alpha_N}|h_{rw}|^2+\sigma_w^2} f_{|h_{rw}|^2}(x)dx \\ &= \frac{P_a H_{aw} e^{\kappa_{rw}} \kappa_{rw}}{\sigma_w^2} E_1(\kappa_{rw}).\end{aligned} \tag{4.46}$$

The optimal transmit power P_a^* is attained by setting the inequality in (4.45) as equality. Therefore, P_a^* is determined as (4.42).

Similarly, the average SNR $\bar{\gamma}_{ar\hat{g}} = \frac{P_a H_{a\hat{g}}+P_r l_{rw}^{\alpha_N}}{\sigma_{\hat{g}}^2}$. Substituting $\bar{\gamma}_{ar\hat{g}}$ and P_a^* into (4.40), the corresponding minimum transmission time T^* is determined as (4.43). □

4.4.4 Joint Optimization of the Transmit Power and Selected Relay

In this subsection, we intend to jointly explore the optimal transmit power of UAV and optimal relay to achieve the overall minimum transmission time. The optimal problem is challenging to solve mathematically since the variability in the worst communication links is associated with different relay. We thus adopt the exhaustive algorithm to find the optimal relay, as shown in Algorithm 2.

4.5 Numerical Results

In this section, we present extensive numerical results to exhibit the performance of the proposed two covert transmission protocols.

4.5.1 Simulation Settings

In the simulations, we define a circular area with a radius of $500m$, and let the density parameter λ varies in the range of $[2 \times 10^{-5}\pi^{-1}, 8 \times 10^{-4}\pi^{-1}]$. Aligning with the approach in [70], we set the time slot duration as Δt = 1ms, and each channel use lasts for 0.01ms. Consequently, the total number of channel uses in a time slot is $n = \frac{\Delta t}{0.01ms} = 100$. Additional simulation parameters are as follows:

Algorithm 2: Optimal relay selection algorithm

Data: Locations of GUs and Willie; Target rate R; Number of channel use n; Noise variance of GUs and Willie σ_g and σ_w; Altitude of the UAV h; CI size M; Channel fading loss exponent α^L and α^N; Covertness constraint ϵ;

Result: Optimal transmit power P_a^*; Optimal relay r^*; Minimum transmission time T^*;

```
for i = 1; i < G; i++ do
    T(i) = ∞;
    P_a(i) = 0;
    R=i;
    for g = 1; g < G − 1; g++ do
        Calculate the optimal transmit power P_a(ig) and minimum
         transmission time T(ig) according to Theorem 4.2 with R act as
         relay;
        if T(ig) is less than T(i) then
            T(i) = T(ig);
            P_a(i) = P_a(ig);
        end
    end
    if T(i) is less than T then
        T = T(i);
        P_a = P_a(i);
        r = R;
    end
end
P_a^* = P_a; T^* = T; r^* = r;
```

UAV's altitude $h = 500m$, file size $M = 1$KB, channel fading loss exponent $\alpha_L = -2$ and $\alpha_N = -3$, target rate $R = 0.1$bpcu (bit per channel use), transmit power at the relay $P_r = -10dBm$, covertness constraint $\epsilon = 0.1$, the S-curve parameters $\sigma = 4.88$ and $f = 0.429$. We further set the noise variance for Willie σ_w^2 and noise variance σ_g^2 for each GU as $\sigma_g^2 = \sigma_w^2 = -70$dBm. For performance comparison, we utilize the center of the minimum circle covering all GUs with the fixed altitude $h = 500m$ as the reference optimal location.

4.5.2 Performance Evaluation

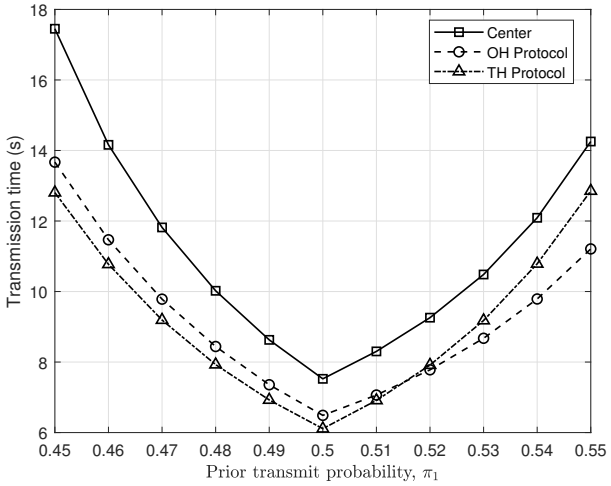

Figure 4.2: Transmission time versus prior transmit probability π_1 under the settings of $\lambda = 1.2 * 10^{-4}$, $r = 500m$ and $\mathbf{q}_w = [600, 0]$.

This subsection provides numerical results to illustrate the impact of system parameters on the transmission time performance. For a given setting of system parameters (like the number of GUs, GU density, radius of considered area, and covertness constraint), we generate 10^4 sets of GU spatial distributions, and then execute the Algorithm 1 and Algorithm 2 to get average minimum transmission time of UAV under the two transmission protocols.

To investigate the impact of prior transmit probability π_1 on covert transmission

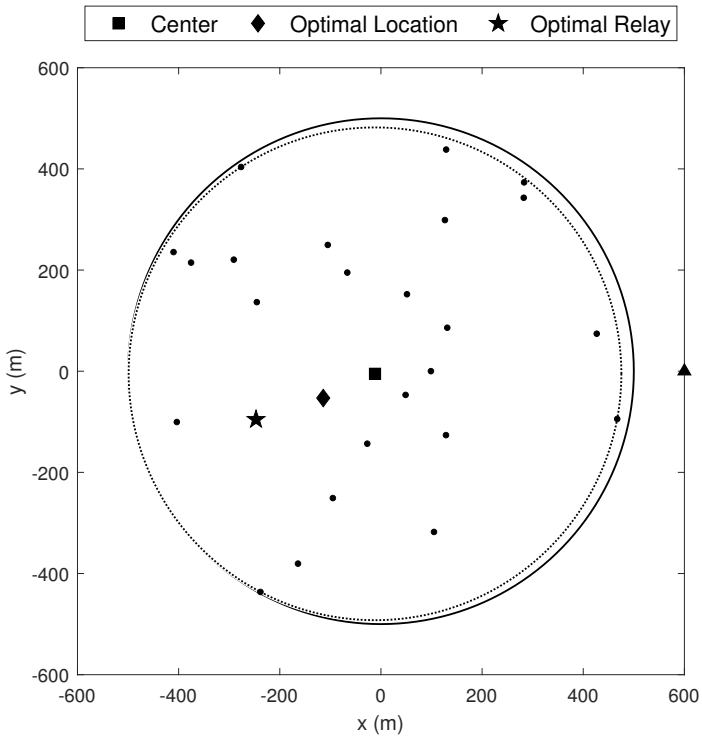

Figure 4.3: Illustration of the optimal location and relay under the settings of $\lambda = 1 * 10^{-4}$, $r = 500m$ and $\mathbf{q}_w = [600, 0]$.

time, Fig. 4.2 illustrates the relationship between transmission time and π_1 under the parameters $\lambda = 1.2 * 10^{-4}$, $r = 500m$, and $\mathbf{q}w = [600, 0]$. The results demonstrate that, across all protocols, transmission time initially decreases and then increases as π_1 increases. This pattern suggests that there is an optimal value for π_1 that minimizes transmission time. Specifically, when $\pi_1 = 0.5$, the transmission time is at its lowest, indicating the optimal prior transmit probability. This optimal value is then used for subsequent analyses to ensure minimal transmission time.

We then provide an illustrative example of two transmission protocols in Fig. 4.3. The black dot represents GUs, the black triangle represents Willie, the dotted circle is the minimal circle covering all GUs, and the realization circle is the considered area. Surprisingly, the optimal UAV location of the OH protocol in the example does not align with and is even a little far away from the center of the minimum circle

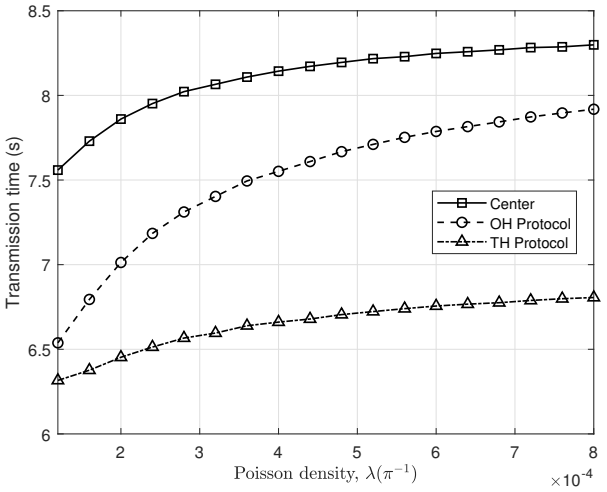

Figure 4.4: Transmission time versus λ under the setting of $\mathbf{q}_w = [600, 0]$.

encompassing all GUs; the optimal relay of the TH protocol is even farther.

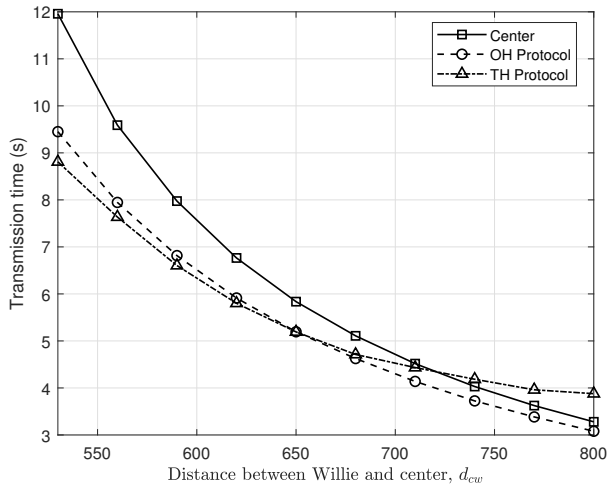

Figure 4.5: Transmission time versus d_{cw} under the setting of $\lambda = 1.2 * 10^{-4} * \pi^{-1}$.

The results in Fig. 4.4 highlight that both the OH and TH transmission protocols achieve shorter transmission times compared to using the center of the minimum circle as the UAV's location, underscoring the efficiency of the new transmission protocols. Furthermore, the TH transmission protocol achieves a significantly shorter transmission time. Notably, a smaller value of λ results in a shorter transmission time. This observation suggests that the proposed transmission protocols are effective in

reducing transmission time, particularly when the number of GUs is relatively small.

We then plot in Fig. 4.5 the relationship between transmission time and the distance d_{cw} from Willie to the center of the considered circle with $\lambda = 1.2{*}10^{-4}{*}\pi^{-1}$. As can be seen from Fig. 4.5, transmission time consistently diminishes as d_{cw} increases. This behavior is attributed to the fact that, with Willie is farther away from GUs, the UAV can employ higher transmit power while satisfying the covertness constraint, resulting in a reduction in transmission time.

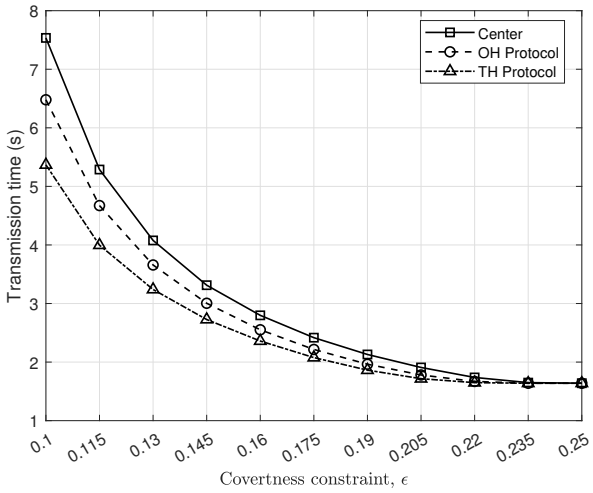

Figure 4.6: Transmission time versus covertness constraint ϵ under the settings of $\lambda = 1.2 * 10^{-4} * \pi^{-1}$ and $\mathbf{q}_w = [600, 0]$.

Finally, we present in Fig. 4.6 how transmission time varies with the covertness constraint ϵ. As illustrated in Fig. 4.6, transmission time decreases with the increase of ϵ (i.e, a relaxation of the covertness constraint). This is attributed to the UAV's ability to transmit CI at a higher power when ϵ is larger, consequently reducing the overall transmission time.

Upon a careful examination of Fig. 4.6, it is evident that the gap between the transmission time of the proposed transmission protocols and that of the utilizing the center of the minimum circle becomes narrow as ϵ decreases, indicating the proposed transmission protocols become more significant as the covertness constraint tends

to be more stringent. Both Fig. 4.5 and Fig. 4.6 underscore the efficiency of the transmission protocols in effectively leveraging multicast transmission potential to reduce the transmission time in the UAV system, especially under more stringent covertness constraints.

4.6 Summary

This chapter introduced two transmission protocols, where in the OH transmission protocol, the PSO-based UAV location and transmit power optimization algorithm is proposed, and in the TH transmission, the optimal relay and transmit power optimization exhaustive algorithm is proposed to facilitate the covert multicast in UAV-enabled communication systems. In contrast to the conventional center location-based transmission, our comprehensive numerical results illustrate that the new transmission protocols can remarkably enhance the time efficiency for covert multicast, particularly in systems with stringent covertness constraints. It is anticipated that this work can serve as a promising solution for future UAV-enabled covert multicast communication systems.

CHAPTER V

Transmission Protocol Design for General Multi-Receiver Scenario

This chapter considers a general multi-receiver scenario, in which a UAV would like to disseminate a common CI to multiple GUs diversely distributed within a circular area while simultaneously evading the detection by a ground warden Willie located in the center of the area. We first propose two effective MG construction algorithms to group all GUs into multiple MGs, and develop a theoretical framework for the performance modeling of each MG in terms of its DEP and transmission time. We also explore the optimal setting of covert transmission power for each MG to achieve the minimum transmission time in the MG. By integrating the aforementioned components, we thus devise a complete and time-efficient covert multicast transmission protocol for the concerned system. Finally, extensive numerical results are provided to illustrate the efficiency of the new transmission protocol under the general multi-receiver scenario.

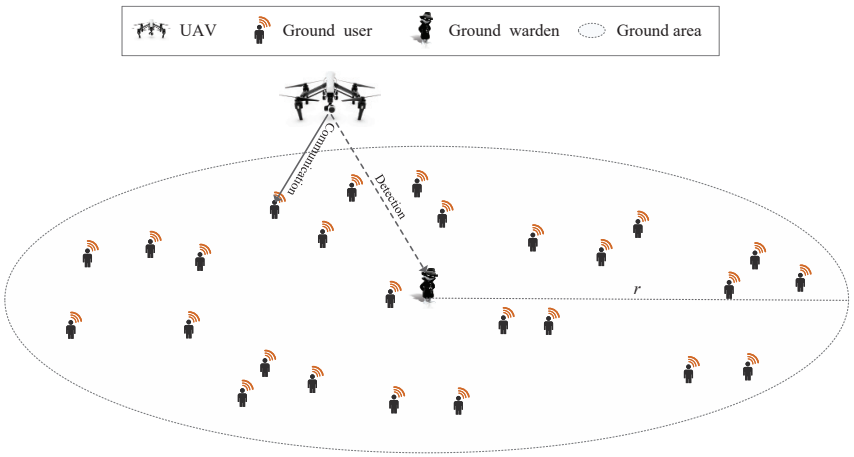

Figure 5.1: Illustration of the system model.

5.1 Preliminaries

5.1.1 System and Channel Model

As shown in Fig. 5.1, we consider a UAV-enabled covert communication system, where UAV (a) acts as a flying base station with altitude h to disseminate a common CI of M bits to G GUs, while simultaneously evading detection by the ground warden (Willie, w). For the considered system, Willie is located in the center of a circular area with radius r, GUs are distributed in this area following the cluster distribution with cluster parameter ρ [78], and the number of the clusters is modeled by a Poisson process with mean λ [79].

Similar as the widely used assumption in existing works on UAV-enabled covert communication [35, 80], we assume that the UAV knows the exact locations of each GU and Willie, which can be achieved by using the standard positioning techniques (e.g., GPS, BeiDou, QZSS or Galileo-based localization)[81]. Since UAV flies with a fixed altitude h, we use its projected two-dimensional coordinates $\mathbf{q}_a = [x_a, y_a]$ to represent its location. The horizontal coordinates of the g-th GU and Willie are denoted as $\mathbf{q}_g = [x_g, y_g]$ and $\mathbf{q}_w = [x_w, y_w]$, respectively.

For UAV-enabled communication scenario, the UAV-ground channel is dominated by the LoS component since the path loss for the UAV-ground channel of the NLoS component is usually much higher than that of the LoS component [35, 80]. Thus, we use the LoS model to characterize the channels from UAV to GUs and to Willie. The channel gain H_{ag} from the UAV to the g-th GU and channel gain H_{aw} from the UAV to Willie are then determined as

$$H_{ag} = \frac{\beta}{\|\mathbf{q}_a - \mathbf{q}_g\|^2 + h^2}, \tag{5.1}$$

$$H_{aw} = \frac{\beta}{\|\mathbf{q}_a - \mathbf{q}_w\|^2 + h^2}, \tag{5.2}$$

where β is the channel power gain at the reference distance of 1 m.

5.1.2 Communication Model

To disseminate the common CI to a group of GUs in its coverage, UAV first divides the CI into m blocks of size $\frac{M}{m}$ bits each, and transmits each block in one time slot with duration Δt. To confuse Willie, UAV selects each time slot with probability π_1 (i.e. does not select this time slot with probability $\pi_0 = 1 - \pi_1$) to transmit a block. If UAV decides to transmit one block in a time slot, she encodes this block into n real value symbols $\mathbf{x} = (\mathbf{x}[1], \cdots, \mathbf{x}[i])$, where each symbol satisfies $\mathbf{x}[i] \sim \mathcal{N}(0, 1)$ and $i = 1, 2, \cdots, n$. UAV then transmits these n symbols to GUs in its coverage by using n channel uses in this time slot. For the i-th symbol $\mathbf{x}[i]$, the received signal $\mathbf{y}_g[i]$ at the g-th GU is determined as

$$\mathbf{y}_g[i] = \sqrt{P_{ag} H_{ag}}\mathbf{x}[i] + \mathbf{n}_g[i], \tag{5.3}$$

where P_{ag} is the transmission power from UAV to g-th GU; $\mathbf{n}_g[i] \sim \mathcal{N}(0, \sigma_g^2)$ represents the additive white Gaussian noise (AWGN) at g-th GU and σ_g^2 is the noise variance.

5.1.3 Detection Model at Willie

Willie adopts the hypothesis test to make a judgment whether the UAV conducts transmission or not by sensing the received signals. For the symbol $\mathbf{x}[i]$, the signal $\mathbf{y}_w[i](i = 1, 2, \cdots, n)$ received by Willie during each time slot can be given by

$$\begin{cases} \mathcal{H}_0: & \mathbf{y}_w[i] = \mathbf{n}_w[i], \\ \mathcal{H}_1: & \mathbf{y}_w[i] = \sqrt{P_{ag}H_{aw}}\mathbf{x}[i] + \mathbf{n}_w[i], \end{cases} \tag{5.4}$$

where $\mathcal{H}_0$ denotes the null hypothesis that the UAV does not transmit the information, $\mathcal{H}_1$ denotes the alternative hypothesis that the UAV transmits the information; $\mathbf{n}_w[i]$ is the AWGN with mean zero and variance σ_w^2 at Willie.

Let $\mathcal{D}_1$ and $\mathcal{D}_0$ denote the binary decisions of Willie that infer whether UAV is transmitting or not, respectively. Therefore, there are two kinds of mistakes that Willie may make, i.e., the false alarm (FA) and the miss detection (MD). Let $P_{FA} = Pr(\mathcal{D}_0|\mathcal{H}_1)$ denotes the false alarm probability, and $P_{MD} = Pr(\mathcal{D}_1|\mathcal{H}_0)$ denotes the miss detection probability. We consider a worst-case scenario, where the transmission power P_{ag}, the channel use n, the prior transmission probability π_1 are known by Willie. The total detection error probability (DEP) at Willie can be given by

$$\xi = \pi_0 P_{FA} + \pi_1 P_{MD}. \tag{5.5}$$

5.2 Overall Transmission Protocol

To enable a flexible trade-off to be initiated between the overall transmission time and covertness guarantee for CI dissemination to all GUs, we define a guard zone around Willie, i.e., a circular region around Willie with radius r_w, as illustrated in Fig. 5.2. For GUs within the guard zone, we adopt the point-to-point transmission protocol to ensure the covertness guarantee. For GUs outside of the guard zone, we

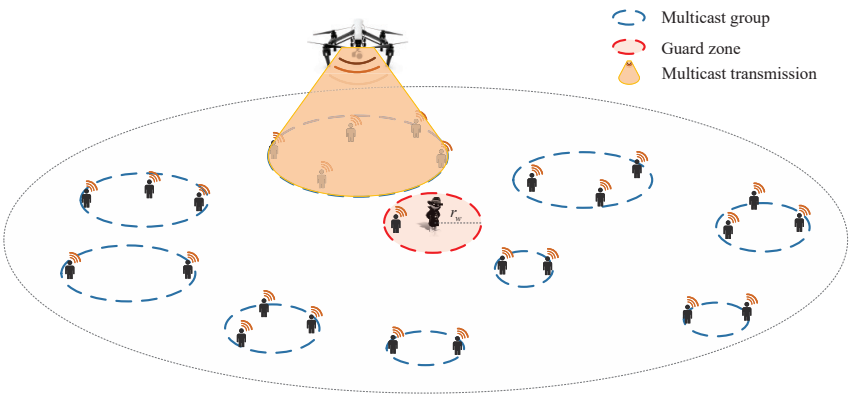

Figure 5.2: Example for illustrating the multicast group.

first apply the K-means++ algorithm [14] or the geometric disk covering (GDC) algorithm [82] to group these GUs into multiple multicast groups (MGs). To conduct the multicast transmission of CI in an MG, we first fix the GU with the worst communication link in the MG, and then determine the optimal transmit power for the MG based on the communication link of this GU. According to the optimal transmit power, we further determine the number of blocks for transmitting the CI in this MG and divide the CI into blocks. Finally, each block is encoded into n symbols and transmitted over n channel uses in a time slot. The overall transmission protocol can be summarized as Protocol 4.

5.3 Protocol Element Design

From Protocol 4 we can see that the proposed transmission protocol involves the GU grouping, detection error probability analysis for an MG, transmission time minimization for the MG, as well as the multicast transmission protocol design for the MG.

Protocol 4: Overall Transmission Protocol

Input: Coordinates of Willie and GUs;
Radius of guard zone;

Step 1: Define a guard zone around Willie;
Step 2: Regard each GU within the guard zone as an MG;
Step 3: Grouping GUs outside of the guard zone into MGs;
Step 4: For each MG process the Step 5-12;
Step 5: Select the GU with the worst communication link in the MG;
Step 6: Based on communication link of this GU, calculate the optimal transmit power;
Step 7: Calculate target blocks size m;
Step 8: Divide CI into m_k^* blocks;
Step 9: Encode one block into target n symbols;
Step 10: Select each time slot to transmit one block with a probability of π_1;
Step 11: Multicast these n symbols of one block to the GUs within one time slot;
Step 12: Repeat Step 9-11 until all blocks are multicast to the GUs.

5.3.1 MG Construction based on GU Grouping

For a group of GUs, we can apply the geometric method in [83] to determine its coverage area (CA), i.e., a minimum circular area (MCA) that covers all GUs in this group. We define a group of GUs as an MG if there is no overlap between its CA and the guard zone. Since we consider the LoS wireless channel model in this work, then the signal loss is strongly dependent on transmission distance. Also, the UAV's hover location is just above the center of the group. Thus, the above condition ensures that even for the GU with the worst communication link to UAV in the group, the received signal power at the GU is still higher than that at Willie, so all the GUs in the group can correctly decode the message while Willie will make wrong decisions with a high probability, enabling the covert multicast communication to be conducted from UAV to all GUs in this group.

Regarding the MG construction, we consider the following two typical algorithms to implement the GU grouping for all GUs outside of the guard zone.

1) K-means++ algorithm: We apply the classical K-means++ algorithm to cluster

GUs into K groups, and then verify whether each of these K groups is an MG. If not, we set $K = K + 1$ and repeat the above process until each group becomes an MG.

2) Geometric disk covering algorithm: The GDC problem aims to cover a set of nodes in a region with the minimum number of disks of a given radius r_m. Here, we adopt a variation of the GDC algorithm named spiral mobile base stations placement algorithm (SMBSP) proposed in [15] to group GUs with radius r_m. We iterative this algorithm with a decreasing radius (e.g. $r_m = r_m - 10$) until each group becomes an MG.

Overall, the MG construction algorithm is summarized in Algorithm 3.

Algorithm 3: MG Construction Algorithm

input: Coordinates of GUs and Willie;
Radius of guard zone;
(Radius of concerned circular area r;)
output: MG set $\mathcal{S}$;
$\mathcal{S} = \{$Each GU within guard zone as an MG$\}$;
Initialize the number of groups $K = 1$ (or the radius $r_m = r$;)
Initialize *overlapped*=**true**;
while *overlapped* **do**
  Execute K-means++ algorithm with K (or execute SMBSP algorithm with r_m), then return the group set $\mathcal{G}$;
  Execute the MCA algorithm for each group in $\mathcal{G}$, then return the CA set $\mathcal{S}'$;
  overlapped=**false**;
  foreach *CA in* $\mathcal{S}'$ **do**
    if *CA is overlapped with the guard zone* **then**
      overlapped=**true**;
      $K = K + 1$ (or $r_m = r_m - 10$);
      break;
    end
  end
end
$\mathcal{S} = \mathcal{S} + \mathcal{S}'$;

5.3.2 Detection Error Probability Analysis for An MG

By employing the MG construction algorithm, we can get the MG set $\mathcal{S}$ with a total of $K = |\mathcal{S}|$ MGs in the set. The UAV then sequentially transmits CI to each MG in $\mathcal{S}$. During the transmission of each MG, the UAV employs the multicast protocol to simultaneously transmit CI to GUs in the MG while avoiding detection by Willie. Notice that the covertness constraint is determined by the optimal DEP at Willie, we then establish the following theorem regarding the optimal DEP at Willie when the UAV transmits CI to the k-th MG ($k = 1, \cdots, K$).

Theorem 5.1. *For the concerned UAV system, when the UAV transmits CI to the k-th MG with transmission power P_{ak} and time slot selection probability π_1 (i.e. does not transmit in a slot with probability $\pi_0 = 1 - \pi_1$), a lower bound $\xi_{k,l}^*$ of the optimal DEP ξ_k^* at Willie is given by*

$$\xi_k^* \geq \xi_{k,l}^* = \min(\pi_0, \pi_1) - \max(\pi_0, \pi_1)\sqrt{\frac{n}{4}\Phi}, \tag{5.6}$$

where $\Phi = \frac{P_{ak}H_{aw}}{\sigma_w^2} - \ln\left(1 + \frac{P_{ak}H_{aw}}{\sigma_w^2}\right)$.

Proof. When the UAV transmits CI to the k-th MG, we denote the probability distribution of the observes vector $\mathbf{y}_{w,k}[i]$ at Willie as $\mathbb{P}_{0,k}$ (resp. $\mathbb{P}_{1,k}$) when $\mathcal{H}_0$ (resp. $\mathcal{H}_1$) is true, and further denote the distribution of the sequence $\mathbf{y}_{w,k} = \{\mathbf{y}_{w,k}[i]\}_{i=1}^n$ received in n channel use as $\mathbb{P}_{0,k}^n$ (resp. $\mathbb{P}_{1,k}^n$). Suppose that Willie adopts an optimal statistical hypothesis test that minimizes the sum of FA and MD, the KL divergence $\mathcal{D}(\mathbb{P}_{1,k}, \mathbb{P}_{0,k})$ from $\mathbb{P}_{1,k}$ to $\mathbb{P}_{0,k}$ can be determined by the same approach of Section 4.3.1 in Chapter IV. □

5.3.3 Transmission Time Minimization for An MG

We first provide the transmission time modeling of an MG, and then examine the optimal setting of transmission power for transmission time minimization in the MG.

For the k-th MG, let T_k denote the transmission time for the UAV to disseminate CI to all the GUs in the MG. We can determine the optimal transmission power and the minimum transmission time of the k-th MG, as summarized in the following theorem.

Theorem 5.2. *For the concerned UAV system, when the UAV transmits CI of bits M to the k-th MG with the time slot selection probability π_1, the channel use n in each time slot, the target rate R and the covertness constraint ϵ, the optimal transmission power P_{ak}^* and the corresponding minimum transmission time T_k^* are determined as*

$$P_{ak}^* = \frac{4\epsilon\sigma_w^2}{H_{aw}}\sqrt{\frac{2}{n}}\frac{\min(\pi_0,\pi_1)}{\max(\pi_0,\pi_1)}, \tag{5.7}$$

and

$$T_k^* = \frac{2M}{\pi_1 nR\left(1+2\varsigma(\gamma_{ak}^*-\vartheta)\right)}, \tag{5.8}$$

where $\gamma_{ak}^* = \frac{P_{ak}^* H_{ak}}{\sigma_k^2}$, ς and ϑ are given in (4.20) of Chapter IV.

Proof. The proof is similar to the Theorem 4.1 in Chapter IV. □

5.4 Numerical Results

In this section, we first conduct simulations to validate the accuracy of the theoretical performance analysis, and then present extensive numerical results to exhibit the performance of the proposed transmission strategy.

5.4.1 Simulation Settings

In the simulations, we consider that there are $G \in [50, 500]$ GUs in a circular area with radius $r = 1000m$, which follow the cluster distribution with the cluster parameter ρ and the mean number of the clusters λ [78, 79]. Same as [70], we set the duration of a time slot as $\Delta t = 1$ms, and set the duration of one channel use as 0.01ms, so the total channel uses in a time slot is $n = \frac{\Delta t}{0.01ms} = 100$. The other parameters

involved in the simulation are set as follows: UAV altitude $h = 500m$, the file size of CI $M = 1$Mb, the channel power gain $\beta = -40$dB, the target rate $R = 0.1$bpcu (bit per channel use), the covertness constraint $\epsilon = 0.1$, and the noise variance of Willie and each GU $\sigma_g^2 = \sigma_w^2 = -70$dBm. Besides, according to the Chapter IV, we chose the optimal time slot selection probability $\pi_1 = 0.5$. For performance comparison, we also implement the point-to-point transmission scheme in our simulation. In this scheme, the UAV conducts point-to-point transmission to transmit the CI directly to each GU in turn. Notice that this scheme just corresponds to the scenario that the radius r_w of the guard zone is large enough that covers all GUs in our proposed scheme.

5.4.2 Model Validation

To validate our theoretical results on the transmission time for an MG, we developed a dedicated MATLAB simulator to simulate the multicast transmission under the proposed transmission strategy [84]. Specifically, under the settings of $G = 50$, $\rho = 0.3$ and $\lambda = 5$, we apply the method in [78, 79] to generate the spatial distribution of these GUs in the concerned circular area with radius $r = 1000m$. An example of such spatial distribution is shown in Fig. 5.3, and the corresponding MGs based on the Algorithm 3 and a guard zone radius of $r_w = 150m$ are illustrated in Fig. 5.4. We treat each GU within the guard zone as an MG, and assign a serial number incrementally to each MG based on the distance between its center and Willie.

For each MG in Fig. 5.4, we summarize in Fig. 5.5 both the theoretical and simulation results on its minimum transmission time. Here, the theoretical result is evaluated by using (5.8), and the simulation result is obtained by averaging the corresponding 10^4 times simulation results of the Protocol 4. It is evident from Fig. 5.5 that the simulation results closely match the theoretical counterparts, so our theoretical framework can efficiently model the fundamental transmission time

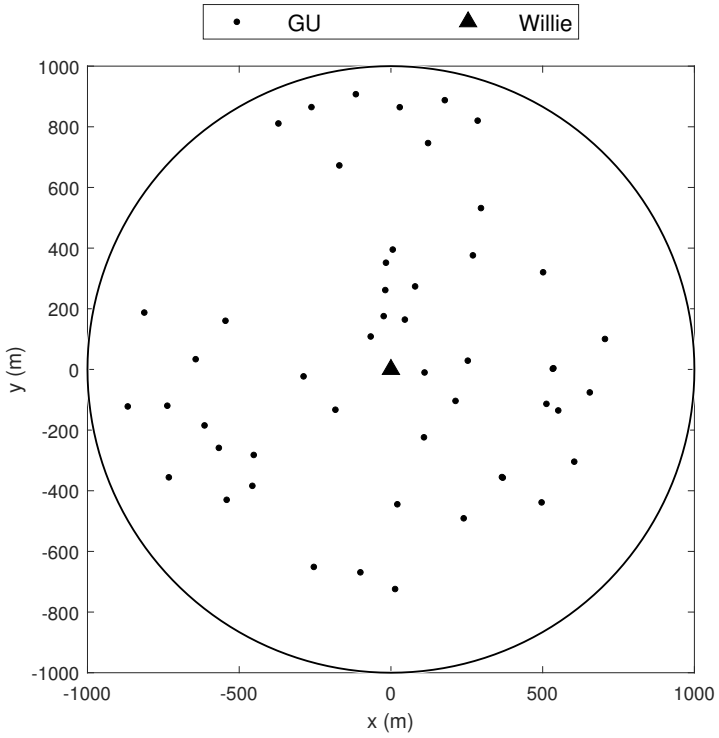

Figure 5.3: Illustration of GU distribution under the settings of $G = 50$, $\rho = 0.3$ and $\lambda = 5$.

performance of the proposed transmission strategy. We can also see from Fig. 5.5 that in general the transmission time of an MG decreases as the MG is located farther away from Willie. This phenomenon is attributed to the fact that when an MG is relatively farther away from Willie, the UAV can then adopt a relatively larger transmission power to transmit CI in the MG while ensuring the covertness. A careful observation of Fig. 5.5a shows that although the 9th MG is further away from Willie than the 8th MG, its transmission time is even longer than that of the 8th MG. This is due to the fact that the 9th MG has a larger coverage area than the 8th MG. This observation indicates that an intricate interplay exists among the coverage, its distance from Willie, and transmission time of an MG.

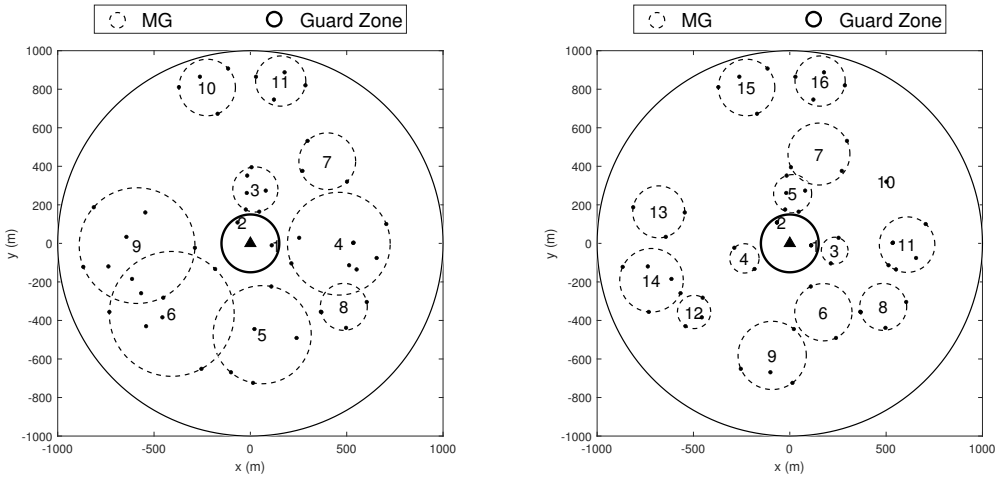

(a) MGs with K-means++ (b) MGs with SMBSP

Figure 5.4: Illustration of MGs under the settings of $G = 50$, $\rho = 0.3$, $\lambda = 5$ and $r_w = 150m$.

5.4.3 Performance Evaluation

This subsection provides numerical results to illustrate the impact of system parameters on the transmission time performance. For a given setting of system parameters (like the number of GUs, cluster parameter, radius of guard zone, and covertness constraint), we first generate 10^4 sets of GU spatial distributions, and then execute 20 times the Algorithm 3 for each GU spatial distribution to get 20 different MG con-

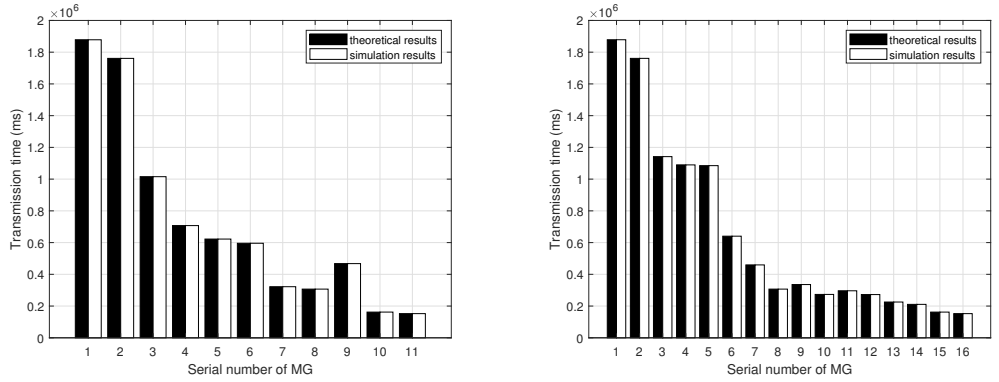

(a) MGs with K-means++ (b) MGs with SMBSP

Figure 5.5: Illustration of the minimum transmission time for MGs in Fig. 5.4.

structions for the GU spatial distribution based on either the K-means++ or SMBSP algorithm. For each MG in a MG construction, we apply (5.8) to evaluate its transmission time, and further get the overall transmission time of the MG construction by summing up the transmission times of all the MGs in this MG construction. Finally, the transmission time for a GU spatial distribution is obtained by taking the average of transmission time of the 20 different MG constructions corresponding to this GU spatial distribution, and the final transmission time under the given setting of system parameters in obtained by taking the average of transmission time of the 10^4 GU spatial distributions.

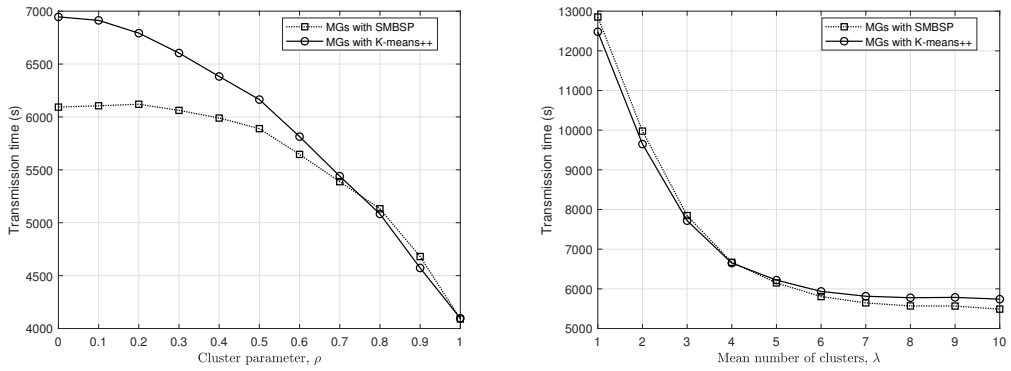

(a) $\lambda = 7$ (b) $\rho = 0.7$

Figure 5.6: Transmission time versus GU spatial distribution parameters (ρ, λ) under the settings of $G = 50$ and $r_w = 150m$.

To explore the impact of GU spatial distribution on the transmission time, we show in Fig. 5.6 how transmission time varies with ρ and λ under the settings of $G = 50$ and $r_w = 150m$. The observation from Fig. 5.6a reveals that the transmission time of the proposed multicast protocol consistently decreases as the cluster parameter ρ increases. This can be attributed to the reason that as ρ increases, GUs in each cluster tend to be more densely clustered within a smaller coverage area, improving the quality of the worst link in each MG and consequently reducing the overall transmission time. We can see from Fig. 5.6b as the mean number of clusters λ increases, the transmission time first rapidly decreases and then remains constant.

This is due to the fact that when λ is small, more GUs will be closer to Willie due to clustering, leading to a higher overall transmission time. On the other hand, when λ is large, more GUs will be farther from Willie due to clustering, resulting in a lower overall transmission time. The results in Fig. 5.6 indicate that when GUs are loosely clustered, the SMBSP algorithm demonstrates shorter transmission times and higher transmission efficiency compared to the K-means++ algorithm. This can be attributed to the SMBSP algorithm's ability to dynamically adjust to variations in user distribution, optimizing resource allocation and reducing latency. In practical applications, this efficiency gain can significantly enhance system performance, particularly in scenarios where rapid data processing and minimal delay are critical. This suggests that the SMBSP algorithm is more suitable for environments with dynamic and sparse user distributions, offering a compelling advantage over traditional clustering methods like K-means++.

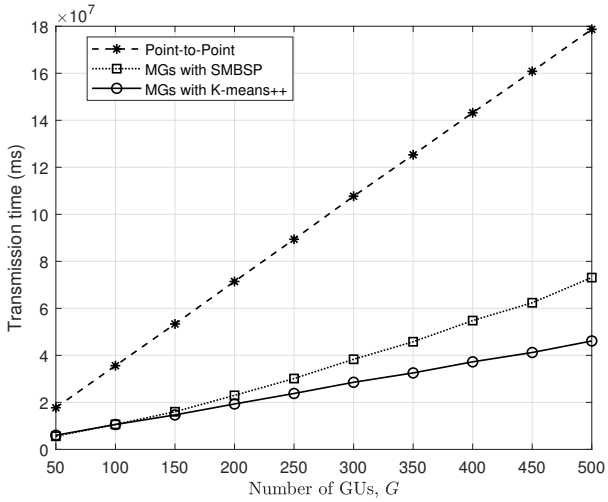

Figure 5.7: Transmission time versus the number of GUs G under the settings of $r_w = 150m$, $\rho = 0.5$ and $\lambda = 10$.

We then plot in Fig. 5.7 the transmission time versus the number of GUs under the settings of $r_w = 150m$, $\rho = 0.5$, and $\lambda = 10$. It is evident from Fig. 5.7 that as the number of GUs increases, the transmission time in general consistently increases,

but the time efficiency of the proposed multicast transmission protocol becomes more significant (in particular the one with K-means++ algorithm). The reason behind this phenomenon is that the multicast transmission protocol with the SMBSP algorithm always employs the circle of the same radius to construct MGs, which is not flexible to adapt to the scenarios with a substantial number of GUs and thus results in a slightly higher transmission time than the one with K-means++ algorithm.

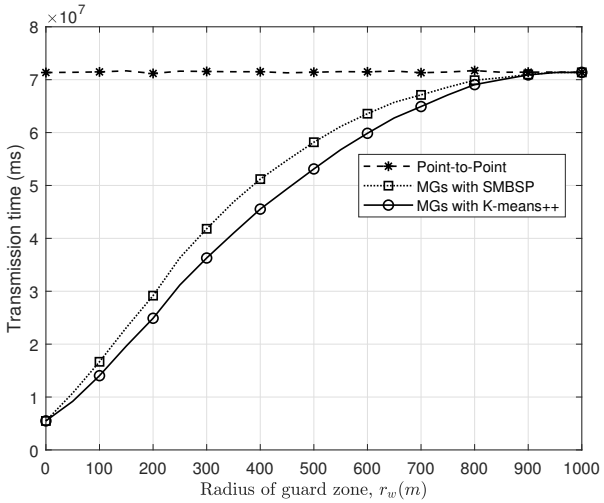

Figure 5.8: Transmission time versus radius of guard zone r_w under the settings of $G = 200$, $\rho = 0.5$ and $\lambda = 10$.

We next illustrate the relationship between the transmission time and the size of guard zone in Fig. 5.8 under the settings of $G = 200$, $\rho = 0.5$ and $\lambda = 10$. From Fig. 5.8 we can see that as the radius of the guard zone increases, the transmission time of the simple point-to-point transmission scheme remains unchanged, but the transmission time of the proposed multicast protocol monotonically increases and finally approaches the transmission time of the point-to-point transmission. The reason is that the guard zone does not affect the distribution of GUs, thereby making the transmission time for the point-to-point scheme remain constant. Conversely, as the radius of the guard zone increases, less GUs will receive CI with the multicast transmission protocol, leading to an increase in transmission time.

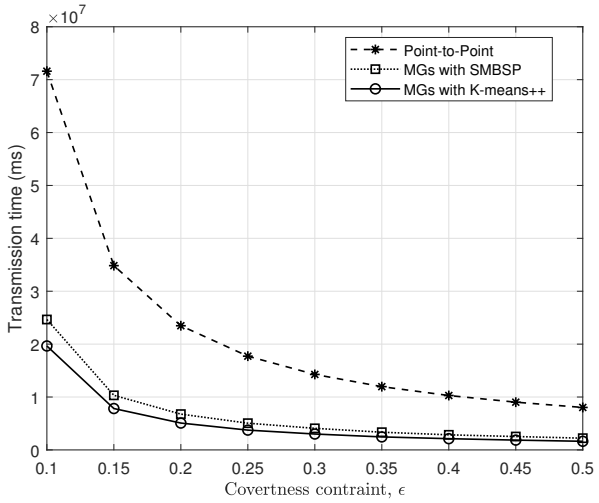

Figure 5.9: Transmission time versus covertness constraint ϵ under the settings of $G = 200$, $r_w = 150m$, $\rho = 0.5$ and $\lambda = 10$.

Finally, we summarize in Fig. 5.9 how transmission time varies with the covertness constraint ϵ. As depicted in Fig. 5.9, the transmission time decreases as ϵ increases (i.e., as the covertness constraint becomes less stringent). This is due to the fact that when ϵ is larger, the UAV can transmit CI with a higher transmission power, reducing the overall transmission time. A careful observation of Fig. 5.9 shows that the gap between the transmission time of the proposed multicast transmission protocol and that of the point-to-point transmission scheme increases as ϵ decreases (i.e., as covertness constraint becomes more stringent), indicating that the new protocol can more efficiently leverage the potential multicast transmission to reduce the transmission when the UAV system is subjected to a more stringent covertness constraint.

5.5 Summary

This chapter proposes a time-efficient transmission protocol for supporting the covert multicast in a UAV-enabled communication system with general multi-receiver scenario by exploring the K-means++ algorithm/SMBSP algorithm for user grouping as well as the transmission power optimization for transmission time minimization.

Compared with the simple point-to-point transmission scheme, our extensive numerical results demonstrate that the new protocol can significantly improve the time efficiency, specially for systems with a large number multicast users and a stringent covertness constraint requirement. It is expected this work can serve as a promising solution and also shed light on the protocol design for future UAV-enabled covert multicast communication systems.

CHAPTER VI

Conclusion

In this thesis, we studied the design of transmission protocols and analyzed covert performance for covert communication in UAV-enabled wireless systems. We first explored the transmission protocol design for covert communication in UAV-enabled wireless systems with a single-receiver scenario and conducted theoretical analysis to derive the corresponding achievable covert throughput performance. We then considered a simple multi-receiver scenario, designed the related transmission protocol, and provided theoretical analysis to demonstrate the covert throughput performance. Finally, we extended our study to the scenario where receivers were diversely distributed in such systems.

For covert communication in UAV-enabled wireless systems with a single-receiver scenario, we studied in Chapter III how a UAV adaptively adopt the OM or DM transmission mode to transmit covert information to a ground user while evading detection by an adversary. For both the OM and DM modes, we first conducted theoretical analysis to reveal the inherent relationship between the transmit rate/transmit power and basic covert performance metrics, including DEP, outage probability, and ECR. To facilitate the transmission mode selection at Alice, we then explored the optimization of transmit rate and transmit power for ECR maximization under the OM and DM modes. Additionally, we proposed a covert transmission protocol based on the

OM/DM transmission mode selection, which allowed the UAV to adaptively select between the OM and DM modes to achieve the maximum ECR at a given UAV location. The main results in Chapter III demonstrated that the hybrid OM/DM transmission mode outperformed the pure OM or DM mode in terms of covert performance.

We investigated in Chapter IV the covert communication in a simple multi-receiver UAV-enabled wireless system, where the UAV aim to disseminate common covert information to GUs within its coverage area while simultaneously evading detection by a ground warden, Willie, outside the covered area. We designed two covert multicast transmission protocols for the system based on one-hop transmission and two-hop transmission, respectively. In the OH transmission protocol, based on the link conditions from the UAV to all GUs, the UAV determined the optimal transmit power and hover location to directly multicast the CI to all GUs to achieve the minimum transmission time. In the TH transmission protocol, the UAV first select the optimal transmit power and an optimal relay from the GUs according to the link conditions among the GUs, UAV, and Willie. The UAV then transmit the CI to the relay, which further multicast the CI to all other GUs by the relay. Related theoretical models were also developed to depict the system performance in terms of DEP and overall transmission time. The main results in Chapter IV demonstrated the efficiency of the proposed two transmission protocols for the simple multi-receiver scenario in UAV-enabled wireless systems.

In Chapter V, we further extended our study to a general multi-receiver scenario, in which a UAV aim to disseminate common CI to multiple GUs diversely distributed within a circular area while simultaneously evading detection by a ground warden, Willie, located in the center of the area. We first proposed two effective MG construction algorithms to group all GUs into multiple MGs and developed a theoretical framework for modeling the performance of each MG in terms of its DEP and transmission time. We also explored the optimal setting of covert transmission power

for each MG to achieve the minimum transmission time. By integrating the aforementioned components, we devised a complete and time-efficient covert multicast transmission protocol for the system. The main results in Chapter V demonstrated the efficiency of the two proposed transmission protocols for the general multi-receiver scenario in UAV-enabled wireless systems.

Overall, the novel covert transmission protocols developed in this thesis offered promising and effective solutions for enhancing covert communication within various UAV-enabled wireless systems. Additionally, the theoretical frameworks presented in this work provide a robust foundation for performance analysis, which can be adapted and applied to other wireless communication systems. These contributions not only advance the state-of-the-art in UAV-enabled covert communication but also provide valuable insights into the broader field of secure wireless communication, guiding future research and development efforts.

This thesis primarily focuses on optimizing key parameters such as frequency selection, transmit mode, user grouping, and transmit power to optimize covert performance, achieving significant improvements in system efficiency and security. However, real-world applications often introduce additional complexity, such as varying environmental conditions and dynamic user behaviors. Recognizing these challenges, a significant direction for future research lies in exploring the joint optimization of additional factors, particularly the UAV's flight speed. By considering flight speed in conjunction with user grouping, trajectory, and transmit power, future studies could further enhance the effectiveness and adaptability of covert multicast communication systems, paving the way for more sophisticated and resilient UAV-enabled networks. This broader optimization approach could yield more comprehensive solutions that are better suited to the diverse and evolving demands of modern wireless communication environments.

APPENDICES

APPENDIX A

Proofs in Chapter III

A.1 Proof of Lemma 2

Here, we provide the calculation steps for (3.26) as follows

$$\int_0^a x f_{|h_{aw}^{o,\mathbb{B}}|^2}(x)dx = xF_{|h_{aw}^{o,\mathbb{B}}|^2}(x)\Big|_0^a - \int_0^a F_{|h_{aw}^{o,\mathbb{B}}|^2}(x)dx. \tag{A.1}$$

Similar to (3.33), we can derive the first term on the right as

$$xF_{|h_{aw}^{o,\mathbb{B}}|^2}(x)\Big|_0^a = a\left(1-\exp\left(-\left[2a(k_{\mathbb{B}}+1)\right]^{\frac{\nu(\sqrt{2k_{\mathbb{B}}})}{2}} e^{\mu(\sqrt{2k_{\mathbb{B}}})}\right)\right). \tag{A.2}$$

Then, we derive the second term on the right as

$$\begin{aligned}
&\int_0^a F_{|h_{aw}^{o,\mathbb{B}}|^2}(x)dx = \int_0^a 1-\exp\left(-[2x(k_{\mathbb{B}}+1)]^{\frac{\nu(\sqrt{2k_{\mathbb{B}}})}{2}} e^{\mu(\sqrt{2k_{\mathbb{B}}})}\right)dx \\
&= a - \int_0^a \exp\left(-[2x(k_{\mathbb{B}}+1)]^{\frac{\nu(\sqrt{2k_{\mathbb{B}}})}{2}} e^{\mu(\sqrt{2k_{\mathbb{B}}})}\right)dx \\
&\overset{(a)}{=} a - \frac{\gamma\left(\frac{2}{\nu(\sqrt{2k_{\mathbb{B}}})}, [2a(k_{\mathbb{B}}+1)]^{\frac{\nu(\sqrt{2k_{\mathbb{B}}})}{2}} e^{\mu(\sqrt{2k_{\mathbb{B}}})}\right)}{(k_{\mathbb{B}}+1)\nu(\sqrt{2k_{\mathbb{B}}})e^{\frac{2\mu(\sqrt{2k_{\mathbb{B}}})}{\nu(\sqrt{2k_{\mathbb{B}}})}}},
\end{aligned} \tag{A.3}$$

where step (a) is according to $\int_0^u x^m e^{-bx^n} dx = \frac{\gamma(v,bu^n)}{nb^v}, v = \frac{m+1}{n}$ as in [63, Eq. (3.381.8)]. Substituting (A.2) and (A.3) into (A.1), we can obtain (3.26).

A.2 Proof of Lemma 4

Here, we provide the calculation steps for (3.42) as follows

$$\int_0^a x f_{|h_{aw}^{d,\mathbb{B}}|^2}(x)dx = xF_{|h_{aw}^{d,\mathbb{B}}|^2}(x)\Big|_0^a - \int_0^a F_{|h_{aw}^{d,\mathbb{B}}|^2}(x)dx. \tag{A.4}$$

According to (3.6), we can derive the first term on the right as

$$xF_{|h_{aw}^{d,\mathbb{B}}|^2}(x)\Big|_0^a = a\sum\nolimits_{r=0}^{S_{\mathbb{B}}} \binom{S_{\mathbb{B}}}{r}(-1)^r e^{-r\xi_{\mathbb{B}}a}. \tag{A.5}$$

Similarly, the second term on the right can be derived as

$$\begin{aligned}\int_0^a F_{|h_{aw}^{d,\mathbb{B}}|^2}(x)dx &= \int_0^a \sum_{r=0}^{S_{\mathbb{B}}} \binom{S_{\mathbb{B}}}{r}(-1)^r e^{-r\xi_{\mathbb{B}}x}dx \\ &= \int_0^a \left[1 + \sum\nolimits_{r=1}^{S_{\mathbb{B}}} \binom{S_{\mathbb{B}}}{r}(-1)^r e^{-r\xi_{\mathbb{B}}x}\right] dx \\ &= a + \sum\nolimits_{r=1}^{S_{\mathbb{B}}} \binom{S_{\mathbb{B}}}{r}\frac{(-1)^r}{r\xi_{\mathbb{B}}}\left(1 - e^{-r\xi_{\mathbb{B}}a}\right).\end{aligned} \tag{A.6}$$

Then, substituting (A.5) and (A.6) into (A.4), we can obtain (3.42).

APPENDIX B

Proofs in Chapter IV

B.1 Proof of the derivation in (4.11)

According to (4.7), due to $x[i] \sim \mathcal{N}(0,1)$, we can get that $\mathbb{P}_{0,k} \sim \mathcal{N}(0,\sigma_0^2)$, and $\mathbb{P}_{1,k} \sim \mathcal{N}(0,\sigma_1^2)$, where $\sigma_0^2 = \sigma_w^2$ and $\sigma_1^2 = P_{ak}H_{aw} + \sigma_w^2$. Let $f_{0,k}(x)$ and $f_{1,k}(x)$ denote the corresponding probability distribution functions of $\mathbb{P}_{0,k}$ and $\mathbb{P}_{1,k}$, respectively. Thus, $f_{0,k}(x) = \frac{1}{\sqrt{2\pi\sigma_0^2}} \exp\left(-\frac{x^2}{2\sigma_0^2}\right)$ and $f_{1,k}(x) = \frac{1}{\sqrt{2\pi\sigma_1^2}} \exp\left(-\frac{x^2}{2\sigma_1^2}\right)$. The relative entropy between $\mathbb{P}_{1,k}$ and $\mathbb{P}_{0,k}$ can be given by

$$\begin{aligned} \mathcal{D}(\mathbb{P}_{1,k}, \mathbb{P}_{0,k}) &= \int_{\mathcal{X}} f_{1,k}(x) \ln \frac{f_{1,k}(x)}{f_{0,k}(x)} dx \\ &= \int f_{1,k}(x) \ln f_{1,k}(x) dx - \int f_{1,k}(x) \ln f_{0,k}(x) dx. \end{aligned} \tag{B.1}$$

For the first part of (B.1), we have

$$\begin{aligned}
&\int f_{1,k}(x) \ln f_{1,k}(x) dx \\
&= \int P_{1,k}(x) \left(\ln \frac{1}{\sqrt{2\pi\sigma_1^2}} + \ln \exp\left(\frac{-x^2}{2\sigma_1^2} \right) \right) dx \\
&= -\frac{1}{2} \ln\left(2\pi\sigma_1^2\right) - \frac{1}{2\sigma_1^2} \int f_{1,k}(x) x^2 dx \\
&= -\frac{1}{2} \left(\ln\left(2\pi\sigma_1^2\right) + 1 \right).
\end{aligned} \tag{B.2}$$

Similarly, the second part of (B.1) can be calculated as

$$\int f_{1,k}(x) \ln f_{0,k}(x) dx = -\frac{1}{2} \left(\ln\left(2\pi\sigma_0^2\right) + \frac{\sigma_1^2}{\sigma_0^2} \right). \tag{B.3}$$

Substituting (B.2) and (B.3) into (B.1), we have

$$\begin{aligned}
\mathcal{D}(\mathbb{P}_{1,k}, \mathbb{P}_{0,k}) &= \frac{1}{2} \left(\frac{\sigma_1^2 - \sigma_0^2}{\sigma_0^2} - \ln \frac{\sigma_1^2}{\sigma_0^2} \right) \\
&= \frac{1}{2} \left[\frac{P_{ak} H_{aw}}{\sigma_w^2} - \ln\left(1 + \frac{P_{ak} H_{aw}}{\sigma_w^2} \right) \right].
\end{aligned} \tag{B.4}$$

BIBLIOGRAPHY

BIBLIOGRAPHY

[1] Y. Zeng, Q. Wu, and R. Zhang, "Accessing from the sky: a tutorial on UAV communications for 5G and beyond," *Proc. IEEE*, vol. 107, no. 12, pp. 2327–2375, Dec. 2019.

[2] H. Wu, X. Tao, N. Zhang, and X. Shen, "Cooperative UAV cluster-assisted terrestrial cellular networks for ubiquitous coverage," *IEEE J. Select. Areas Commun.*, vol. 36, no. 9, pp. 2045–2058, Aug. 2018.

[3] M. Cui, G. Zhang, Q. Wu, and D. W. K. Ng, "Robust trajectory and transmit power design for secure UAV communications," *IEEE Trans. Veh. Technol.*, vol. 67, no. 9, pp. 9042–9046, Jun. 2018.

[4] L. Chen, L. Chen, S. Jordan, Y.-K. Liu, D. Moody, R. Peralta, R. Perlner, and D. Smith-Tone, *Report on post-quantum cryptography.* US Department of Commerce, National Institute of Standards and Technology, 2016.

[5] X. Zhou, L. Song, and Y. Zhang, *Physical Layer Security in Wireless Communications.* CRC Press, 2013.

[6] G. J. Simmons, "The prisoners' problem and the subliminal channel," in *Advances in Cryptology: Proceedings of Crypto 83.* Springer, 1984, pp. 51–67.

[7] B. J. Xiang, S. Y. Zheng, H. Wong, Y. M. Pan, K. X. Wang, and M. H. Xia, "A flexible dual-band antenna with large frequency ratio and different radiation properties over the two bands," *IEEE Trans. Antennas Propag.*, vol. 66, no. 2, pp. 657–667, Dec. 2017.

[8] J. F. Zhang, Y. J. Cheng, Y. R. Ding, and C. X. Bai, "A dual-band shared-aperture antenna with large frequency ratio, high aperture reuse efficiency, and high channel isolation," *IEEE Trans. Antennas Propag.*, vol. 67, no. 2, pp. 853–860, Nov. 2018.

[9] Y. Li and J. Wang, "Dual-band leaky-wave antenna based on dual-mode composite microstrip line for microwave and millimeter-wave applications," *IEEE Trans. Antennas Propag.*, vol. 66, no. 4, pp. 1660–1668, Feb. 2018.

[10] S. Vuppala, S. Biswas, and T. Ratnarajah, "An analysis on secure communication in millimeter/micro-wave hybrid networks," *IEEE Trans. Commun.*, vol. 64, no. 8, pp. 3507–3519, July 2016.

[11] O. Semiari, W. Saad, and M. Bennis, "Joint millimeter wave and microwave resources allocation in cellular networks with dual-mode base stations," *IEEE Trans. Wireless Commun.*, vol. 16, no. 7, pp. 4802–4816, May 2017.

[12] N. D. Sidiropoulos, T. N. Davidson, and Z.-Q. Luo, "Transmit beamforming for physical-layer multicasting," *IEEE Trans. Signal Processing*, vol. 54, no. 6, pp. 2239–2251, June 2006.

[13] Z. Lin, M. Lin, T. de Cola, J.-B. Wang, W.-P. Zhu, and J. Cheng, "Supporting iot with rate-splitting multiple access in satellite and aerial-integrated networks," *IEEE Internet Things J.*, vol. 8, no. 14, pp. 11 123–11 134, Jan. 2021.

[14] D. Arthur and S. Vassilvitskii, "K-means++: the advantages of careful seeding," in *Proc. Annu. ACM-SIAM Symp. Discrete Algorithms*, 2007, pp. 1027–1035.

[15] J. Lyu, Y. Zeng, R. Zhang, and T. J. Lim, "Placement optimization of UAV-mounted mobile base stations," *IEEE Commun. Lett.*, vol. 21, no. 3, pp. 604–607, Nov. 2016.

[16] B. A. Bash, D. Goeckel, and D. Towsley, "Limits of reliable communication with low probability of detection on AWGN channels," *IEEE J. Sel. Areas Commun.*, vol. 31, no. 9, pp. 1921–1930, Aug. 2013.

[17] P. H. Che, M. Bakshi, and S. Jaggi, "Reliable deniable communication: Hiding messages in noise," in *Proc. IEEE Int. Symp. Info. Theory*, Oct. 2013, pp. 2945–2949.

[18] L. Wang, G. W. Wornell, and L. Zheng, "Fundamental limits of communication with low probability of detection," *IEEE Trans. Inf. Theory*, vol. 62, no. 6, pp. 3493–3503, Jun. 2016.

[19] A. Abdelaziz and C. E. Koksal, "Fundamental limits of covert communication over MIMO AWGN channel," in *Proc. IEEE Conf. Commun. Network Security*, Dec. 2017, pp. 1–9.

[20] S. Lee, R. J. Baxley, M. A. Weitnauer, and B. Walkenhorst, "Achieving undetectable communication," *IEEE J. Sel. Top. Signal Process.*, vol. 9, no. 7, pp. 1195–1205, Apr. 2015.

[21] K. Li, P. A. Kelly, and D. Goeckel, "Optimal power adaptation in covert communication with an uninformed jammer," *IEEE Trans. Wireless Commun.*, vol. 19, no. 5, pp. 3463–3473, Feb. 2020.

[22] K. Shahzad and X. Zhou, "Covert wireless communications under quasi-static fading with channel uncertainty," *IEEE Trans. Inf. Forensics Secur.*, vol. 16, pp. 1104–1116, Oct. 2020.

[23] K. Shahzad, X. Zhou, and S. Yan, "Covert communication in fading channels under channel uncertainty," in *Proc. IEEE 85th Veh. Technol. Conf.*, Jun. 2017, pp. 1–5.

[24] K. Shahzad, X. Zhou, S. Yan, J. Hu, F. Shu, and J. Li, "Achieving covert wireless communications using a full-duplex receiver," *IEEE Trans. Wireless Commun.*, vol. 17, no. 12, pp. 8517–8530, Nov. 2018.

[25] R. Soltani, D. Goeckel, D. Towsley, B. A. Bash, and S. Guha, "Covert wireless communication with artificial noise generation," *IEEE Trans. Wireless Commun.*, vol. 17, no. 11, pp. 7252–7267, Nov. 2018.

[26] T.-X. Zheng, H.-M. Wang, D. W. K. Ng, and J. Yuan, "Multi-antenna covert communications in random wireless networks," *IEEE Trans. Wireless Commun.*, vol. 18, no. 3, pp. 1974–1987, Feb. 2019.

[27] J. Bai, J. He, Y. Chen, Y. Shen, and X. Jiang, "On covert communication performance with outdated CSI in wireless greedy relay systems," *IEEE Trans. Inf. Forensics Secur.*, vol. 17, pp. 2920–2935, Aug. 2022.

[28] L. Lv, Q. Wu, Z. Li, Z. Ding, N. Al-Dhahir, and J. Chen, "Covert communication in intelligent reflecting surface-assisted NOMA systems: Design, analysis, and optimization," *IEEE Trans. Wireless Commun.*, vol. 21, no. 3, pp. 1735–1750, Aug. 2021.

[29] M. T. Mamaghani and Y. Hong, "Aerial intelligent reflecting surface enabled terahertz covert communications in beyond-5G Internet of Things," *IEEE Internet Things J.*, vol. 9, no. 19, pp. 19 012–19 033, Mar. 2022.

[30] M. V. Jamali and H. Mahdavifar, "Covert millimeter-wave communication: Design strategies and performance analysis," *IEEE Trans. Wireless Commun.*, Nov 2021.

[31] J. Zhang, M. Li, S. Yan, C. Liu, X. Chen, M.-J. Zhao, and P. Whiting, "Joint beam training and data transmission design for covert millimeter-wave communication," *IEEE Trans. Inf. Forensics Secur.*, vol. 16, pp. 2232–2245, Jan. 2021.

[32] J. Zhang, M. Li, M.-J. Zhao, X. Ji, and W. Xu, "Multi-user beam training and transmission design for covert millimeter-wave communication," *IEEE Trans. Inf. Forensics Secur.*, vol. 17, pp. 1528–1543, Mar. 2022.

[33] C. Wang, Z. Li, and D. W. K. Ng, "Covert rate optimization of millimeter wave full-duplex communications," *IEEE Trans. Wireless Commun.*, vol. 21, no. 5, pp. 2844–2861, Oct. 2021.

[34] X. Zhou, S. Yan, J. Hu, J. Sun, J. Li, and F. Shu, "Joint optimization of a UAV's trajectory and transmit power for covert communications," *IEEE Trans. Signal Process.*, vol. 67, no. 16, pp. 4276–4290, July 2019.

[35] H. Rao, S. Xiao, S. Yan, J. Wang, and W. Tang, "Optimal geometric solutions to UAV-enabled covert communications in line-of-sight scenarios," *IEEE Trans. Wireless Commun.*, vol. 21, no. 12, pp. 10 633–10 647, June 2022.

[36] X. Jiang, X. Chen, J. Tang, N. Zhao, X. Y. Zhang, D. Niyato, and K.-K. Wong, "Covert communication in UAV-assisted air-ground networks," *IEEE Wireless Commun.*, vol. 28, no. 4, pp. 190–197, Mar. 2021.

[37] S. Yan, S. V. Hanly, and I. B. Collings, "Optimal transmit power and flying location for UAV covert wireless communications," *IEEE J. Sel. Areas Commun.*, vol. 39, no. 11, pp. 3321–3333, Jun. 2021.

[38] X. Zhou, S. Yan, D. W. K. Ng, and R. Schober, "Three-dimensional placement and transmit power design for UAV covert communications," *IEEE Trans. Veh. Technol.*, vol. 70, no. 12, pp. 13 424–13 429, Oct. 2021.

[39] X. Chen, M. Sheng, N. Zhao, W. Xu, and D. Niyato, "UAV-relayed covert communication towards a flying warden," *IEEE Trans. Commun.*, vol. 69, no. 11, pp. 7659–7672, Aug. 2021.

[40] R. Zhang, X. Chen, M. Liu, N. Zhao, X. Wang, and A. Nallanathan, "UAV relay assisted cooperative jamming for covert communications over Rician fading," *IEEE Trans. Veh. Technol.*, vol. 71, no. 7, pp. 7936–7941, Apr. 2022.

[41] L. Jiao, R. Zhang, M. Liu, Q. Hua, N. Zhao, A. Nallanathan, and X. Wang, "Placement optimization of UAV relaying for covert communication," *IEEE Trans. Veh. Technol.*, vol. 71, no. 11, pp. 12 327–12 332, July 2022.

[42] X. Chen, Z. Chang, M. Liu, N. Zhao, T. Hämäläinen, and D. Niyato, "UAV-IRS assisted covert communication: Introducing uncertainty via phase shifting," *IEEE Wirel. Commun. Lett.*, Oct. 2023.

[43] C. Wang, X. Chen, J. An, Z. Xiong, C. Xing, N. Zhao, and D. Niyato, "Covert communication assisted by UAV-IRS," *IEEE Trans. on Commun.*, vol. 71, no. 1, pp. 357–369, Jan. 2022.

[44] Y. Qian, C. Yang, Z. Mei, X. Zhou, L. Shi, and J. Li, "On joint optimization of trajectory and phase shift for IRS-UAV assisted covert communication systems," *IEEE Trans. Veh. Technol.*, Apr. 2023.

[45] S. Bi, L. Hu, Q. Liu, J. Wu, R. Yang, and L. Wu, "Deep reinforcement learning for IRS-assisted UAV covert communications," *China Commun.*, May 2023.

[46] M. Tatar Mamaghani and Y. Hong, "Aerial intelligent reflecting surface-enabled terahertz covert communications in beyond-5G internet of things," *IEEE Internet of Things Journal*, vol. 9, no. 19, pp. 19 012–19 033, Oct. 2022.

[47] Y. Su, S. Fu, J. Si, C. Xiang, N. Zhang, and X. Li, "Optimal hovering height and power allocation for UAV-aided NOMA covert communication system," *IEEE Wirel. Commun. Lett.*, Feb. 2023.

[48] D. Deng, S. Dang, X. Li, D. W. K. Ng, and A. Nallanathan, "Joint optimization for covert communications in UAV-assisted NOMA networks," *IEEE Trans. Veh. Technol.*, Aug. 2023.

[49] K. Venugopal, M. C. Valenti, and R. W. Heath, "Device-to-device millimeter wave communications: Interference, coverage, rate, and finite topologies," *IEEE Trans. Wireless Commun.*, vol. 15, no. 9, pp. 6175–6188, June 2016.

[50] Y. Zhu, G. Zheng, and M. Fitch, "Secrecy rate analysis of UAV-enabled mmwave networks using Matérn hardcore point processes," *IEEE J. Sel. Areas Commun.*, vol. 36, no. 7, pp. 1397–1409, Apr. 2018.

[51] C. You and R. Zhang, "3D trajectory optimization in Rician fading for UAV-enabled data harvesting," *IEEE Trans. Wireless Commun.*, vol. 18, no. 6, pp. 3192–3207, Apr. 2019.

[52] S. Shimamoto *et al.*, "Channel characterization and performance evaluation of mobile communication employing stratospheric platforms," *IEICE Trans. Commun.*, vol. 89, no. 3, pp. 937–944, Mar. 2006.

[53] M. K. Simon and M.-S. Alouini, *Digital communication over fading channels*. John Wiley & Sons, 2005.

[54] J. G. Andrews, T. Bai, M. N. Kulkarni, A. Alkhateeb, A. K. Gupta, and R. W. Heath, "Modeling and analyzing millimeter wave cellular systems," *IEEE Trans. Commun.*, vol. 65, no. 1, pp. 403–430, Oct. 2016.

[55] T. Bai and R. W. Heath, "Coverage and rate analysis for millimeter-wave cellular networks," *IEEE Trans. Wireless Commun.*, vol. 14, no. 2, pp. 1100–1114, Oct. 2014.

[56] H. Alzer, "On some inequalities for the incomplete gamma function," *Math. Comp.*, vol. 66, no. 218, pp. 771–778, 1997.

[57] S. Shellhammer, "Performance of the power detector with noise uncertainty," *Doc. IEEE 802.22-06/0134r0*, July 2006.

[58] T. V. Sobers, B. A. Bash, S. Guha, D. Towsley, and D. Goeckel, "Covert communication in the presence of an uninformed jammer," *IEEE Trans. Wireless Commun.*, vol. 16, no. 9, pp. 6193–6206, Sept. 2017.

[59] H. ZivariFard, M. R. Bloch, and A. Nosratinia, "Covert communication in the presence of an uninformed, informed, and coordinated jammer," in *2022 IEEE Int. Symp. on Info. Theory (ISIT)*. IEEE, June 2022, pp. 306–311.

[60] A. Browder, *Mathematical analysis: an introduction*. Springer Science & Business Media, 2012.

[61] D. Mishra and S. De, "i^{2}RES: Integrated information relay and energy supply assisted RF harvesting communication," *IEEE Trans. Commun.*, vol. 65, no. 3, pp. 1274–1288, Dec. 2016.

[62] M. Z. Bocus, C. P. Dettmann, and J. P. Coon, "An approximation of the first order Marcum Q-function with application to network connectivity analysis," *IEEE Commun. Lett.*, vol. 17, no. 3, pp. 499–502, Jan. 2013.

[63] I. S. Gradshteyn and I. M. Ryzhik, *Table of integrals, series, and products*. Academic press, 2014.

[64] A. Li, Q. Wu, and R. Zhang, "UAV-enabled cooperative jamming for improving secrecy of ground wiretap channel," *IEEE Wireless Commun. Lett.*, vol. 8, no. 1, pp. 181–184, Aug. 2018.

[65] M. R. Akdeniz, Y. Liu, M. K. Samimi, S. Sun, S. Rangan, T. S. Rappaport, and E. Erkip, "Millimeter wave channel modeling and cellular capacity evaluation," *IEEE J. Sel. Areas Commun.*, vol. 32, no. 6, pp. 1164–1179, Jun. 2014.

[66] C. Liu, M. Li, S. V. Hanly, I. B. Collings, and P. Whiting, "Millimeter wave beam alignment: Large deviations analysis and design insights," *IEEE J. Sel. Areas Commun.*, vol. 35, no. 7, pp. 1619–1631, Apr. 2017.

[67] J. Zhang, X. Chen, M. Li, and M. Zhao, "Optimized throughput in covert millimeter-wave UAV communications with beam sweeping," *IEEE Wireless Commun. Lett.*, vol. 10, no. 4, pp. 720–724, Dec. 2020.

[68] W. Khawaja, I. Guvenc, D. W. Matolak, U.-C. Fiebig, and N. Schneckenburger, "A survey of air-to-ground propagation channel modeling for unmanned aerial vehicles," *IEEE Commun. Surv. Tutor.*, vol. 21, no. 3, pp. 2361–2391, May 2019.

[69] K. Haneda, J. Zhang, L. Tan, G. Liu, Y. Zheng, H. Asplund, J. Li, Y. Wang, D. Steer, C. Li *et al.*, "5G 3GPP-like channel models for outdoor urban microcellular and macrocellular environments," in *2016 IEEE 83rd VTC spring*. IEEE, May 2016, pp. 1–7.

[70] F. Shu, T. Xu, J. Hu, and S. Yan, "Delay-constrained covert communications with a full-duplex receiver," *IEEE Wirel. Commun. Lett.*, vol. 8, no. 3, pp. 813–816, Jan. 2019.

[71] J. Wang, W. Tang, Q. Zhu, X. Li, H. Rao, and S. Li, "Covert communication with the help of relay and channel uncertainty," *IEEE Wireless Communications Letters*, vol. 8, no. 1, pp. 317–320, Sept. 2018.

[72] P. Fisher and Others, "Negative binomial distribution." *Ann. Eugen.*, vol. 11, pp. 182–787, 1941.

[73] Z. Xiang, W. Yang, Y. Cai, J. Xiong, Z. Ding, and Y. Song, "Secure transmission in a NOMA-assisted IOT network with diversified communication requirements," *IEEE Internet Things J.*, vol. 7, no. 11, pp. 11 157–11 169, May 2020.

[74] G. Durisi, T. Koch, and P. Popovski, "Toward massive, ultrareliable, and low-latency wireless communication with short packets," *Proc. IEEE*, vol. 104, no. 9, pp. 1711–1726, Aug. 2016.

[75] J. Sánchez-García, D. G. Reina, and S. Toral, "A distributed PSO-based exploration algorithm for a UAV network assisting a disaster scenario," *Future Generation Computer Systems*, vol. 90, pp. 129–148, Jan. 2019.

[76] T. Riihonen, S. Werner, and R. Wichman, "Hybrid full-duplex/half-duplex relaying with transmit power adaptation," *IEEE transactions on wireless communications*, vol. 10, no. 9, pp. 3074–3085, July, 2011.

[77] Y. Hu, J. Gross, and A. Schmeink, "On the capacity of relaying with finite blocklength," *IEEE Transactions on Vehicular Technology*, vol. 65, no. 3, pp. 1790–1794, Feb. 2015.

[78] C. H. Stapper, "On yield, fault distributions, and clustering of particles," *IBM J. Res. Dev.*, vol. 30, no. 3, pp. 326–338, May 1986.

[79] J. Lyu, H.-m. Wang, and K.-w. Huang, "Physical layer security in D2D underlay cellular networks with poisson cluster process," *IEEE Trans. Commun.*, vol. 68, no. 11, pp. 7123–7139, Aug. 2020.

[80] X. Zhou, S. Yan, F. Shu, R. Chen, and J. Li, "UAV-enabled covert wireless data collection," *IEEE J. Sel. Areas Commun.*, vol. 39, no. 11, pp. 3348–3362, Jun. 2021.

[81] S. Minaeian, J. Liu, and Y.-J. Son, "Vision-based target detection and localization via a team of cooperative UAV and UGVs," *IEEE Trans. Syst. Man Cybern.: Syst.*, vol. 46, no. 7, pp. 1005–1016, Nov. 2015.

[82] A. Srinivas, G. Zussman, and E. Modiano, "Construction and maintenance of wireless mobile backbone networks," *IEEE/ACM Trans. Networking*, vol. 17, no. 1, pp. 239–252, Feb. 2009.

[83] C.-F. Huang, Y.-C. Tseng, and L.-C. Lo, "The coverage problem in three-dimensional wireless sensor networks," *J. Interconnect. Netw.*, vol. 8, no. 03, pp. 209–227, Oct. 2007.

[84] W. Zhang, "MATLAB simulator for time-efficient covert multicast in UAV-enabled wireless communication systems," 2023, [online]. available: https://github.com/zhangwenhao/multicast_transmission_protocol_simulator.

Publications

Jounal Articles

[1] Wenhao. Zhang, J. He, Y. Shen and X. Jiang. "Covert communication in hybrid microwave/mmWave UAV-enabled systems with transmission mode selection," *Computer Communications*, vol. 219, pp. 216-228, April 2024.

Conference Papers

[2] Wenhao. Zhang, J. He and X. Jiang. "Transmit power and flying location optimization for time-efficient covert multicast in UAV-enabled wireless communication systems," *2024 International Conference on Networking and Network Applications (NaNA)*, Yinchuan, China, 2024.